Design and Performance of Cost-Effective Ultra High Performance Concrete for Bridge Deck Overlays

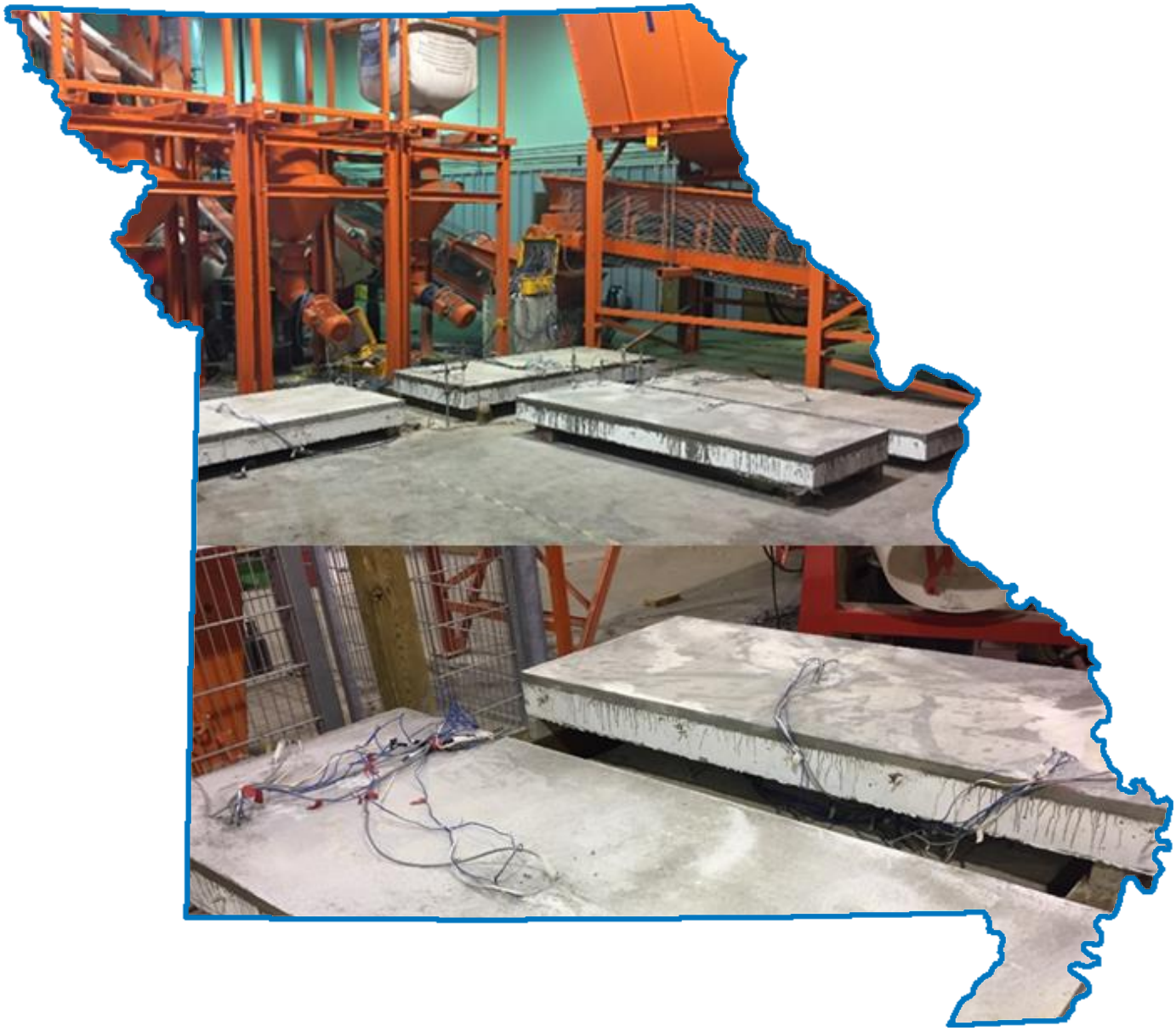

Prepared by:
Kamal H. Khayat, P.Eng., Ph.D.
Mahdi Valipour, Ph.D.
Missouri University of Science and Technology
Center for Infrastructure Engineering Studies

Final Report Prepared for Missouri Department of Transportation
April 2018 Project TR201704 Report cmr18-006

TECHNICAL REPORT DOCUMENTATION PAGE

1. Report No. cmr 18-006	**2. Government Accession No.**	**3. Recipient's Catalog No.**
4. Title and Subtitle Design and Performance of Cost-Effective Ultra High Performance Concrete for Bridge Deck Overlays		**5. Report Date** January 2018 Published: April 2018 **6. Performing Organization Code**
7. Author(s) Kamal H. Khayat, P.Eng., Ph.D. https://orcid.org/0000-0003-1431-0715 Mahdi Valipour, Ph.D. https://orcid.org/0000-0002-0739-0211		**8. Performing Organization Report No.**
9. Performing Organization Name and Address Department of Civil, Architectural and Environmental Engineering Missouri University of Science and Technology 1401 N. Pine St., Rolla, MO 65409		**10. Work Unit No.** **11. Contract or Grant No.** MoDOT project # TR201704
12. Sponsoring Agency Name and Address Missouri Department of Transportation (SPR) Construction and Materials Division P.O. Box 270 Jefferson City, MO 65102		**13. Type of Report and Period Covered** Final Report (July 2016-February 2018) **14. Sponsoring Agency Code**

15. Supplementary Notes

Project title: Design of Ultra High Performance Concrete for Thin Overlays. Conducted in cooperation with the U.S. Department of Transportation, Federal Highway Administration. MoDOT research reports are available in the Innovation Library at http://www.modot.org/services/or/byDate.htm.

16. Abstract

The main objective of this research was to develop a cost-effective ultra-high performance concrete (UHPC) for bonded bridge deck overlays. The high durability and mechanical properties of such repair material can offer shorter traffic closures and prolong the service life of the bridge deck. The UHPC was optimized using supplementary cementitious materials (SCMs), proper combinations of sands, and adequate selection of fiber types and contents. Packing density studies included paste, sand, and fiber combinations. The robustness of optimized UHPC mixtures to variations of mixing and curing temperatures was examined. The efficiency of various shrinkage mitigation approaches for reducing autogenous and drying shrinkage of optimized UHPC mixtures was evaluated. This included the use of CaO-based and MgO-based expansive agents, shrinkage-reducing admixture, and pre-saturated lightweight sand. Test results indicate that the optimized UHPC mixtures exhibited relatively low autogenous shrinkage and drying shrinkage. All tested UHPC mixtures exhibited high mechanical properties and excellent frost durability. The use of 60% lightweight sand led to a significant reduction in autogenous shrinkage from 530 to 35 με. The optimized UHPC mixtures were cast as thin bonded overlays of 25, 38, and 50 mm (1, 1.5, and 2 in.) in thickness over pavement sections measuring 1 × 2.5 m^2 (10.7 x 27 ft2). Early-age and long-term deformation caused by concrete, humidity and temperature gradients, as well as cracking and delamination were monitored over time. Test results indicate that there was no surface cracking or delamination in UHPC overlays after more than 200 d of casting. After laboratory investigations, a life cycle cost analysis (LCCA) was determined for the selected concrete mixtures with different mixture compositions and performance characteristics. Results indicate that, based on both deterministic and probabilistic results, UHPC overlay with minimum 25 mm (1 in.) thickness is a more cost-effective option compared with other commonly used materials, such as latex-modified concrete and conventional bonded concrete overlays.

17. Key Words Fibers; Greenhouse gases; Overlays (Pavements); Pavement performance; Service life; Ultra high performance concrete	**18. Distribution Statement** No restrictions. This document is available through the National Technical Information Service, Springfield, VA 22161.

19. Security Classif. (of this report) Unclassified.	**20. Security Classif. (of this page)** Unclassified.	**21. No. of Pages** 132	**22. Price**

Missouri University of Science and Technology

Center for Infrastructure Engineering Studies

Final Report:

DESIGN AND PERFORMANCE OF COST-EFFECTIVE ULTRA HIGH PERFORMANCE CONCRETE FOR BRIDGE DECK OVERLAYS

January 2018

Prepared by:

Kamal H. Khayat, P.Eng., Ph.D.

Mahdi Valipour, Ph.D.

ABSTRACT

The main objective of this research was to develop a cost-effective ultra-high performance concrete (UHPC) for bonded bridge deck overlays. The high durability and mechanical properties of such repair material can offer shorter traffic closures and prolong the service life of the bridge deck. The UHPC was optimized using supplementary cementitious materials (SCMs), proper combinations of sands, and adequate selection of fiber types and contents. Packing density studies included paste, sand, and fiber combinations. The robustness of optimized UHPC mixtures to variations of mixing and curing temperatures was examined. The efficiency of various shrinkage mitigation approaches for reducing autogenous and drying shrinkage of optimized UHPC mixtures was evaluated. This included the use of CaO-based and MgO-based expansive agents, shrinkage-reducing admixture, and pre-saturated lightweight sand. Test results indicate that the optimized UHPC mixtures exhibited relatively low autogenous shrinkage and drying shrinkage. All tested UHPC mixtures exhibited high mechanical properties and excellent frost durability. The use of 60% lightweight sand led to a significant reduction in autogenous shrinkage from 530 to 35 με. The optimized UHPC mixtures were cast as thin bonded overlays of 25, 38, and 50 mm (1, 1.5, and 2 in.) in thickness over pavement sections measuring 1 × 2.5 m^2 (10.7 x 27 ft^2). Early-age and long-term deformation caused by concrete, humidity and temperature gradients, as well as cracking and delamination were monitored over time. Test results indicate that there was no surface cracking or delamination in UHPC overlays after more than 200 d of casting. After laboratory investigations, a life cycle cost analysis (LCCA) was determined for the selected concrete mixtures with different mixture compositions and performance characteristics. Results indicate that, based on both deterministic and probabilistic results, UHPC overlay with minimum 25 mm (1 in.) thickness is a more cost-effective option compared with other commonly used materials, such as latex-modified concrete and conventional bonded concrete overlays.

ACKNOWLEDGMENTS

This project was supported by the Missouri Department of Transportation (MoDOT), the RE-CAST (Research on Concrete Applications for Sustainable Transportation) Tier-1 University Transportation Center (UTC) at Missouri University of Science and Technology (Missouri S&T), and the Center for Infrastructure Engineering Studies (CIES).

Authors would like to give special thanks to Dr. Weina Meng. The authors would also like to sincerely thank the staff of the Center for Infrastructure Engineering Studies (CIES); Ms. Abigayle Sherman, Ms. Gayle Spitzmiller, and Mr. Jason Cox for their great help and support. The authors would like to thank Mr. John Bullock, Mr. Brian Swift, and Mr. Gary Abbott for their technical assistance.

DISCLAIMER

TABLE OF CONTENTS

LIST OF FIGURES

LIST OF TABLES

1. INTRODUCTION

1.1. NEED FOR RESEARCH

Rigid concrete pavements consist usually of base and sub-base layers which last for 300 to 40 years or more. On the other hand, while the wearing coarse materials has a shorter service life. Intensive efforts are devoted to introducing a new generation of materials to enhance the performance of surface wearing layers in concrete pavements, thus prolonging the service life of pavement system. Given their superior mechanical properties and durability, overlays cast using ultra-high performance concrete (UHPC) can provide significant improvement in durability and service life of the pavement. In addition, the absence of mechanical consolidation due to the high fluid nature of the UHPC materials can reduce construction time for the installation of a new overlay and/or the rehabilitation of an existing pavement system.

Degradation of concrete bridge decks can be found in the form of spalling, delamination, scaling due to poor material design, freeze-thaw damage, and/or corrosion of reinforcing steel bars associated with the infiltration of chloride ions and moisture or inadequate clear cover (Shann, 2012; Krauss et al., 2009). Overlays are often applied to bridge decks to protect the superstructure from these deterioration mechanisms (Knight et al., 2004; Griffin et al., 2006). Traditional overlays have several limitations, such as a relatively short service life, typically between 5 and 25 years. This can result in continuous maintenance, repair, and replacement of the bridge system. Furthermore, overlay construction often requires the use of experienced contractors and specialized equipment for proper implementation. The latter can significantly increase the dead load. The use of some overlay materials often develop compatibility issues associated with differences in time-dependent properties between the existing concrete and overlay materials (Shann, 2012; Krauss et al., 2009).

Due to cost considerations and weight limitations, the thickness of overlay materials used in pavement and bridge decks is generally limited. In general, shallow overlays are more prone to have a high risk of shrinkage cracking. Therefore, the incorporation of the proper type of steel and/or synthetic fibers is sometimes used to minimize the risk of cracking and delamination. In addition, the use of fibers can reduce the depth of pavement overlay, thus reducing the overall costs and speeding up the construction process (Shann, 2012). This research aimed at developing thin UHPC overlays that can be used bridge deck construction and rehabilitation.

1.2. OBJECTIVE AND SCOPE OF WORK

The main objective of this research is to develop a cost-effective UHPC material for thin bonded overlays targeted for bridge deck applications to enhance the service life.

A comprehensive investigation involving laboratory material performance evaluation was conducted to develop the mixture design methodology and validate the material performance. The research project consisted of following main tasks:

- Developed a systematic mixture design procedure of UHPC to achieve a densely-compacted cementitious matrix with enhanced fresh and mechanical properties and relatively low cost. A number of cost-effective UHPC mixtures, including high-volume supplementary cementitious materials (SCMs), conventional concrete sand, and relatively low fiber content were proposed. The mixtures were evaluated to determine key properties, such as workability, shrinkage, and durability.
- Evaluate the robustness of optimized UHPC mixtures due to temperature variations. Robustness was evaluated for UHPC made with silica fume, Class C fly ash, and ground granulated blast-furnace slag at different casting and curing temperatures of 10, 23, and 30 °C (50, 73.4, and 86 °F). The investigated properties included rheology, workability, setting time, mechanical properties, as well as autogenous and drying shrinkage.
- Given the critical effect of autogenous and drying shrinkage on the performance of thin overlay systems, the benefits of using the combined addition of shrinkage mitigating admixtures along with lightweight sand were evaluated. The effect of initial moist curing on shrinkage and compressive strength of the UHPC was of special interest.
- The performance of optimized UHPC mixtures for thin-bonded overlay applications was investigated for relatively small concrete pavement sections made with thin overlays made with different materials and thicknesses. Emphasis was placed on the evaluation of shrinkage deformation and the variations of relative humidity (RH) and temperature through the overlay material.
- The life cycle cost analysis (LCCA) of the optimized UHPC mixtures made with different mixture compositions and performance characteristics was investigated. The LCCA provided an engineering economic analysis tool that can allow transportation officials to quantify the differential costs of alternative investment options for a given project.

2. LITERATURE REVIEW

2.1. NEED FOR CONCRETE OVERLAYS

A large percentage of bridges in the United States will reach their design service life in the upcoming decades. More than 11% are currently listed as structurally deficient, and over 12% are rated as functionally obsolete (Shann, 2012; Krauss et al., 2009). The quality of the concrete bridge decks can be one of the main factors to cause the degradation of an entire bridge system (Knight et al., 2004). This is because the deck provides not only the riding surface, but also as acts as a barrier against environmental impacts, such as de-icing agents, various environmental conditionsas well as traffic loading and abrasion, which can lead to bridge deck's degradation (Krauss et al., 2009; Krstulovic-Opara et al., 1995).

The main purpose of constructing concrete overlays is to optimize and/or extend the remaining life of the existing bridge deck by placing an additional layer of concrete above it. The benefits of concrete overlay include expedited construction, reduced cost, increased structural integrity, improved riding quality, and protection of the structure against deleterious environmental effects.

Concrete overlays on pavements or bridge decks can strengthen the structure against further deterioration due to fatigue cracking. They are also effective means to enhance pavement sustainability by improving surface reflectance, increasing structural longevity, and enhancing surface profile stability. The overlays can serve as complete preventive maintenance or rehabilitation solutions or can be used in conjunction with spot repairs of isolated distresses. In addition, concrete overlays can provide cost-effective solutions for pavement and bridge deck repairs. Concrete overlays can be placed using conventional concrete pavement practices. One of the best benefits of the concrete overlay is that the pavement or bridge can be opened to traffic within a day of placement as well as use of accelerated construction practices throughout the normal construction season (Shann, 2012).

Concrete overlays can be categorized into two types: bonded concrete overlay and unbonded concrete overlay. In bonded concrete overlays, there are ultra-thin and thin whitetoppings and bonded concrete overlay. These concrete overlays require good bond between the concrete overlay and the existing pavement. In unbonded concrete overlays, there are conventional whitetopping and unbonded overlays (Shann, 2012).

2.2. BONDED AND UNBONDED CONCRETE OVERLAYS

A bonded concrete overlay is a relatively thin concrete that is used to resurface an existing concrete pavement or bridge deck. Such overlay is typically 50 to 100 mm (2 to 4 in.) in thickness, and its performance depends on the bond strength of the overlay to the existing pavement. The purpose of a bonded concrete overlay is to rehabilitate deteriorating concrete pavement to increase load capacity and ride quality. A bonded concrete overlay is recommended when the existing pavement is considered to be in fair or good condition with minor surface distresses and less than a few punch-outs per lane mile (Kim, 2011).

An effective bond is necessary in the case of the bonded concrete overlay. Proper bond will provide monolithic behavior, ensuring that the stiffness of the rehabilitated pavement can carry the traffic load as one structure. Since bonded concrete overlays rely on the existing pavement to assist in carrying the traffic load, the condition of the existing pavement affects the performance of the rehabilitated pavement. Proper repairs or upgrades should be made to provide adequate support as required by design. In addition, if joints are made, well designed joint spacing helps to reduce curling and bending stresses due to traffic and environmental loads. It is crucial that the transverse joints in the bonded concrete overlays match those in the existing pavement to promote monolithic behavior.

In a bonded concrete overlay, different modes of failure can occur, and the loss of bond is one of the critical issues. The bond between the overlay and the existing pavement can be lost due to lack of quality control in surface preparation or placement during construction. Another failure mode is delamination due to differences in coefficient of thermal expansion (CTE). If a bonded concrete overlay has a CTE that is greater than that of the existing pavement, the overlay can expand or contract more than the existing pavement. This results in shear stress at the bond, and eventually cracking and delamination of the overlay. Generally, these stresses are greater at the edges of the overlay section and along cracks compared to bonded areas in the middle of the section. This is due to curling and warping at the top of the overlay as temperature and moisture change more rapidly at the top surface than that of the rest of the slab depth (Kim, 2011).

On the other hand, an unbonded concrete overlay is categorized as relatively thick concrete overlay used to resurface an existing concrete pavement. This type of overlay is typically 130 to 280 mm (5 and 11 in.) in thickness and is designed to perform without bonding to the existing pavement. The unbonded concrete overlay is used when the existing pavement is

severely deteriorated with major surface distresses. A separation layer is used to maintain separation between the concrete overlay and the existing pavement to ensure that cracks are not reflected through the overlay material (Kim, 2011).

Several factors play a significant role in determining the performance of unbonded concrete overlays. The effectiveness of the separation layer is critical. An effective separation layer should act as a shear plane that prevents the migration of cracks from the existing pavement into the overlay. In addition, the separation layer prevents bonding between the new and the old layers allowing them to move independently. Also, a well-constructed drainage system can prevent the building up of pore pressure from the traffic loads. The system serves to prolong the life of the overlay by reducing pumping, asphalt stripping of the separation layer, faulting, and cracking.

Different failure modes can take place in unbonded concrete overlays. The failure due to an inadequate separation layer is one of them. The separation layer prevents reflective cracks. If the new overlay is not structurally separated from the deteriorated existing pavement, the movement of the two structures will affect each other, which will induce heavy reflective stress to the overlay. In addition, poor drainage can be considered as another failure mode. The higher elevation of the pavement necessitates a change in the drainage grade lines. Additional right-of-way may be required to provide the proper slopes for the ditches (Kim, 2011).

The characteristics of various overlay materials are compared in Table 2-1. Each overlay material has advantages and disadvantages, and therefore, care should be taken to select the proper type of overlay materials, depending on the type of repair/rehabilitation. In the case of a bonded overly for pavements and bridge decks, high-performance concrete (HPC) with low overlay thickness can be an effective method to ensure long average lifespan compared to the other types of overlay materials given the low permeability, high mechanical properties, and good durability. The use of properly designed UHPC materials may present a cost-effective solution since the thickness of the overlay can be further reduced.

2.3. CHARACTERISTICS OF UHPC AND GOVERNING FEATURES

UHPC is categorized as a relatively new class of concrete that can develop extremely high durability and mechanical properties compared to conventional concrete. UHPC can be considered as part of the family of engineered cementitious composites (Habel et al., 2015). It

can be defined as a cement-based concrete having a compressive strength equal to or greater than 150 MPa (21.8 ksi) (Naaman and Wille, 2012; Resplendino, 2012). In addition, this novel material is characterized as concrete with a very low water-to-cementitious materials (w/cm), high binder content, and optimum packing density. The packing density is required to eliminate capillary pores and provide an extremely dense matrix. (Naaman and Wille, 2012; Resplendino, 2012). In most cases, UHPC contains micro steel fibers, which can enhance the materials' ductility and mechanical properties. Aïtcin (2000) described how UHPC can achieve such a high strength as follows: "We know how to make 150 MPa (21.8 ksi) concrete on an industrial basis. Because at such a high level of strength, it is the coarse aggregate which becomes the weakest link in concrete; it is only necessary to take out coarse aggregate, to be able to increase concrete compressive strength and make reactive powder concrete having a compressive strength of 200 MPa (29 ksi); it is only necessary to confine this reactive powder concrete in thin-walled stainless steel tubes to see the compressive strength increased to 375 MPa (54.4 ksi); and when the sand is replaced by a metallic powder, the compressive strength of concrete increases to 800 MPa (116 ksi)".

Due to the large difference in elastic moduli between aggregate and cement paste, conventional concrete (CC) and high performance concrete (HPC) have a mismatch in the properties of different constituent materials. The mismatch can be significantly reduced in UHPC through selecting constituent materials with similar elastic moduli (Gao et al., 2005). Another problem in CC and HPC is weaker interfacial transition zones between the aggregate and cement paste compared to UHPC.

Table 2-1 Comparisons of different overlays (Shann, 2012)

Overlay type	Latex-modified concrete (LMC)	Silica fume modified concrete (SFMC)	Low slump dense concrete (LSDC)	Fiber-reinforced concrete
Cost ($)/S.F.	18-39	More expensive than LMC	13-19	1.4-2.6
Alternative names or types	Latex-modified mortar2 and high strength LMC4	Microsilica modified concrete (MMC), Silica fume concrete (SFC).	-	-
Avg. thickness	1.25”, 1.25-3”, 1.5”, 2.25”	1.25”, 2”, 2.25”	2-3”, 2”	1”, 2.75”
Service-life	14-29 yr	5-10 yr	16-32 yr	
Mixture components	Portland cement, latex (typically styrene-butadiene), water, coarse and fine aggregates, and antifoamer. Steel or synthetic fibers are often used.	Silica fume, portland cement, water, coarse and fine aggregates, high-range water reducer, and air-entraining admixture. Steel or synthetic fibers are often used.	-	Steel, glass, synthetic, plastic fibers, or blends are used with Portland cement, water, and coarse and fine aggregates. High-range water reducer and air-entraining admixture are often needed. Fly ash or microsilica can be added. Steel or synthetic fibers have been used.
w/cm	0.35, 0.37, 0.4	0.35-0.4	-	0.4
Modulus of elastistic	3.8 ksi	4.1 ksi	-	4.9 ksi
Compressive strength	High early age and 28 d compressive strength	High early age and 28 d compressive strength	5,000 psi at 7 d is required	High early age compressive strength, but low at 28 and 90 d
Tensile strength	710 psi at 28 d for splitting tensile strength	680 psi at 28 d for splitting tensile strength	-	825 psi at 28 d for splitting tensile strength
Resistance to Cl ion penetration	ASTM rating "Low"	ASTM rating "Very low"	-	ASTM rating "Moderate"
Chloride permeability specification	1000 Coulombs at 90 d	1000 coulombs at 90 d	-	-

Table 2-1 Comparisons of different overlays (Cont'd)

Overlay type	Latex-modified concrete (LMC)	Silica fume modified concrete (SFMC)	Low slump dense concrete (LSDC)	Fiber-reinforced concrete
Construction notes	Substrate should be wetted before application of bonding agent, requires special mixing equipment and contractor experience, and is sensitive to weather conditions. Burlap and/or plastic are used during curing, very limited widow for finishing (15-30 min), but typical concrete finishing machines can be used	Fog sprays are used to control water evaporation. Wet burlap sacks and polyethylene sheets should be placed quickly to avoid plastic shrinkage. Overlay should be continuously wet and the area should be well drained. Bull float trowel are often used after screeding. Can be tined, broomed, burlap, or turfed finish early	Requires experienced contractors. Bonding agents should be applied to a dry substrate. Wind fences are commonly used. Mechanical tamping is used in some cases to obtain proper densification, but care must be taken as it is not difficult to overwork the surface. Overlay must be screed and finished immediately	-
State use	WV, DE, IL, IN, KS, KY, MA, MI, MO, NC, OK, PA, RI, SD, TN, WA, Ontario	WV, NY, OR, OH, RI	KY, MN, NY, ND, IA, KS, MI, MO, ND, SD, Puerto Rico	-
Overall pros	High bond strength, good durability, high abrasion and skid resistance, low permeability, low cracking, short cure time, quick installation, and long estimated service-life	Low permeability, high early and ultimate strength, good bond strength, high abrasion and skid resistance, high electrical resistance (suppresses the corrosion reaction in concrete)	Low permeability, good durability, long estimated service-life, and increased structural capacity	Post cracking tensile capacity. High early strength. High ductility due to fibers. Many possibilities of specialization within mix design
Overall cons	High cost, placement difficulties and need for experienced contractors. If improperly constructed, cracking and/or debonding are often major issues. Wear has been noted in wheel paths. Some have experienced long curing times. A few mix designs (primarily older designs) have issues with odor, toxicity, and flammability	Premature cracking, spalling and delamination due to surface shrinkage and strength failure at interfaces have been experienced	Difficulties of placement and consolidation, long cure times, higher dead loads. Susceptible to cracking. Vulnerable to weather conditions	Additional dead load, not as high compressive strength long-term as some high strength alternatives. Chloride resistance is not superior to other overlay types

Table 2-1 Comparisons of different overlays (Cont'd)

Overlay type	Hot-mix asphalt (HMA) single or multi-layer	Polymer-concrete (PC)	High-performance concrete overlay (HPC)	Portland cement concrete overlay (PCC) standard concrete and reinforced concrete overlay.
Cost ($) /S.F.	3.1-7.6	10-17	17-25	22-36
Alternative names or types	Layered overlays are also called sandwich seal overlays.	-		Structural bridge deck overlays (SBDO).
Average thickness	2-3.25"	0.5-1.4"	1.6-3.5"	3-3.8"
Average lifespan	10-15 yrs	9-18 yr	16-29 yr	15-24 yr
Mix design - Mix components	Can be made with one asphalt layer or as a multiple, sandwich layer. Asphalt and bridge deck sealant (rubber, fiberglass, bitumen, polyester membrane). Layered Overlay includes a tack coat	Aggregate and binder. Binder can be epoxy, polyester styrene, or methacrylate. No Portland cement or water is used	-	Type I Portland cement, water, and coarse and fine aggregate. High early strength Portland cement is also used
Comparison	-	Often used as a preventative measure on newer deck. Lower dead load	-	Used in deck rehabilitation more than other overlays
Curing and construction duration	Total construction time is around 3 d	Total construction can take less than 24 h	Total construction time can take over 7 d	1-2 day moist curing
Construction notes	Substrate repairs must be made before overlay placement. Typical asphalt paving equipment and procedures are used. Sealant is placed between bridge deck and first asphalt layer.	Substrate roughening is vital to this overlay's success. Must follow temperature and humidity tolerances. Usually two-component systems: one component contains resin and the second contains the curing agent or initiator. Uniformly graded aggregates are used with slurry and premixed overlays. Gap graded aggregates are used with multiple-layer overlays and are broadcast on the top of slurry and some premix overlays.	Typically contains low w/c ratio. Admixtures may be added for improved workability	Substrate surface preparation is typically achieved through hydro demolition

Table 2-1 Comparisons of different overlays (Cont'd)

Overlay type	Hot-mix asphalt (HMA) single or multi-layer	Polymer-concrete (PC)	High-performance concrete overlay (HPC)	Portland cement concrete overlay (PCC) standard concrete and reinforced concrete overlay.
State use	CO, CT, IL, KY, NE, NY, RI, SD, TN, UT, VT, Alberta, Ontario, Quebec	AK, CA, CO, GA, ID, IL, KS, MA, ME, MO, NM, NV, NY, OK, OR, TN, UT, BT, WY, VA	AK, AZ, ID, IL, KS, MI, MO, NE, NY, OK, OR, WV, WY, Alberta	No agencies reported using PCC overlays for new construction, though half of the agencies surveyed used PCC for over 25years
Overall pros	Low cost, ease and speed of installation, improves ride-ability, effective	High early compressive strength, high bond strength, good durability and skid resistance, low permeability, low dead load. Does not require modification of approaches or existing expansion joints.	Low permeability, good durability, high strength. High cost-effective performance	Long life, familiar and quick installation, good record. Good alternative to repair and replacement.
Overall cons	The layered asphalt overlay can trap moisture in the deck, which can damage bond and/or reinforcement. Short service-life and timely maintenance is required. Some have found difficulty of removal. Effectiveness of membrane is unknown. Poor performance has been found on curved bridges. Does not contribute structurally to the superstructure.	Installation difficulties. Some have found low durability. Higher cost. Cannot be used as a replacement for bridge deck concrete.	Installation difficulties. Cracking has been found during curing. Long cure times. Higher cost.	Long construction time and high cost. Low bond strength. Not conductive to decks containing slag.

Figure 2-1 illustrates a representation of the force transfer within the CC and UHPC. In the case of the CC, the force or load is transferred only among aggregates. In the UHPC, all the material constituents, including cement paste, fiber, and aggregates, take part in the force transfer. This can result in a significant improvement in the mechanical properties of such novel material.

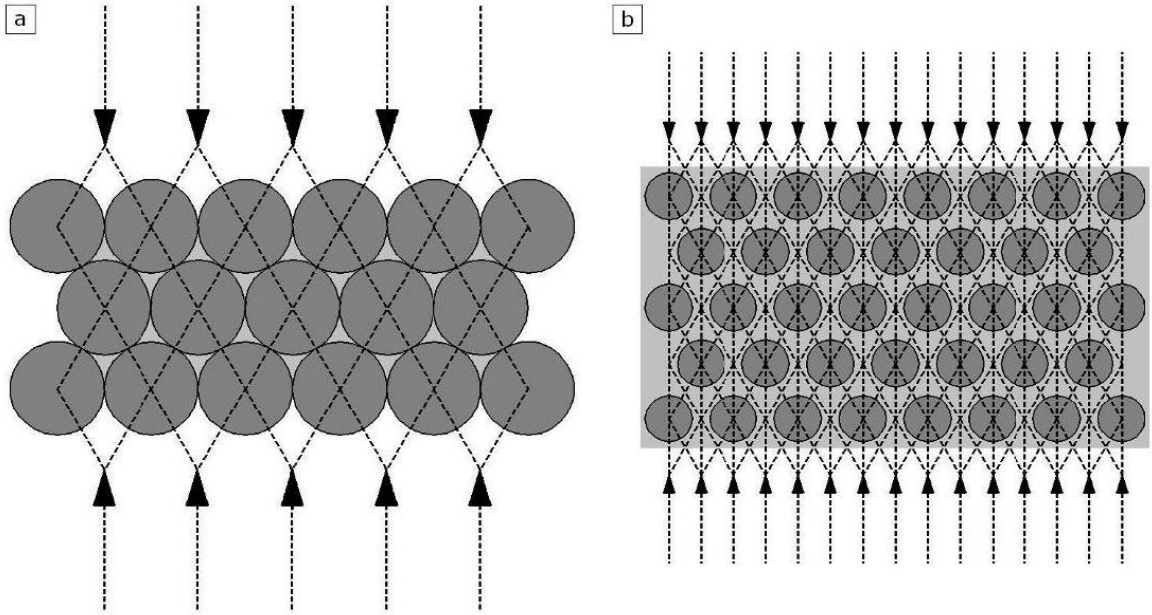

Figure 2-1 Depiction of force transfer within: (a) conventional concrete; (b) UHPC (Walraven, 2002; Voort et al., 2008)

Some of the mixture design principles involved in UHPC include the enhancement of homogeneity by the elimination of coarse aggregate and increased packing density by optimization of the granular skeleton of the mixture through wide distribution of powder size classes. The addition of SCMs, such as silica fume, fly ash, and slag, and the use of low water-to-cementitious materials (w/cm) ratio can result in significant improvement in the mechanical properties and durability of the non-fibrous UHPC matrix. Employing post-set heat-treatment can enhancement the microstructure of UHPC. The improvement of ductility, tensile strength, and crack resistance can be achieved by the incorporation of small rigid fibers, such as steel fibers (Richard and Cheyrezy, 1995). UHPC has high packing density which can be achieved by optimizing the proportioning of different components (Richard and Cheyrezy, 1995). The particles should be selected to fill up the voids between large particles and smaller particles, leading to a smaller volume of gaps within the aggregate skeleton.

The concept of packing density, i.e. the ratio of the volume of solids to a given volume, is introduced to evaluate the arrangement of granular mixtures. Figure 2-2 illustrates how the concept of packing density can be applied to three granular systems, i.e. single-, binary-, and ternary- systems (Stovall et al., 1986). The single-sized aggregate can be packed together to

occupy only a limited space, i.e. it can achieve only a relatively low packing density. However, the multi-sized aggregates can be packed together much more effectively to achieve higher packing density, i.e. binary and ternary mixtures. For a given volume of cement paste, the increase in packing density of the aggregates can increase the workability of concrete at the same w/cm, or increase the strength of concrete by reducing the w/cm at a given workability.

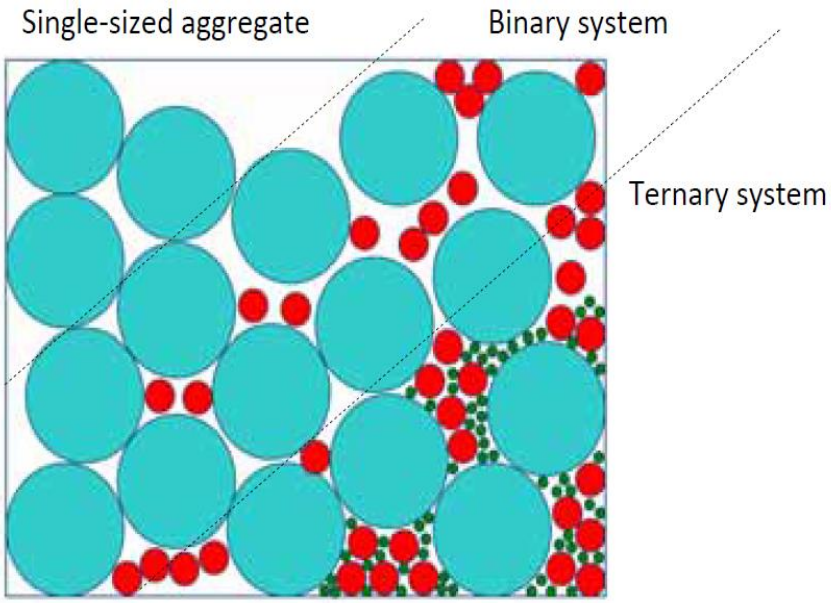

Figure 2-2 Typical packing arrangements of single, binary, and ternary mixtures (Stovall et al., 1986)

Key engineering properties of CC, HPC, and UHPC are compared in Table 2-2. It is important to review different components and the microstructural properties of typical UHPC mixtures. Sand, cement, silica fume, crushed quartz, fibers, high-range water reducer (HRWR), and/or superplasticizer (SP), as well as water, are the main components of UHPC, as presented in Table 2-3.

Table 2-2 Comparison of properties of CC, HPC, and UHPC (Ahlborn et al., 2008)

Material characteristics	Conventional concrete	HPC	UHPC
Maximum aggregate size, (in.)	0.75-1.00	0.38-0.50	0.016-0.024
w/cm	0.40-0.70	0.24-0.35	0.14-0.27
Mechanical properties			
Compression strength (ksi)	3.0-6.0	6.0-14.0	25.0-33.0
Split cylinder tensile strength (ksi)	0.36-0.45	-	1.0-3.5
Poisson's ratio	0.11-0.21	-	0.19-0.24
Creep coefficient, Cu	2.35	1.6-1.9	0.2-0.8
Porosity (%)	20-25	10-15	2-6
Fracture energy (k-in/in.^{2})	0.00057-0.00086	-	0.057-0.228
Young's modulus (ksi)	2000-6000	4500-8000	8000-9000
Modulus of rupture 1st crack (ksi)	0.4-0.6	0.8-1.2	2.4-3.2
Flexure strength - ultimate (ksi)	-	-	3.0-9.0
Shrinkage	-	Post cure 40-80×10^{-5}	Post cure <1×10^{-5}, No autogenous shrinkage after cure
Coefficient of thermal expansion (/°F)	4.1-7.3×10^{-6}	-	7.5-8.6 ×10^{-6}
Ductility	-	-	250 Times > NSC
Durability			
Freeze/thaw resistance	10%	90%	100%
Chloride penetration (Coulomb)	> 2000	500-2000	< 100
Air permeability (k) at 24 hr and 40°C, (in.^{2})	4.65×10^{-14}	0	0
Water absorption at 225 hr (lb/in.^{2})	4×10^{-3}	5×10^{-4}	7.1×10^{-5}
Chloride ion diffusion coefficient (by steady state diffusion), (in.^{2}/s)	1.55×10^{-9}	7.75×10^{-10}	3.1×10^{-11}
Penetration of carbon / sulfates	-	-	None
Mass of scaled off (lb/ft^2)	> 0.205	0.016	< 0.002

2.4. CASE STUDIES: USE OF UHPC IN BRIDGE STRUCTURAL ELEMENTS

2.4.1. Sustainable and Advanced Materials for Road Infrastructures (SAMARIS)

The UHPC, CEMTEC$_{multiscale®}$ family, was applied for the rehabilitation and widening purposes on a bridge over the river La Morge in Switzerland in 2004, as a part of the SAMARIS European project. The bridge was deteriorated as a result of chloride ingress. The rehabilitation process was conducted in three phases. Firstly, the bridge was widened using a prefabricated UHPFRC edge beam on a new reinforced concrete beam. Secondly, the upper surface of the

bridge deck contaminated by chloride ingress was replaced by UHPC layer with a thickness 30 mm (1.17 in.). Finally, the concrete surface of the upstream curb was rehabilitated with 30 mm (1.17 in.) of UHPC. The details of this bridge are shown in Figure 2-3. UHPC used in this project had the microsilica-to-cement and water-to-binder ratios of 0.26 and 0.125, respectively. The UHPC was comprised of cement (1430 kg/m^3, 2410 lb/yd^3), microsilica, fine quartz sand with a maximum grain size of 0.5 mm (0.02 in.). The total fiber volume of 706 kg/m^3 (1190 lb/yd^3) (9 vol.%) including microfibers, steel wool (2 to 3 mm (0.08 to 0.12 in.) length), in combination with macrofibers (10 mm (0.4 in.) length and an aspect ratio of 50), was used. The average values of 28-day compressive strength and modulus of elasticity were 182 MPa (26.4 ksi) and 47 GPa (6,816 ksi), respectively. Construction cost analysis indicated that the cost of rehabilitation with UHPC was about 10% higher than the conventional option of using repair mortar with waterproofing membrane (Bruhwiler and Denarie, 2008).

Table 2-3 Range of UHPC mixture components (Dugat et al., 1996; Castellote et al., 2003; Droll, 2004)

Components	Typical range (kg/m^3)	Mass ratio to cement	Volume fraction (%)
Sand	490 - 1390	1.43	38.8
Cement	610 - 1080	1.00	22.7
Silica fume	50 - 334	0.32	10.6
Crushed quartz	0 - 410	0.30	8.1
Fibers	40 - 250	0.21	2.0
Superplasticizer	9 - 71	0.02	1.4
Water	126 - 261	0.23	16.5

*Superplasticizer is expressed as the weight of the solid fraction; the liquid fraction is included in the water weight.
Note: 1 kg/m^3 = 1.686 lb/yd^3

2.4.2. Application of UHPC on Barrier Walls as Protection Layers

The concrete crash barrier wall of a highway bridge severely suffering from de-icing salts ingress was rehabilitated using UHPC in 2006, as shown in Figure 2-4. A UHPC layer with thickness of 30 mm (1.2 in.) and w/cm of 0.17 was applied on the barrier wall. The UHPC layer was made with 1100 kg/m³ (1854 lb/yd^3) cement, 26% silica fume, by mass of cement, quartz-sand, and 6% steel fibers, by volume of concrete. UHPC mixture was prepared in a concrete ready mix plant and hauled to the job site by a conventional truck. Four months after rehabilitation, no crack was observed (Bruhwiler and Denarie, 2008).

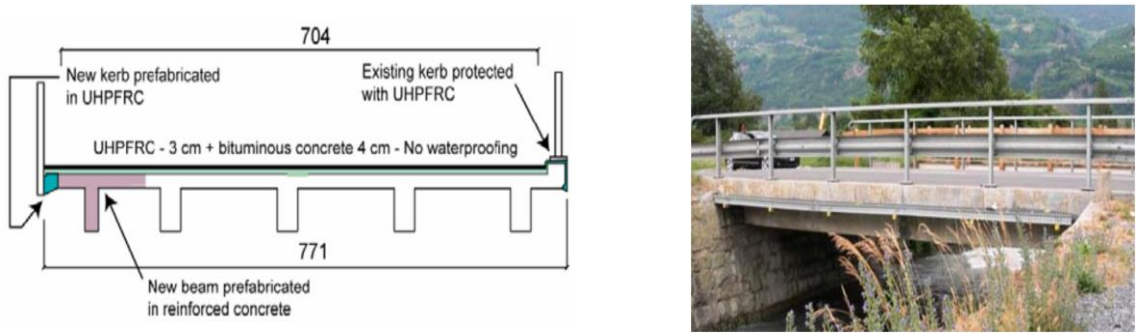

Figure 2-3 Bridge cross section after rehabilitation with UHPC – (dimensions in cm) (Bruhwiler and Denarie, 2008)

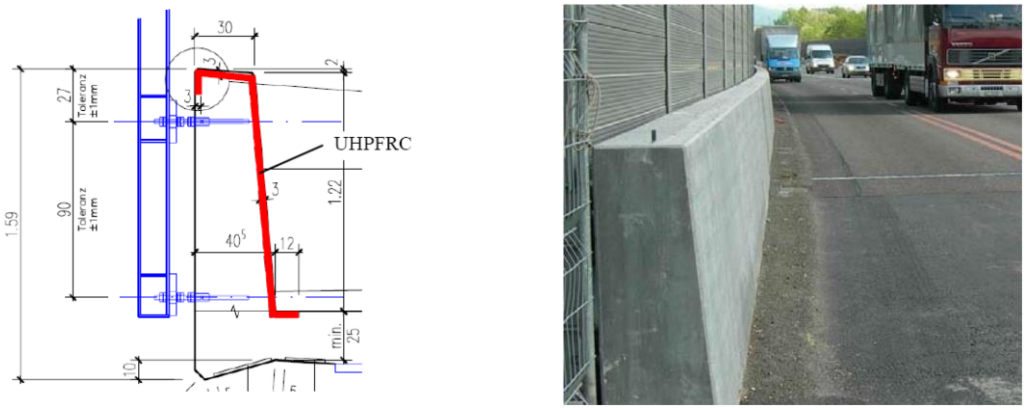

Figure 2-4 Typical cross section of the crash barrier wall and view after rehabilitation (Bruhwiler and Denarie, 2008)

2.4.3. Rehabilitation of a Bridge Pier Using Prefabricated UHPC Shell Elements

As shown in Figure 2-5, an existing 40-year-old reinforced concrete bridge pier subjected to severe environmental exposure of de-icing salt splashes was protected by 40 mm (1.57 in.) prefabricated UHPC elements in 2007. Before the UHPC installation, chloride-contaminated concrete, about 100 mm (4 in.) thickness, was removed. UHPC used in this project was made with 0.155 w/c, containing 1300 kg/m³ (2191 lb/yd^3) of cement, silica fume, quartz-sand, steel fibers, and superplasticizer (Bruhwiler and Denarie, 2008).

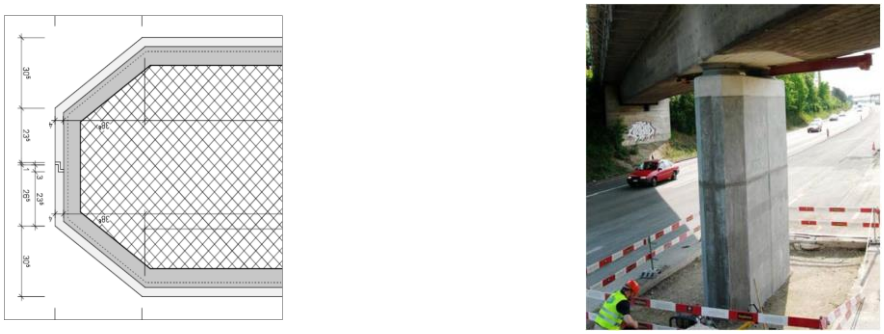

Figure 2-5 Strengthening of an industrial floor (Bruhwiler and Denarie, 2008)

2.4.4. Strengthening of an Industrial Floor

In this project, the load-bearing capacity of a 50-year-old reinforced concrete slab with an area of 720 m^2 (860 yd^3) was enhanced by applying a 40-mm (1.57 in.) UHPC overlay. The UHPC was proportioned with 1300 kg/m^3 (2191 lb/yd^3) of cement, along with silica fume, quartz-sand, steel fibers, and superplasticizer, and w/cm of 0.155 (Bruhwiler and Denarie, 2008). Details of the overlay design and casting are presented in Figure 2-6.

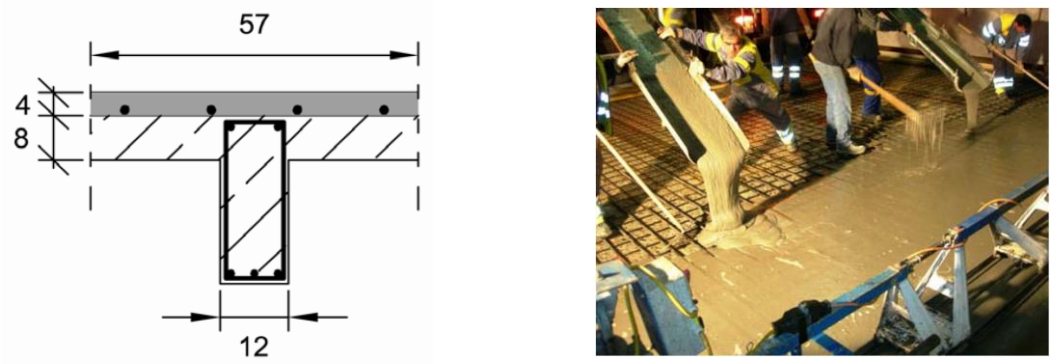

Figure 2-6 Cross-section (dimensions in cm) with UHPC layer (in grey) and view of UHPC casting performed (Bruhwiler and Denarie, 2008)

2.4.5. LOG ČEZOŠKI Bridge, Slovenia

As shown in Figure 2-7, UHPC was used to rehabilitate a bridge deck, measuring 65 m (213 ft) in length with a 5% longitudinal slope over the Šoka River in Slovenia in 2009. The UHPC was applied to protect the full upper face of the bridge deck, footpath, and external faces of the curbs. In this project, the UHPC thickness varied between 25 and 30 mm (1 to 1.17 in.). UHPC mixture design included 763 kg/m^3 (1286 lb/yd^3) cement, 763 kg/m^3 (1286 lb/yd^3) limestone filler, 153 kg/m^3 (259 lb/yd^3) microsilica fume, with W/(C+LF+SF) of 0.155. A

mixture of micro-steel wool (1 mm (0.04 in.) length) and macrofibers (10 mm (0.4 in.) length and aspect ratio of 50), with a total dosage of 706 kg/m^3 (1190 lb/yd^3) (9% vol.) was incorporated. The average mixing time of UHPC for this project was 12 minutes. The UHPC overlay was moist-cured for 7 d after casting (Bruhwiler and Denarie, 2008).

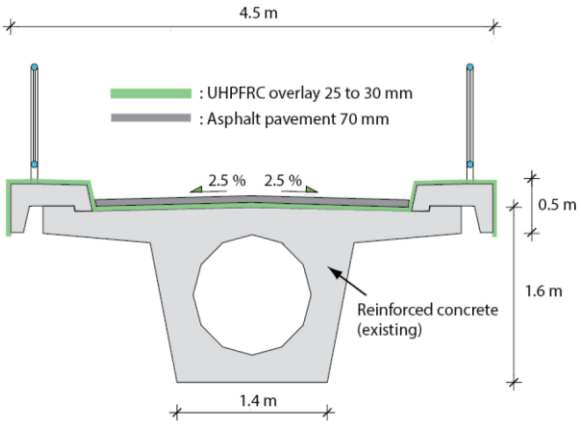

Figure 2-7 Cross section of bridge with concept of rehabilitation (Bruhwiler and Denarie, 2008)

2.4.6. Pinel Bridge, France The Pinel Bridge (Figure 2-8 and 2-9) was constructed using CC in 1996 in France. The bridge has two lanes with a filler beam deck with two span lengths of 1220 and 1480 m (4001 and 4854 ft). In 2007, it was decided to extend the lanes from two to five using prefabricated UHPC to increase traffic volume capacity on the bridge. The depth of the seventeen UHPC beams was 620 mm (24.4 in.). The UHPC was produced using 2360 kg (5200 lb) of premix, 45 kg (100 lb) of superplasticizer, 195 kg (430 lb) of water, and 195 kg (430 lb) of steel fibers, yielding 28-day compressive strength of 165 MPa (23.9 ksi) (Matteis et al., 2008).

2.4.7. Experimental Validation of a Ribbed UHPC Bridge Deck in France

An experimental validation of a ribbed UHPC bridge deck made of two segments assembled by post-tensioning was conducted as part of the MIKTI French R&D national project focusing on steel-concrete composite applications, as shown in Figure 2-10 and 2-11. One of the segments was made of Ductal®-FM and the other of BSI®. The UHPC ribbed slab was supported by two longitudinal steel beams. The slab thickness was 0.05 m (0.16 ft) and the total thickness with the ribs was 0.38 m (1.25 ft) (Toutlemonde et al., 2007).

Figure 2-8 General view of the existing bridge (Matteis et al., 2008)

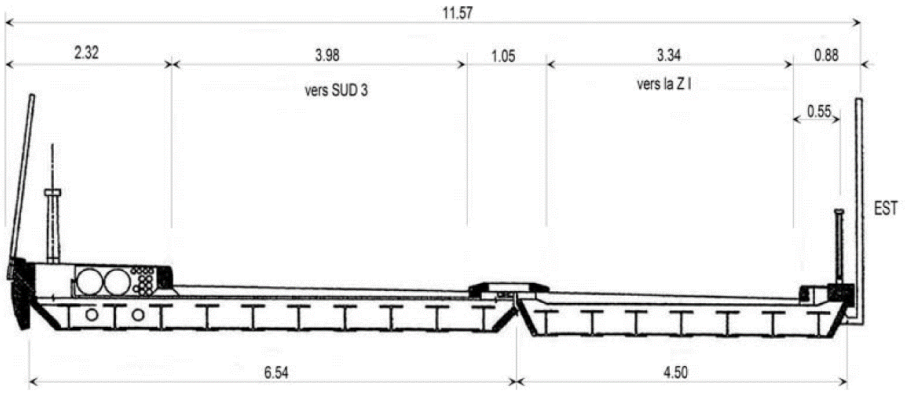

Figure 2-9 Deck cross section of the existing bridge (Matteis et al., 2008)

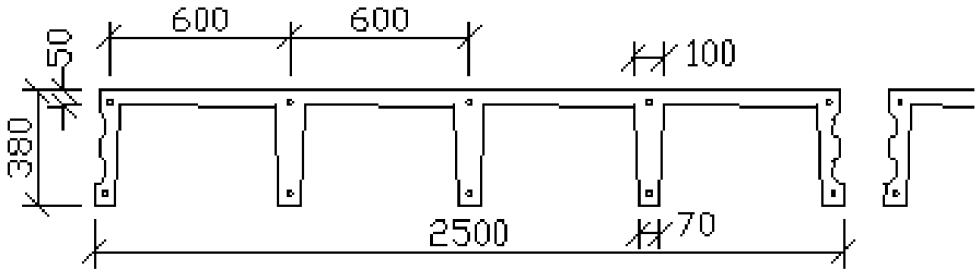

Figure 2-10 Longitudinal cross-section of precast segments. Longitudinal ribs are 50 mm-wide only at the bottom. (lengths in mm) (Toutlemonde et al., 2007)

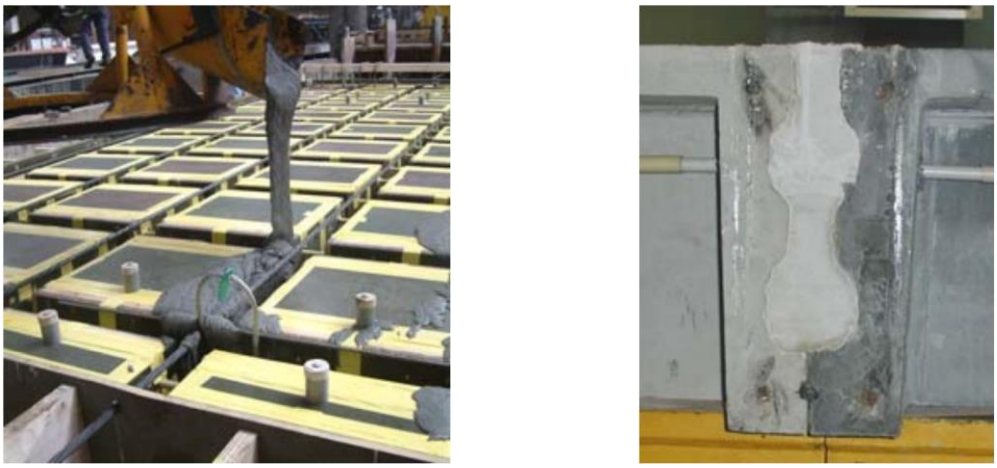

(a) (b)

Figure 2-11 Model ribbed slab for validation tests. a) casting; b) cold joint (Toutlemonde et al., 2007)

2.4.8. Sherbrooke Pedestrian Bridge, Canada

A new pedestrian bridge was constructed over the Magog River in Sherbrooke, Quebec, Canada in 1997 (Figure 2-12) using a reactive powder concrete (RPC) prepared in a concrete precast plant. The bridge had a single lane measuring 60 m (197 ft) in length. The bridge was precast in six segments measuring 10 m (32.8 ft) long and 3 m (9.8 ft) height) each with a space truss system. Using UHPC allowed the top deck slab to be as low as 30 mm (1.2 in.), using no passive reinforcement in the bridge (Russell and Graybeal, 2013).

Figure 2-12 Sherbrooke pedestrian bridge (Russell and Graybeal, 2013)

2.4.9. Glenmore/Legsby Pedestrian Bridge

As shown in Figure 2-13, the Glenmore/Legsby Pedestrian Bridge was another example constructed using Ductal over an eight-lane highway in Calgary, Alberta, Canada. This bridge was a single span measuring 53 m (174 ft) in length. Post-tensioned girders were 3.6-m (11.8-ft) wide at the mid-span. The T-shaped girders were 11-m (36-ft) deep and 33.6-m (110-ft) long. A high shear mixer was employed to deliver proper and sufficient mixture for this application which required 40 m^3 (52.3 yd^3) UHPC. The prepared Ductal was hauled to the job site from the batch plant using CC trucks (Russell and Graybeal, 2013).

Figure 2-13 The Glenmore/Legsby pedestrian bridge, Calgary, Alberta, Canada (Russell and Graybeal, 2013)

2.4.10. Mars Hill Bridge

The Mars Hill bridge (Figure 2-14) located in Wapello County, Iowa, was built in 2006 and was the first bridge in the United States made of UHPC (Russell and Graybeal, 2013). Three prestressed bulb-tee girders of this bridge were fabricated using Ductal UHPC. The girders were 33.5 m (110 ft) long and 1.14 m (3.7 ft) deep with a cast-in-place concrete bridge deck. Other bridge parts were constructed using CC materials. Ductal UHPC consisting of fine sand, cement, silica fume, and quartz sand were incorporated in UHPC mixture in low w/cm between 0.15 and 0.19. The achieved average 28-d compressive strength ranged from 125 - 207 MPa (18 - 300 ksi), depending on the mixing and curing process. To improve ductility, steel or polyvinyl

alcohol (PVA) fibers at an amount of 2%, by volume of concrete, were included to improve ductility.

Figure 2-14 Mars Hill Bridge, Wapello County, IA, USA (Russell and Graybeal, 2013)

2.5. UHPC AS BONDED OVERLAY

UHPC has extremely high impermeability, negligible dry shrinkage if properly cured, and excellent post-cracking tensile capacity. UHPC also exhibits high compressive strength, ranging from 125 to 230 MPa (18 to 33 ksi) at 28 d, depending on the curing regime. This is required for the rehabilitation of bridge decks when added load capacity and load transfer is desired (Graybeal, 2006; Misson, 2008). Furthermore, UHPC develops high early strength, which can reduce traffic closure time and increase the rate of precast bed turnover. In order to fully benefit from the superior properties of UHPC, the bond integrity of the novel material to the conventional concrete deck systems need to be evaluated. The thickness of the UHPC overlay should be optimized to reduce the dead load while maintaining the integrity of the bond interface.

In spite of the aforementioned benefits of UHPC over conventional overlay materials, its high initial cost can limit its broad use. Bonneau et al. (1996) reported the UHPC's price as \$1400/m^3 (\$1071/yd^3) in 1996 in Europe, which was decreased to \$750/m^3 (\$574/yd^3) in 2000 with more common use (Blais and Couture, 1999). The cost estimation of the UHPC was \$2620/m^3 (\$2005/yd^3) in North America in 2007 (Suleiman et al., 2008). More recently, a 30 mm (1.2 in.) thick UHPC was used as an overlay to repair a short span of a heavy traffic road bridge (Bruhwiler and Denarie, 2008; Denarie et al., 2005). Two alternatives were suggested in this overlay project, which were the rehabilitation using UHPC without water proofing

membrane and typical repair mortar with water proofing membrane. Cost analysis for the two alternatives indicated that the UHPC overlay would have 12% higher material cost than the mortar overlay. However, the typical mortar overlay necessitates longer traffic closure time due to the drying process before applying the water proofing membrane when compared to the UHPC overlay. This can reduce the traffic disruption and provide superior mechanical properties and durability (Denarie et al., 2005).

The flexural behavior of a UHPC overlay was investigated by Yuguang et al. (2008) using a multilayer model. This research was done by varying the numbers of rebar and fiber volumes (0, 0.8%, and 1.6%). The results indicated that a 30.5 mm (1.2 in.) thick UHPC overlay made without any rebar can endure the maximum traffic load.

Lee and Wang (2005) evaluated the compressive strength, bond strength, and steel pullout capacity. The results indicated that the use of a 10-mm (0.4-in.) thick RPC or UHPC bonding layer increases compressive and flexural strengths between 150% and 200% over a CC overlay. In addition, the abrasion resistance of an RPC overlay was approximately eight times greater than that of the CC overlay. Bernardi et al. (2016) reported the successful use of UHPC overlay with 45 mm (1.75 in.) in thickness reinforced with 3.25% steel fibers for bridge deck rehabilitation in Switzerland in 2014. The details of this application are shown in Figure 2-15 and 2-16. The overlay repair included reinforcing rebar and UHPC to strengthen the existing deck that was damaged by alkali-silica reactivity. Similarly, a successful use of UHPC measuring 38 mm (1.5 in.) in thickness applied on a 30 m (98 ft) long bridge was also reported in Iowa, USA.

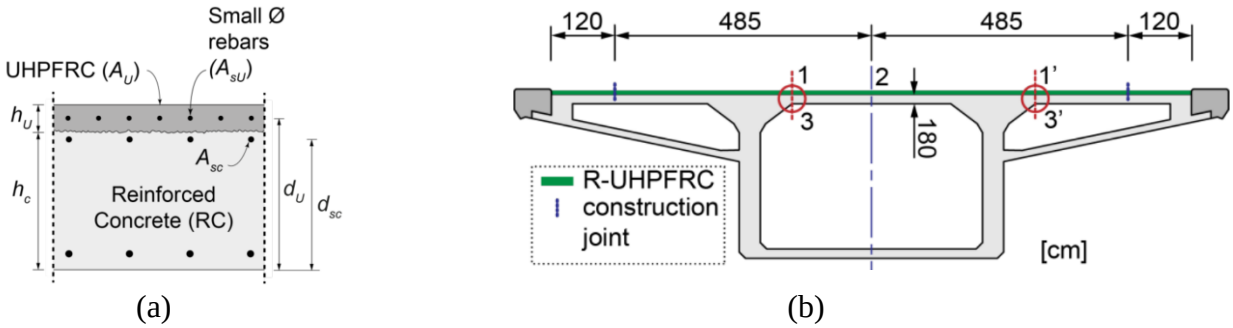

Figure 2-15 Cross-section details of the project: (a) typical composite cross section and (b) geometry of the box girders cross-section

Figure 2-16 Implementation details of UHPC overlay application

2.6. STRESS AND STRAIN IN BONDED CONCRETE OVERLAYS

This section presents the status of stress distribution in a system of composite overlay due to moisture variation. Figure 2-17 illustrates the variation of normal stress (σ_{xx}) over the section width at 10 d, including the restrained shrinkage stress, total stresses, and relaxation because of restrained creep. The shrinkage stress was reduced gradually because of creep relief at the critical point of the center line (Lange and Shin, 2001; Beushausen and Alexander, 2007; Tran et al., 2007; Rahman et al., 2000).

Figure 2-18 illustrates the variation of tensile stresses (σ_{yy}) over the section width of the composite system at the interface. As shown, peeling stresses govern at the edge of the system (Lange and Shin, 2001; Beushausen and Alexander, 2007; Tran et al., 2007; Rahman et al., 2000). At a short distance (20 mm (0.75 in.)) from the edge, the peeling stresses drop in magnitude and alter from tensile to compressive. The unbalanced moment that σ_{xx} stress makes through the overlay depth results in σ_{yy} stress field at the interface. Figure 2-19 presents the shear stress (τ_{xy}) variation at the interface over the width section. As shown, the considerable value of shear stress concentrating at the overlay edges, moderately decrease towards the center and become zero when it reaches the center. Thus, the combination of biaxial tensile and shear state of stress at the interface can most likely make a zone to initiate the interface failure (Lange and Shin, 2001; Beushausen and Alexander, 2007; Tran et al., 2007; Rahman et al., 2000).

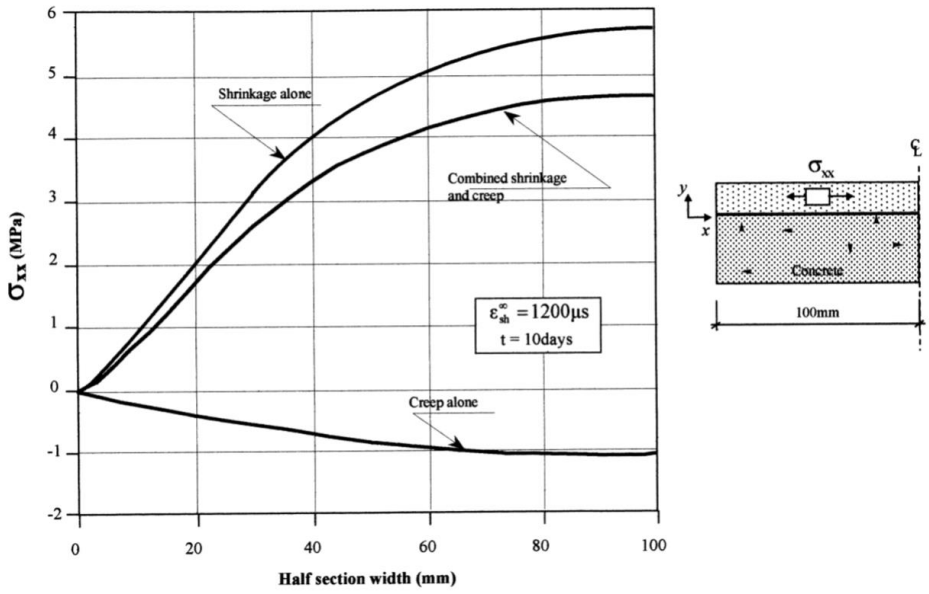

Figure 2-17 Variation of normal stress (σ_{xx}) across the width at top at (10 d) (Rahman et al., 2000), (Note: 1 mm = 0.039 in., 1 MPa = 145 psi)

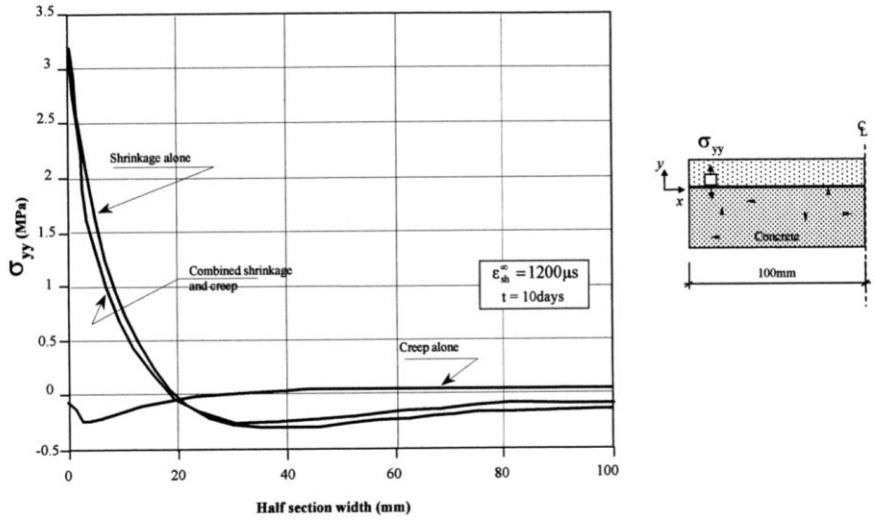

Figure 2-18 Variation of tensile stress (σ_{yy}) across the width at top at (10 d) (Rahman et al., 2000), (Note: 1 mm = 0.039 in., 1 MPa = 145 psi)

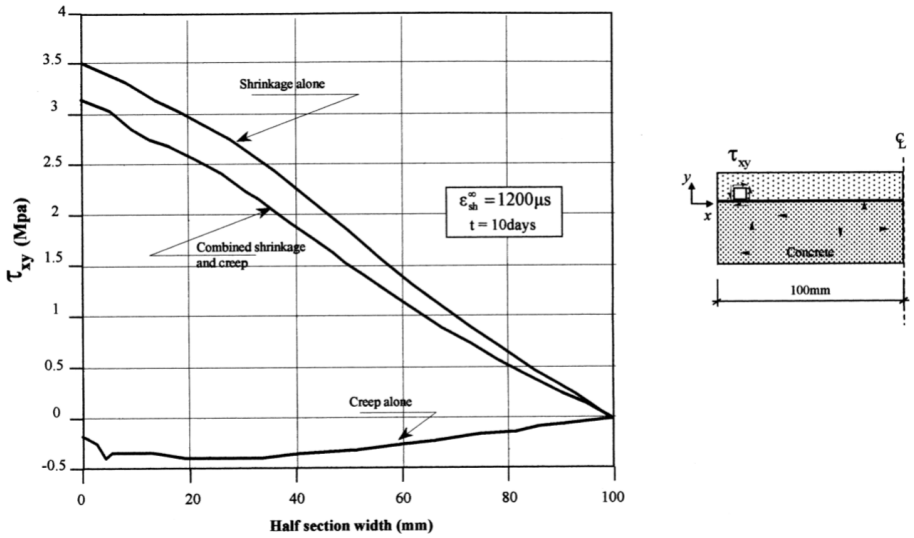

Figure 2-19 Variation of shear stress (τ_{xy}) at the interface over the width section (Rahman et al., 2000), (Note: 1 mm = 0.039 in., 1 MPa = 145 psi)

3. OPTIMIZATION AND PERFORMANCE OF COST-EFFECTIVE UHPC

This chapter presents a mixture design method for UHPC prepared with high-volume supplementary cementitious materials (SCMs) and conventional concrete sand. The method involves the optimization of binder combinations to enhance packing density, compressive strength, and rheological properties. The w/cm is then determined for pastes prepared with the selected binders. The sand gradation is optimized using the modified Andreasen and Andersen packing model to achieve the maximum packing density. The binder-to-sand volume ratio is then determined based on the void content, required lubrication paste volume, and compressive strength. The optimum fiber volume is selected based on flowability and flexural performance. The high-range water reducer (HRWR) dosage and w/cm are then adjusted according to the targeted mini-slump flow and compressive strength. Finally, the optimized UHPC mixture designs are evaluated to determine key properties that are relevant to the intended applications. This mixture design approach was applied to develop cost-effective UHPC. The results indicate that the optimized UHPC can develop 28 d compressive strength of 125 MPa (18.1 ksi) under standard curing condition and 168 - 178 MPa (24.4 - 25.8 ksi) by heat curing for one day. Such mixtures have a unit cost per compressive strength at 28 d of 4.1 to 4.5 \$/m^3/MPa (0.46 to 0.5 \$/yd^3/ksi) under standard curing.

3.1. MATERIALS, MIXERS, AND SPECIMEN PREPARATIONS

In this study, the cementitious materials included Class C fly ash (FAC), Ground-granulated blast-furnace slag (GGBS), silica fume (SF), and Type III Portland cement (C). The characteristics of the investigated raw materials are listed in Table 3-1. Fine SF with particles smaller than 1 μm (3.9×10^{-5} in.) in diameter was used; the mean diameter of the SF is about 0.15 μm (5.9×10^{-6} in.), and the specific surface area determined using the Brunauer, Emmet, and Teller (BET) method is 18,500 m^2/kg (90,325 ft^2/lb). Missouri River sand (0-4.75 mm (0-0.19 in.)) and masonry sand (0 - 2.00 mm (0-0.08 in.)) were used under saturated surface dry (SSD) condition. The water absorptions of the river sand and masonry sands are 0.14% and 0.06%, respectively. A polycarboxylate HRWR was used to enhance the workability. The HRWR has a solid mass content of 23% and a specific gravity of 1.05. Straight steel fibers with a 0.2 mm (0.008 in.) diameter and 13 mm (0.5 in.) length were used to enhance the mechanical

properties. The tensile strength and elastic modulus of the steel fiber are 1.9 and 203 GPa (276 and 29,443 ksi), respectively.

All mixtures were prepared and tested at room temperature (23 ± 2 °C (73 ± 36 °F)). Two mixers were used, including a 12-L (3.2 gal) Hobart mixer and a 150-L (39.6 gal) EIRICH mixer. The Hobart mixer was used for optimizing the individual components of UHPC, and the EIRICH mixer was employed for finalizing the UHPC mixtures. A specific mixing procedure was employed for each mixer. When the Hobart mixer was used, the mixing procedure was composed of the following three steps: (1) dry cementitious materials and/or sand were mixed for 2 min at 1 rps; (2) 90% of the mixing water and 90% of the HRWR were added and the mixture was mixed for 3 min at 2 rps; (3) the rest of the water and HRWR were added and the mixture was mixed for 9 min at 2 rps. When the EIRICH mixer was used, the mixing procedure was composed of five steps: (1) the mixer was pre-wetted; (2) the sand and cementitious materials were added into the mixer and mixed for 2 min at 1 rps; (3) 90% of the total liquid (water + HRWR), by volume, was added and mixed for 2 min at 6 rps; (4) the rest of the liquid was introduced, and the materials were mixed for 4 min at 6 rps; (5) the fibers were gradually added over a period of 1 min; (6) the materials were mixed for 2 min at 10 rps. While mixing, the pan speed of the mixer was fixed at 2 rps.

For each mixture, specimens were cast in one lift without mechanical consolidation. The molds were immediately covered with wet burlaps and plastic sheets after casting. They were demolded after one day and then cured in lime-saturated water at 23 ± 1 °C (73 ± 34 °F) until the testing time (standard curing). To investigate the effect of curing regime on compressive strength, two sets of UHPC specimens were prepared and tested. One set with standard curing, while the other set with heat curing. Heat curing was performed at a maximum temperature of 90 °C (194 °F) for 24 h. The specimens were then cured in lime-saturated water for 7 d, followed by air-curing at room temperature.

3.2. PROPOSED MIXTURE DESIGN PROCEDURE AND EXPERIMENTAL PROGRAM

The proposed UHPC mixture design method consists of six main steps, as illustrated in Figure 3-1. These incluede: (1) determine binder candidates; (2) preliminarily select a w/cm; (3) determine the sand combination; (4) assess the binder-to-sand volume ratio (V_b/V_s); (5) optimize

the fiber content; and (6) evaluate and adjust the UHPC mixture. Step 1 is composed of three sub-steps: (1a) select binder combination candidates based on flow characteristics; (1b) narrow down the binder candidates according to the combined effects of minimum water content (MWC), relative water demand (RWD), and HRWR demand, as well as 1 and 28 d compressive strengths; (1c) finalize the binder combinations based on the rheological properties.

Table 3-1 Physical and chemical composition of raw materials

	C	FAC	SF	GGBS	Missouri river sand	Masonry sand
SiO_2 (%)	19.72	36.5	95.5	36.8	80.3	86.5
Al_2O_3 (%)	5.10	24.8	0.7	9.2	10.5	0.39
Fe_2O_3 (%)	2.76	5.2	0.3	0.76	3.43	1.47
CaO (%)	64.50	28.1	0.4	37.1	1.72	9.42
MgO (%)	2.30	5	0.5	9.5	1.70	0
SO_3 (%)	3.25	2.5	0	0.06	1.07	0
Na_2Oeq. (%)	0.33	0	0.4	0.34	–	0
C_3S (%)	65.23	–	–	–	–	–
C_2S (%)	7.33	–	–	–	–	–
C_3A (%)	8.85	–	–	–	–	–
C_4AF (%)	8.40	–	–	–	–	–
Loss of ignition (%)	2.6	0.3	2.6	5.1	1.28	0.24
Blaine surface area (m^2/kg)	562	465	–	589	–	–
B.E.T. (m^2/kg)	–	–	18,200	–	–	–
Specific gravity	3.15	2.70	2.20	2.90	2.65	2.64

Note: 1 m^2/kg = 4.88 ft^2/lb

3.2.1. Step 1: Optimize Binder Combinations for Paste

With the initially-selected binder combinations, which aim at using high-volume SCMs in proportioning UHPC, flow tests are conducted to evaluate the minimum water content (MWC) and relative water demand (RWD) of binders under wet conditions in order to screen candidates for binders. The paste mixtures with lower MWC are advantageous in terms of the packing density, and thus, the corresponding binders are selected for further optimization. To further narrow down the candidates of the optimum binder combinations, the HRWR demand and compressive strength of the binders selected based on flow characteristics are then evaluated. For a given sand and fiber content, any change in the rheological characteristics is directly related to

the changes in the paste matrix (Wu et al. 2014). Therefore, final binder selection is based on rheological properties of the successful binder systems. The three sub-steps are elaborated as follows.

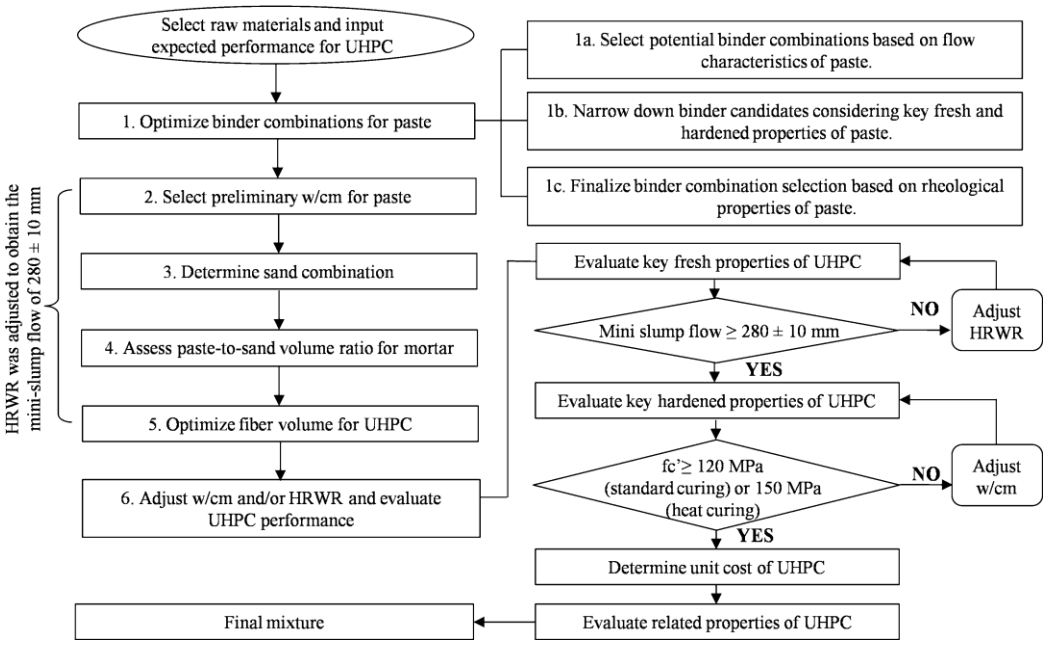

Figure 3-1 Procedure of mixture design methodology for UHPC

3.2.1.1 Sub-step 1 a: Select binder candidates based on flow characteristics

A mini-slump test is conducted in accordance with ASTM C 230/C 230 M. For each of the test binders, seven mixtures are prepared with various w/cm, by volume, values ranging from 0.4 to 1.0. This is carried out to establish a relationship between fluidity and w/cm for each binder combination, as illustrated in Figure 3-2. The intercept on the vertical axis represents the MWC required to initiate flow, and the slope of the relationship represents the RWD. Assuming there is no air entrapped in the paste, the volume occupied by the water content can be taken as the minimum void content. Therefore, a low MWC represents a high packing density of the binder (Hwang et al. 2006). A high RWD indicates that a given increase in w/cm can result in a small impact on the flowability. Thus, mixtures with high RWD are more robust to variations in water content (Hwang et al. 2006). Therefore, binder combinations with low MWC and high RWD are desirable for designing UHPC.

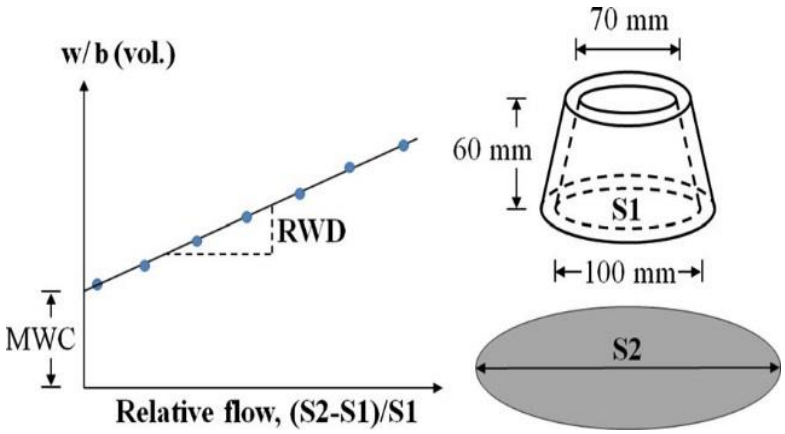

Figure 3-2 MWC and RWD in the mini-slump flow test, (Note: 1 mm = 0.039 in.)

3.2.1.2 Sub-step 1 a: Sub-step 1b: Narrow down binder candidates

To further narrow down the binder combinations, key fresh and hardened properties of the selected binder combinations are evaluated. The 1 and 28 d compressive strengths are measured in accordance with ASTM C 109. The HRWR dosage is adjusted to obtain a mini-slump flow of 280 ± 10 mm (10.9 ± 0.4 in.), which is commonly adopted to ensure good flowability and low air entrapment (Dudziak et al. 2008). The flow time is measured using a mini V-funnel in accordance with the EFNARC (2002). The mixtures with higher compressive strength and lower HRWR demand are preferred.

A radar chart is employed to display multivariate criteria for the selection of binder (Khayat et al. 2014). The criteria include the MWC, RWD, HRWR demand, and 1 and 28 d compressive strengths. The plot consists of a sequence of equi-angular spokes (radii), and each spoke represents one variable. The length of each spoke is proportional to the magnitude of the corresponding variable. Each variable is assigned with a specific weight factor. The data points of each spoke are sequentially connected and formed a specific area. A larger area indicates a better performance of the mixture (Khayat et al. 2014).

3.2.1.3 Sub-step 1c: Finalize the binder selection

The rheological properties of the paste mixtures with the selected binders in Sub-step 1b are tested using a coaxial rheometer (Anton Paar MCR 302) at different ages, up to 60 min. The w/cm is fixed at 0.63. The mini-slump spread value is fixed at 280 ± 10 mm (10.9 ± 0.4 in.) by adjusting the HRWR dosage.

The plastic viscosity (μ_p) is measured at 20, 40, and 60 min after water addition. The paste in the rheometer undergoes a 60 s pre-shearing period at a shear rate of 100 s^{-1}. This operation could minimize the structural build-up of paste at rest. Then, the shear rate is reduced by 10 s^{-1} for every 5 s until zero. The dynamic yield stress (τ_0) and μ_p are calculated using the Bingham fluid model (Tattersall et al. 1983), as shown in Eq. 3.1:

$$\tau = \tau_0 + \mu_p \dot{\gamma} \tag{3.1}$$

where γ denotes the shear rate. A relatively low value of μ_p is more desirable to ensure the proper filling capacity.

3.2.2. Step 2: Preliminarily Select a w/cm for Paste

The w/cm of UHPC is typically in the range of 0.15-0.25 (Willeet al. 2011). Paste mixtures of the selected binder combinations were proportioned with w/cm ranging between 0.18 and 0.23. The selection of the appropriate w/cm is based on HRWR demand and 28 d compressive strength under standard curing. The selected w/cm is applied in the later investigations to determine the optimum sand and fiber content (see Steps 3 and 4). The preliminary w/cm may be slightly adjusted in the final UHPC mixtures to achieve a good balance between flowability and strength which is elaborated in Step 6.

3.2.3. Step 3: Determine Sand Gradation

The modified Andreasen and Andersen model acts as a targeted function for the optimization of sand gradation, as shown in Eq. 3.2 (Funk and Dinger, 1994):

$$P(D) = \frac{D^q - D_{\min}^q}{D_{\max}^q - D_{\min}^q} \tag{3.2}$$

where P(D) represents the weight percentage of sand passing the sieve with size D; D_{max} is the maximum particle size (μm) (in.); D_{min} is the minimum particle size (μm) (in.); and q is the

distribution modulus which is related to the sand particle size. For fine particles, q can be set at 0.23 (q < 0.25) (Yu et al. 2014). The sand proportions are adjusted until the best fit is achieved between the composed gradation and the targeted curve, using an optimization algorithm based on the least square method. When the discrepancy between the targeted curve and the composed sand gradation is minimized, the sand combination can be considered as optimum.

According to the excess thickness theory (Li et al. 2011), the fluid paste volume should be high enough to fill voids between sand particles and provide a lubrication layer that envelops the particles to achieve a high flowability (Koehler et al. 2007). The bulk density of the compacted sand blend can be determined using a Gyrator compactor testing machine. A sand sample can be compacted by a continuous kneading action consisting of axial pressure and shear. The applied overhead air pressure is set at 4 ± 10^5 Pa. The gyrator angle and cycle number are fixed at 2° and 200, respectively. The working speed is 1 rps. The void content (α) of the compacted sand blend can then be calculated as:

$$\alpha = (1 - \gamma_{RM} / \rho_{RM}) \times 100 \tag{3.3}$$

$$\rho_{RM} = \rho_{Ri} \times \sum_{i-1}^{n} (V_{Ri} / V_{RM}) \tag{3.4}$$

where γ_{RM} is the bulk density of dry sand blend; V_{Ri} and V_{RM} are absolute volumes of river sand and sand blend, respectively; and ρ_{Ri} and ρ_{RM} are the densities of river sand and sand blend, respectively.

3.2.4. Step 4: Determine V_b/V_s of Mortar

The primary paste volume, denoted by V_b, takes into account the paste volume that is necessary to fill the void content of the sand and lubricate the sand particles. The primary paste can be calculated using the approach proposed by (Koehler et al. 2007):

$$V_b = V_{\exp} + V_{void} \tag{3.5}$$

$$V_{\exp} = 8 + (16 - 8) / 2(R_{S,A} - 1) \tag{3.6}$$

$$V_{void} = \alpha(100 - V_{\exp}) / 100 \tag{3.7}$$

$$V_S = (V_{\exp} + V_{void}) / (100 - V_{\exp} - V_{void}) \tag{3.8}$$

where V_S expresses as the sand volume; V_{exp} denotes excess paste volume (vol.%); V_{void} is void content in mortar (vol. %); and $R_{S,A}$ is a coefficient related to the shape and the angularity of sand in the range of 1-5 (Koehler et al. 2007).

The minimum V_b/V_S value can provide the necessary paste for filling ability. However, the minimum value is not necessarily appropriate for a specific requirement of strength. Therefore, additional experiments need to be carried out to validate the optimum value of V_b/V_S using mortar mixtures. The 28 d compressive strength of each mortar mixture with a V_b/V_S value can be evaluated. The HRWR dosage is adjusted to obtain a mini slump flow of 280 ± 10 mm (10.9 ± 0.4 in.).

3.2.5. Step 5: Determine Fiber Content of UHPC

The fiber content of UHPC commonly ranges from 2% to 5% (Park et al. 2012). The optimum fiber content is determined based on key fresh and mechanical properties of UHPC mixtures made with different fiber contents. The mini V-funnel and mini-slump tests are used to express workability. The HRWR dosage is adjusted to obtain a mini-slump flow of 280 ± 10 mm (10.9 ± 0.4 in.). Flexural load deflection relationships are determined in accordance with ASTM C 1609 to evaluate the first cracking strength and load capacity. Beam specimens (304.8 × 76.2 × 76.2 mm^3 (0.02 × 0.005 × 0.005 $in.^3$)) are tested after 28 d standard curing.

3.2.6. Step 6: Adjust w/cm and/or HRWR and Evaluate Performance of UHPC

In this step, trial batches are prepared to verify compliance of selected mixtures with mini-slump flow of 280 ± 10 mm (10.9 ± 0.4 in.) and 28 d compressive strength C120 MPa under standard curing and/or C150 MPa under heat curing. If the mixture does not achieve the targeted performance, either the HRWR dosage or w/cm value can be adjusted. For the selected mixture(s), key properties of the UHPC should be determined, as elaborated below.

3.2.6.1 Fresh properties

The HRWR dosage is adjusted to secure an initial mini-slump flow of 280 ± 10 mm (10.9 ± 0.4 in.). The unit weight and air content are measured in accordance with ASTM C 138 and ASTM C 231, respectively. The initial and final setting times are tested in accordance with ASTM A403. A ConTech 5 viscometer can be employed to determine τ_0 and μ_p of the UHPC.

Typically, the measurements begin at 10 min after water addition with samples subjected to pre-shear at a rotational velocity of 0.50 rps during 25 s, followed by a stepwise reduction in rotational velocity. The τ_0 and μ_p are then calculated using the Bingham fluid model (Tattersall et al. 1983), as shown in Eq. 3.1.

3.2.6.2 Mechanical properties

Compressive strength and flexural properties can be tested at different ages. The elastic modulus can be determined in accordance with ASTM C 469. The splitting tensile strength can be measured in accordance with ASTM C 496. Three samples are replicated in each test.

3.2.6.3 Autogeneous and drying shrinkage

The autogenous shrinkage can be evaluated in accordance with ASTM C 1698 using samples in corrugated plastic tubes and stored immediately after casting at 20 ± 0.5 °C (20 ± 33 °F) and 50 ± 2% relative humidity (RH). The first measurement is taken right after the final setting. The second measurement is taken at 12 hr after final setting. Other measurements are carried out daily within the 1st week, and then, weekly until 28 d after final setting. Drying shrinkage can be evaluated using prism specimens in accordance with ASTM 596, until 91 d after 7 d moist curing.

3.2.6.4 Durability

If deemed necessary, some durability characteristics of the optimized UHPC mixture can be investigated. For example, the electrical resistivity can be measured in accordance with ASTM C 1760, and frost durability can be determined in accordance with the ASTM C 666, Procedure A.

3.3. EXPERIMENTAL VALIDATIONS

As stated earlier, the study aimed at using high volume SCMs and locally available conventional concrete sand in proportioning UHPC to reduce the material's unit cost. An example of using the mixture design method in details is presented as follows.

3.3.1. Optimize Binder Combinations for Paste

3.3.1.1 Select binder candidates based on flow characteristics of paste

The initial binder combinations contained SF ≤ 25%, vol. %, and FAC and/or GGBS ≥ %, vol. %, as listed in Table 3-2. Twenty seven binder systems were investigated, which consisted of the reference, 14 binary, nine ternary, and three quaternary binders. The binary binders were categorized into three groups: (i) four GGBS systems, (ii) four FAC systems, and (iii) six SF systems. The ternary binders included four FAC-SF systems and five GGBS-SF systems. Quaternary binders were prepared with FAC-SF-GGBS.

Figure 3-3 compares the MWC and RWD results of the 27 binder combinations, which are listed in Table 3-2. The FAC and GGBS systems exhibited lower MWC values than that of the reference made with 100% cement. The MWC value decreased with the increase of FAC content due to the lubrication effects of FAC (Termkhajornkit et al. 2001). However, GGBS had an optimum amount that allowed the lowest MWC, due to its higher Blaine fineness than that of the cement, which improves the grain size distribution of the powder component and reduces the water demand (Parka et al. 2005). However, GGBS has irregular shapes and large specific areas that may result in an increase of the MWC. The MWC values of the SF binary systems were close to that of the reference mixture. The small and spherical SF particles can fill the voids between cement particles, which reduce the water demand. However, the fine SF particles are highly chemically reactive and can adsorb HRWR, which is adverse for the MWC (Otsubo et al. 1980).

Figure 3-3 indicates that the use of SCMs could increase the RWD and lead to a greater robustness. For the binary systems, the FAC60 mixture provided the smallest MWC and the largest RWD. For the GGBS binary system, the G50 mixture had the best performance (smallest MWC and largest RWD). For the SF binary system, the SF5 mixture gave the best performance. For the GGBS-SF ternary systems, the use of 5% SF slightly reduced the MWC and increased the RWD, compared with the corresponding GGBS binary systems. The fine SF particles filled the voids between the bigger cement and GGBS particles and formed a gel that reduced the friction between the particles (Parka et al. 2005), thus reducing the MWC. However, using 5% or 8% SF in the FAC-SF ternary systems did not demonstrate significant improvement for the corresponding FAC binary systems. Particularly, the use of 5% SF led to a notable increase in MWC and reduction in RWD when 60% FAC was used. In summary, the G50SF5 mixture

provided the highest packing density (smallest MWC) and robustness (largest RWD). All quaternary systems offered low MWC and high RWD, as indicated in Figure 3-3.

Table 3-2 Codification of initial investigated binders (vol.%)

Group	Code	C	GGBS	FAC	SF
1	Ref	100	–	–	–
2	G40	60	40	–	–
	G50	50	50	–	–
	G60	40	60	–	–
	G70	30	70	–	–
3	FAC30	70	–	30	–
	FAC40	60	–	40	–
	FAC50	50	–	50	–
	FAC60	30	–	60	–
4	SF5	95	–	–	5
	SF8	92	–	–	8
	SF11	89	–	–	11
	SF14	86	–	–	14
	SF20	80	–	–	20
	SF25	75	–	–	25
5	FAC40SF5	55	–	40	5
	FAC50SF5	45	–	50	5
	FAC50SF8	42	–	50	8
	FAC60SF5	35	–	60	5
6	G40SF5	55	40	–	5
	G50SF5	45	50	–	5
	G60SF5	35	60	–	5
	G50SF8	42	50	–	8
	G50SF11	39	50	–	11
7	F40S5G10	45	10	40	5
	F40S5G20	35	20	40	5
	F40S5G30	25	30	40	5

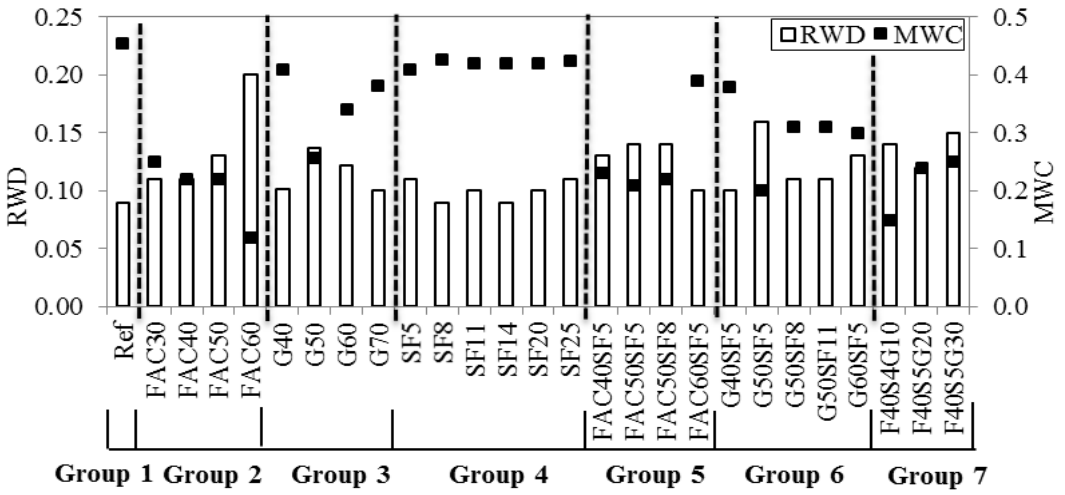

Figure 3-3 Effect of binder type on MWC and RWD

Out of the 27 binder combinations shown in Figure 3-3, 18 binders that have relatively low MWC (high packing density) were selected. Two combinations having the lowest MWC were selected in group 3. For Groups 2, 4, 5, 6, and 7, three mixtures were selected since the second and third mixtures have similar performance.

3.3.1.2 Narrow down binder combinations

In this step, the w/cm was fixed at 0.20. Figure 3-4 shows the results of HRWR demand (active solid material in HRWR divided by binder, wt. %), and 1 and 28 d compressive strengths of paste mixtures. Under standard curing, the FAC binary systems, except for the FAC60 mixture, achieved higher 1 day compressive strengths but lower 28 d compressive strengths than those of the GGBS binary systems. Using high-volume GGBS or FAC could lead to 75% lower HRWR demand compared with the reference mixture. The use of SF did not influence the HRWR demand and 28 d compressive strength significantly but increased the 1 day compressive strength considerably. For example, the use of 5% SF resulted in 95.8 MPa (13.9 ksi) 1 d compressive strength which is more than twice that of the reference mixture (45.8 MPa (6.6 ksi)). The SF binary systems demonstrated the highest 1 d compressive strength compared to other binary systems but also the highest HRWR demand. Except for the FAC40SF5G10 mixture, the 28 d compressive strength of the 17 binder combinations was in the range of 125 - 158 MPa (18.1 - 22.9 ksi). The HRWR demand of the binders with high-volume SCM was one-third of those of the reference and the SF binary systems.

In this study, the weighted factors that were used in radar chart analysis were selected to secure the high performance of UHPC intended for overlay application. The factors for the 1 day compressive strength, 28 d compressive strength, MWC, flow time, RWD, and HRWR demand were 2, 4, 3, 3, 2 and 3, respectively. Figure 3-5 shows the area obtained from the radar charts. The FAC60 had the largest area, followed by G50SF5, G50, FAC40SF5, FAC40, and G50SF11 mixtures. The top six binder combinations were selected for evaluating the rheological properties.

3.3.1.3 Finalize binders based on rheological properties for paste

Seven binder combinations, including the reference (Ref) and six candidates selected from the previous steps, were further evaluated in terms of the rheological properties. Since the w/cm and initial mini-slump flow were fixed for all mixtures, spreads of μ_p at 20 min between the mixtures were mainly due to their differences in packing densities and water film thicknesses that depend on the HRWR dosage and binder in use (Ferraris et al. 2001). Figure 3-6 shows the variation in μ_p from 20 to 60 min after water addition. At 20 min, the G50SF5 mixture achieved the lowest μ_p, whereas the reference paste had the highest μ_p. A lower μ_p of binders indicated additional water amount, thicker water film, and lower friction between particles (Wong et al. 2008). Between 20 and 60 min, the μ_p values did not change significantly and had similar rates of increase in μ_p.

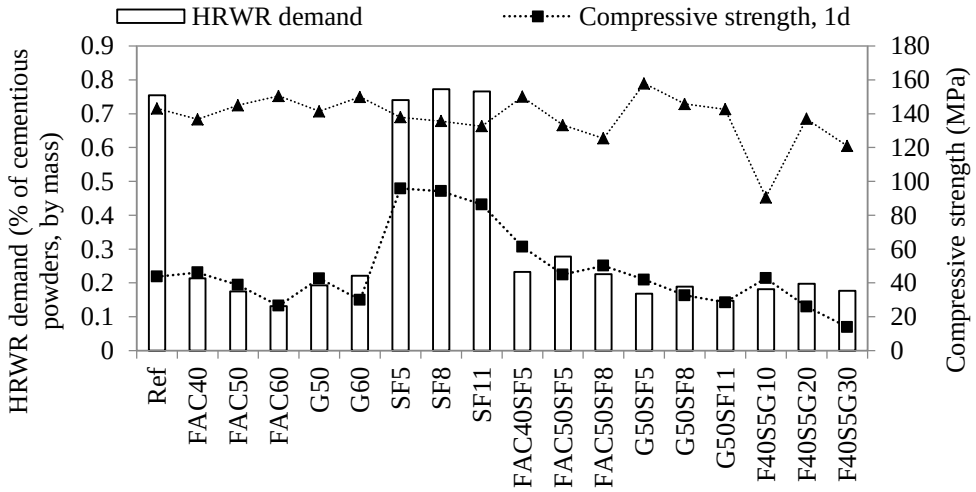

Figure 3-4 HRWR demand and 1- and 28 d compressive strength of paste, (Note: 1 MPa = 145 psi)

Low μ_p is desirable to achieve good filling capacity (Mechtcherine et al. 2015). Relatively low μ_p can also help fibers get evenly distributed in the matrix and improve the flexural performance. Mixtures that are highly viscous can entrap air, and, thus have reduced strength. Therefore, the G50SF5, FAC40SF5, G50, and FAC60 mixtures were selected for further evaluation.

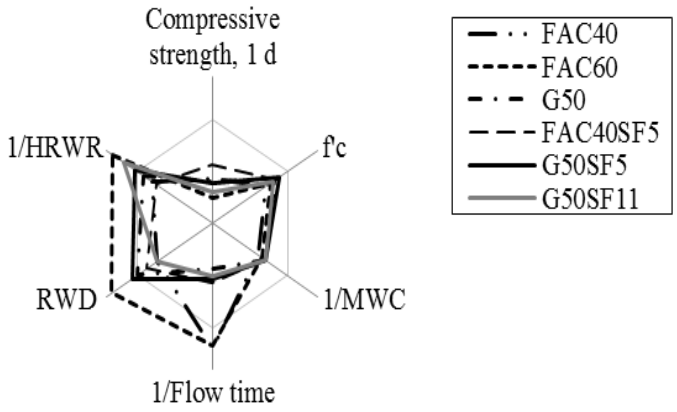

(a)

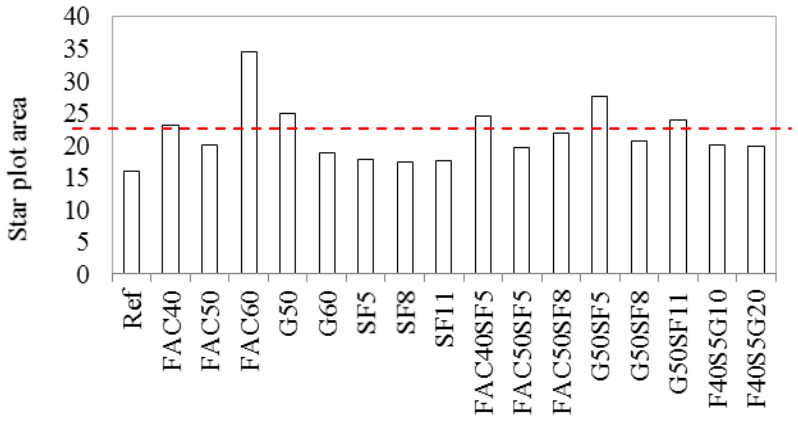

(b)

Figure 3-5 Multi-variable analysis: (a) radar chart and (b) areas in radar chart

3.3.2. Preliminarily Select a w/cm for Paste

A w/cm in the range of 0.18-0.23 was investigated for the four optimum binders. As indicated in Figure 3-7, when the w/cm was increased from 0.18 to 0.23, the 28 d compressive

strengths under standard curing did not decrease significantly (<10%), but the HRWR demand was reduced by about 40-60%. When the w/cm was increased from 0.20 to 0.23, the HRWR demand did not change significantly. Therefore, a w/cm of 0.2 was preliminarily selected, which allowed high compressive strength and flowability.

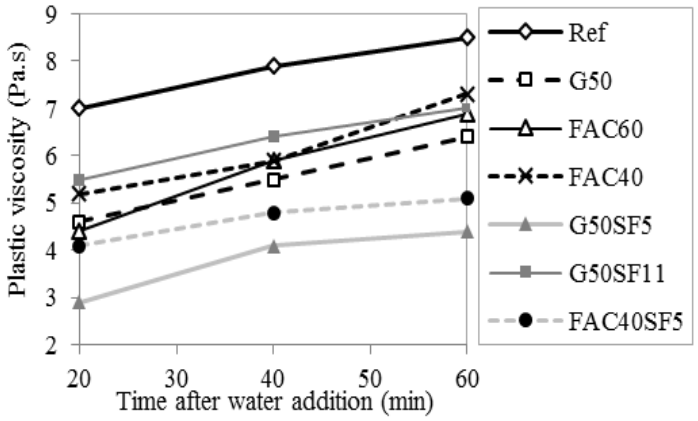

Figure 3-6 Time versus plastic viscosity of paste mixtures

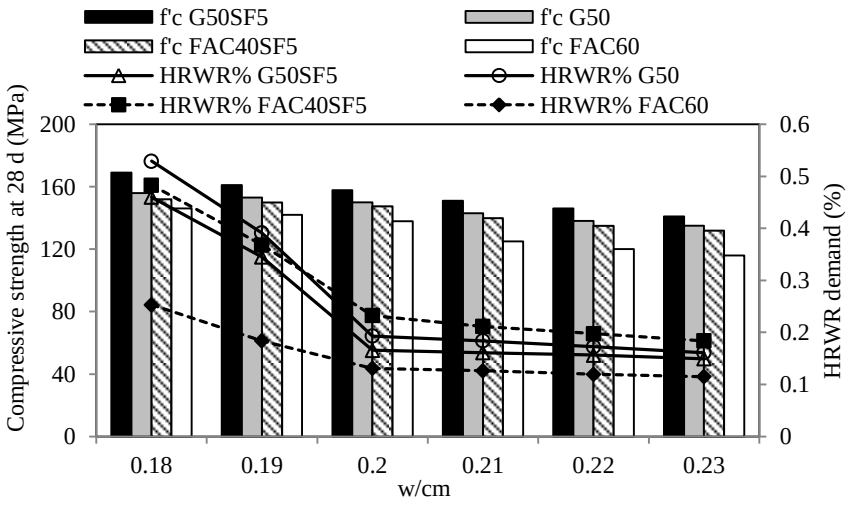

Figure 3-7 HRWR demand and compressive strength at 28 d for different w/cm, (Note: 1 MPa = 145 psi)

3.3.3. Determine Sand Combination

The D_{max} and D_{min} values were determined by the sieve sizes of 4.75 and 0.15 mm (0.2 and 0.006 in.), respectively. The optimized sand combination can result in an optimized gradation curve that could be achieved with the minimum deviation from the target gradation

curve, as shown in Figure 3-8. For the river sand and masonry sand employed in this study, the optimized sand combination to meet the targeted particle size distribution consisted of 70% of river sand and 30% of masonry, by mass.

In order to validate the suitability of the optimized sand to achieve high packing density, the densities of different sand combinations were measured using a gyrator compaction testing procedure. The combination of 70% river sand and 30% masonry sand indeed resulted in the highest bulk packing density (1870 kg/m^3 (3152 lb/yd^3)) compared to the density of other sand blends.

By applying the Eqs. 3.3 and 3.4, the void content (a) can be determined as: α = (1 - 1870/ 2640) 9 100 = 30. This value is required for evaluating the binder-to-sand volume ratio (V_b/V_S).

3.3.4. Determine V_b/V_s

The minimum V_b/V_S is determined to be 0.6 according to Eqs. 3.5-3.8, where $R_{S,A}$ equals 2 (Koehler et al. 2007). The flow properties and compressive strength for mortars with V_b/V_S values of 0.6, 0.7, 0.8, 0.9, 1.0 and 1.3 were tested, as shown in Table 3-3. The mixtures were prepared with the same binder made with 50% GGBS, 5% SF, and 45% cement. The w/cm was set to 0.2. As the V_b/V_S value was increased from 0.6 to 1.3, the HRWR demand and flow time were increased from 0.12% to 0.30% and from 46 to 129 s, respectively. The corresponding 1 day compressive strength was increased from 40 to 42 MPa (5.8 to 6.1 ksi), respectively, and the 7- and 28 d compressive strengths were increased from 75 to 90 MPa (10.1 to 13 ksi) and from 100 to 124 MPa (14.5 to 18 ksi), respectively. Therefore, as V_b/V_S value increased from 1.0 to 1.3, the compressive strength results did not change considerably, but the HRWR demand and flow time were significantly increased. The V_b/V_S value was determined to be 1.0, which resulted in optimized mixture with relatively low HRWR demand and viscosity, low paste content, and high compressive strength.

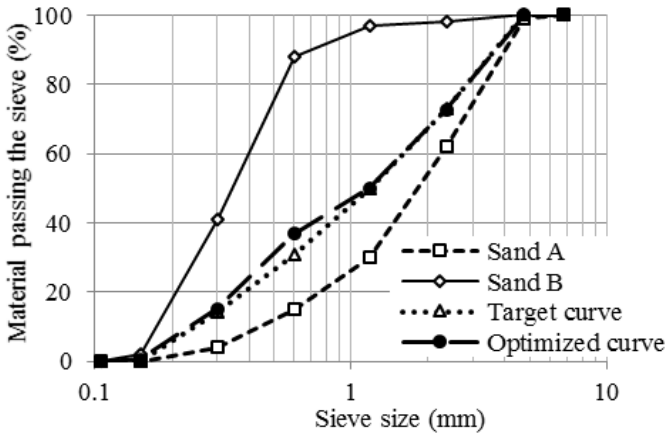

Figure 3-8 Sand gradation, (Note: 1 mm = 0.039 in)

3.3.5. Determine Fiber Content

Short steel fibers were used to enhance the post-cracking performance. As the fiber content was increased from 0 to 2.5% with a step size of 0.5%, as shown in Table 3-4, the HRWR demand, which was required to ensure the slump flow of 280 ± 10 mm (10.9 ± 0.4 in.) was increased from 0.28% to 0.69%, and the flow time was increased from 12 to 35 s. Particularly, when the fiber volume percentage, denoted by V_f, was increased from 2% to 2.5%, the HRWR dosage and flow time were increased by 72% and 94%, respectively.

For the flexural properties, the first cracking load is expressed as f_1, which corresponds to the load at the appearance of the first crack, as shown in Table 3-4. The peak load is denoted by f_p. The mid-span deflections corresponding to f_1 and f_p are denoted by and d_1 and d_p, respectively. The area under the load versus deflection curve between deflection values of 0 to L/150 (L = 202 mm (7.9 in.)) is referred to as T_{150}, which represents the toughness and is an indicator of energy dissipation. As the fiber content increased from 0 to 2%, the f_1 and f_p increased by 20% and 48%, respectively. However, no significant change was observed in f_p and T_{150} when the fiber content further increased from 2% to 2.5%. The highest f_p and T_{150} were secured by the use of 2% steel fibers which is considered as the optimum fiber content.

Table 3-3 Compressive strengths of different binder-to-sand ratios (V_b/V_S)

V_b/V_s	HRWR demand (%)	Flow time (sec.)	Compressive strength (MPa)		
			1 d	7 d	28 d
0.6	0.12	46	40	75	100
0.7	0.18	64	41	80	106
0.8	0.21	79	43	83	111
0.9	0.25	92	42	85	115
1.0	0.28	104	42	88	123
1.3	0.30	129	42	90	124

Table 3-4 Performance of UHPC made with different fiber contents

Code	V_f (%)	HRWR demand (%)	Slump flow (mm)	Flow time (sec.)	28 d compressive strength (MPa)	f_1 (MPa)	d_1 (mm)	f_p (MPa)	d_p (mm)	T_{150} (J)
Ref.-no fiber	0.0	0.28	29.0	12	123	13.7	0.10	13.7	0.10	1.0
Steel-0.5%	0.5	0.28	29.0	20	124	14.9	0.10	14.9	0.10	24.5
Steel-1.0%	1.0	0.28	28.5	22	124	15.9	0.07	16.5	0.61	38.4
Steel-1.5%	1.5	0.29	28.0	24	125	16.2	0.11	19.6	0.77	41.3
Steel-2.0%	2.0	0.40	28.0	18	125	16.5	0.08	20.3	1.05	50.2
Steel-2.5%	2.5	0.69	28.0	35	126	12.7	0.07	19.7	1.65	49.7

Note: 1 mm = 0.039 in., 1MPa = 145 psi

3.3.6. Evaluate and Adjust Designed UHPC Mixtures

Based on the above investigations, four mixtures were selected for further evaluation. Table 3-5 lists the four mixtures and a proprietary UHPC mixture taken as the reference mixture. These mixtures were prepared using the EIRICH mixer. The UHPC mixtures were designed to have a mini-slump flow diameter of 280 ± 10 mm (10.9 ± 0.4 in.), by adjusting the HRWR dosage, without consolidation. The w/cm was not changed since all the mixtures achieved 28 d compressive strengths higher than 120 MPa (17.4 ksi) under standard curing.

3.3.6.1 Fresh and physical properties

Table 3-6 summarizes the results of fresh properties. All the mixtures were self-consolidating and stable. The mini V-funnel flow times and plastic viscosities of the mixtures ranged from 12 s to 46 s and 23 - 50 Pa, respectively. The reference mixture exhibited the lowest flow time and plastic viscosity, which were 12 s and 23 Pa.s, respectively. The highest flow time and plastic viscosity, which were 46 s and 50 Pa.s, respectively, were obtained by the G50 mixture. The HRWR demands of all the mixtures were in the range of 0.5% to 1.4%. The

HRWR demand was the lowest for the FAC60 mixture and the highest for the G50SF5 mixture. The FAC40SF5 mixture demonstrated the longest initial setting time of 10 h and final setting time of 15 hr. The G50SF5 had the shortest initial and final setting time of 2 and 6 hr, respectively.

Table 3-5 Proportioning of the designed UHPC mixtures (unit: kg/m^3)

Code	Cement	SF	FAC	GGBS	Quartz sand	Fine sand	Sand A	Sand B	HRWR	Total water	Steel fibers
Ref.	712	231	–	–	1020	211	–	–	6.5	164	156
G50SF5	548	42	–	535	–	–	694	304	16.0	167	156
G50	593	–	–	546	–	–	698	295	12.5	182	156
FAC40SF5	663	42	367	–	–	–	703	308	12.0	171	156
FAC60	486	–	556	–	–	–	715	304	5.5	188	156

Note: 1 kg/m^3 = 1.685 lb/yd^3

3.3.6.2 Compressive strengths

Compressive strengths of the selected mixtures at 28 d under standard and heat curing methods were compared, as listed in Table 3-6. The 28 d compressive strength of the reference mixture was 135 MPa (19.6 ksi) and that of the designed mixtures was up to 125 MPa (18.1 ksi), under standard curing. The designed mixtures had slightly lower compressive strengths than that of the reference mixture. This may be due to the low silica fume content of the designed UHPC mixtures compared with the reference mixture. The designed UHPC mixtures achieved 28 d compressive strength up to 178 MPa (25.8 ksi) under heat curing, which was 12% lower than that of the reference UHPC (202 MPa (29.3 ksi)). The FAC60 mixture had 136 MPa (19.7 ksi) under initial heat curing, which is under the target value of 150 MPa (21.7 ksi).

3.3.6.3 Unit cost per compressive strength under standard curing

The unit cost per strength, defined as the ratio of the unit cost ($/m^3), is normalized by the 28 d compressive strength under standard curing conditions, as shown in Table 3-6. The unit cost includes the costs of all ingredients necessary for producing the UHPC mixtures with the exception of transportation cost. The unit cost of the selected cement, SF, FAC, GGBS, local river sand, masonry sand, quartz sand, HRWR, and steel fiber are 0.2, 0.66, 0.03 0.05, 0.014, 0.007, 2.2, 3.8 and 1.0 $/kg (0.4, 1.3, 0.06, 0.1, 0.03, 0.001, 4.4, 7.7 and 2 $/lb), respectively. These costs apply to St. Louis, MO, in 2016. The FAC and GGBS have 75% lower unit cost than

the cement. The local river sand has about 99.5% lower unit cost than the special finely-ground quartz sand. Thus, the use of high volume SCMs and local river sand could significantly reduce the unit cost of the UHPC. The unit cost per strength was 14.8 $/m^3/MPa (5.8 $/yd^3/ksi) for the reference mixture, and 3.5, 4.2, 4.3 and 4.7 $/m^3/MPa (1.4, 1.6, 1.7, 1.8 $/yd^3/ksi) for the designed FAC 60, G50, FAC40SF5, and G50SF5 mixtures, respectively. This corresponds to 68% to 76% reduction in unit cost per unit compressive strength.

3.3.6.4 Other mechanical properties

Table 3-6 summarizes the test results of the splitting tensile strength, Young's modulus, and flexural properties of the investigated UHPC mixtures under standard curing. The G50SF5 and FAC60 mixtures offered the highest and the lowest splitting tensile strengths of 14.3 and 10.3 MPa (2.0 and 1.5 ksi), respectively. The FAC40SF5 and FAC60 gave the highest and the lowest elastic moduli of 51.6 and 45.8 GPa (7,484 and 6,643 ksi), respectively. For the flexural properties, the flexural strengths of the five mixtures were close and ranged from 19.7 to 22.8 MPa (2.9 to 3.3 ksi). The G50 mixture had the highest first cracking and peak loads and toughness. The reference mixture had the lowest flexural strength and T_{150}.

3.3.6.5 Shrinkage

Autogenous shrinkage, which is caused by volume reduction due to chemical reactions during hydration and self-desiccation, contributes mostly to the total shrinkage in UHPC (Bao et al. 2015). Table 3-6 shows the results of the 28-d autogenous shrinkage measured since the final setting. The reference mixture had the highest 28-d autogenous shrinkage, which was 731 με, due to the high silica fume content. The lowest autogenous shrinkage of 253 με was obtained by the G50 mixture. The G50SF5, FAC60 and FAC40SF5 mixtures had 28 d autogenous shrinkage values of 602, 593 and 545 με, respectively.

The drying shrinkage values were measured after 7 d of moist curing. The end of the moist curing was chosen as "time zero" (t=0). The reference mixture reached a total drying shrinkage of 600 με, which was the highest value compared with the other designed mixtures. The G50 mixture displayed the minimum drying shrinkage, which was only 55 με. The total shrinkage of the UHPC can be considered as the initial autogenous shrinkage after 7 d, when autogenous shrinkage was stabilized, plus the drying shrinkage determined following 7 d of

moist curing. The G50 mixture had the lowest total shrinkage of 309 με. The reference mixture obtained the highest total shrinkage, which was 1331 με.

Table 3-6 Mechanical properties and durability of the UHPC mixtures

Code		Ref.	G50SF5	G50	FAC40SF5	FAC60
Flow time (sec.)		12	30	37	39	46
HRWR demand (%)		0.69	1.38	1.06	1.01	0.51
Mini slump flow (mm)		275	280	285	285	285
Yield stress (Pa)		39	35	37	34	30
Plastic viscosity (Pa·s)		23	39	50	44	29
Air content (%)		4	5	5	4	3.5
Specific gravity		2.47	2.45	2.43	2.44	2.41
Initial setting (h)		5	2	6	10	6
Final setting (h)		10	6	12	15	12
Compressive strength at 1 d - standard curing (MPa)		53	52	64	65	69
Compressive strength at 28 d - standard curing (MPa)		135	125	124	124	120
Compressive strength at 28 d - heat curing (MPa)		202	178	170	168	136
Splitting tensile strength (MPa)		12	14	12	12	10
Unit costs normalize by compressive strength ($/m^3/MPa)		14.8	4.7	4.2	4.3	3.5
Modus of elasticity (GPa)		53	50	50	52	46
Flexural performance	First cracking load (kN)	22	21	24	21	20
	Peak load (kN)	21	29	33	31	28
	δ_1 (mm)	0.092	0.085	0.080	0.093	0.089
	δ_p (mm)	0.701	0.690	0.653	0.820	0.635
	Peak strength (MPa)	19.7	20.2	22.8	21.3	20.1
	T_{150} (J)	40.4	48.8	51.5	51.1	49.4
Surface conductivity (kΩ·cm)		45	30	28	38	34
Durability factor (%)		99.8	99.8	99.8	99.7	99.7
Autogenous shrinkage at 28 d (με)		731	602	253	545	593
Drying shrinkage at 98 d (με)		600	430	56	466	500

Note: 1 mm = 0.039 in., 1MPa = 145 psi, 1Pa = 0.000145 psi, 1GPa = 145 ksi, 1 kN = 225 lb,
1 kΩ·cm = 0.394 kΩ·in., 1 $/m^3/MPa = 110.94 $/yd^3/psi

3.3.6.6 Electrical resistivity

The electrical resistivity affects the corrosion resistance of the material. Test results of surface resistivity, which is an indicator of electrical resistivity, of the five UHPC mixtures determined at 28 d, are shown in Table 3-6. Mixtures with a surface conductivity greater than 20 kΩ cm (7.9 kΩ-in.) can be considered to have a low risk of corrosion rate (Broomfield 2011).

Hence, all the mixtures that had surface conductivities of 30-45 kΩ cm (11.8-15 kΩ-in.) can be considered to exhibit a low risk of corrosion rate. The reference mixture with high silica fume content had the highest electrical resistivity. The G50 mixtures had the lowest electrical resistivity.

3.3.6.7 Freezing and thawing

The variations in durability factor of the UHPC mixtures after 300 freeze-thaw cycles are shown in Table 3-6. All the UHPC mixtures exhibited adequate resistance to freezing and thawing with durability factors of nearly 100%. The freezing/thawing testing was initiated after 56 d of moist curing given the high volume of SCMs. The excellent frost durability is associated with the very low permeability of the material.

3.4. SUMMARY

A mixture design methodology is presented for producing cost-effective UHPC with high-volume SCMs and conventional concrete sand. Based on the reported studies, the following conclusions can be drawn:

(1) The MWC can first be used as an indicator of the packing density of binders in wet condition to narrow down binder systems and reduce the required number of experiments. The binder composition of UHPC can then be optimized with consideration of the HRWR demand, rheological properties, MWC, RWD, and compressive strength properties. A radar chart can be then employed for the analysis. Based on this approach the following binder combinations were selected: G50, G50SF5, FAC60, and FAC40SF5.

(2) The second step is to determine the preliminary w/cm based on the 28 d compressive strength and HRWR demand value for paste mixtures prepared with the optimum binder combinations with w/cm values of 0.18-0.23. The optimum value for the selected binders was 0.20.

(3) The modified Andreasen and Andersen model can be used to optimize sand gradation. In this study, 70% river sand and 30% masonry sand were selected to achieve the highest packing density.

(4) The next step involves the determination of the binder-to-sand volume ratio (V_b/V_s). Mortar mixtures made with the selected w/cm and G50SF5 binder were prepared with

V_b/V_s values of 0.6, 0.7, 0.8, 0.9, 1.0 and 1.3. Based on flow properties and 28 d compressive strength, the optimum V_b/V_s was determined to be 1.0.

(5) The optimum fiber content for the UHPC is experimentally determined given the flowability and flexural properties of UHPC made with various fiber contents. For the steel fibers considered in this study, 2% fiber volume was selected.

(6) For the UHPC mixtures prepared with the various binder systems and optimized mixture proportioning, the UHPC mixtures were self-consolidating, stable, and had 28 d compressive strengths of 120 - 125 MPa (17.4 - 18.1 ksi) under standard curing condition. The strength can reach up to 178 MPa (25.8 ksi) by applying heat curing at a maximum temperature of 90 °C (194 °F) for one day followed by 7 d moist curing. For the selected UHPC mixtures, the 28 d splitting tensile strength, modulus of elasticity, flexural strength, and toughness (T_{150}) were 11.6-14.3 MPa (1.7-2.1 ksi), 48.8-51.6 MPa (7.1-7.5 ksi), 20.2-21.3 MPa (2.9-3.1 ksi) and 50 ± 1.5 kN mm (439 ± 13.2 lb in.), respectively.

(7) The designed UHPC mixtures exhibited relatively low autogenous shrinkage and drying shrinkage. The G50 mixture had the lowest autogenous and drying shrinkage of 253 με at 28 d and 56 με at 98 d, respectively. All tested UHPC mixtures exhibited a very high electrical resistivity and excellent frost durability.

(8) The unit cost per compressive strength of the UHPC mixtures designed with high volume of SCMs and concrete sand can range between 3.5 and 4.7 $\$/m^3/MPa$ (455 and 528 $\$/yd^3/psi$). The mixture FAC60 was the most cost-effective mixture, which also developed better workability and lower unit cost per compressive strength of 3.7 $\$/m^3/MPa$ (411 $\$/yd^3/psi$) than other.

4. ROBUSTNESS OF UHPC AT DIFFERENT CASTING AND CURING TEMPERATURES

The concrete temperature during mixing and curing can have marked influence on key properties, including workability, setting time, mechanical properties as well as autogenous and drying shrinkage, of UHPC. The work described in this chapter aims at investigating the effect of casting and curing temperatures on such properties of UHPC. The UHPC was mixed and cured at 10, 23, and 30 ºC (50, 73.4, and 86 ºF).

4.1. MATERIAL AND MIXTURE PROPORTIONS

Table 4-1 summarizes the physical and chemical characteristics of cementitious materials. A Type III portland cement, densified silica fume (SF), a Class C fly ash (FAC), and ground granulated blast-furnace slag (GGBS) were employed for the binder. Two natural siliceous sand of 0 - 4.75 mm (0 - 0.2 in.) (sand A) and 0 - 2 mm (0 - 0.08 in.) (sand B) with a specific gravity of 2.6 were used. The sand A-to-sand B ratio was proportioned at 70: 30, by mass, which was found to yield the highest packing density for the proposed UHPC mixtures (Meng et al., 2017). A quartz sand (0 - 0.6 mm (0 - 0.02 in.)) was used for the reference UHPC. A polycarboxylate-based HRWR with a solid content of 23% and a specific gravity of 1.05 was used to enhance fluidity retention and fiber distribution of the UHPC. Brass coated straight steel fibers measuring 13 mm (0.5 in.) in length and 0.2 mm (0.008 in.) in diameter were incorporated at 2%, by volume of concrete, to improve ductility. The aspect ratio and tensile strength of the fibers are 40 and 2.16 GPa (5,801 and 313 ksi), respectively.

Table 4-2 summarizes the mixture proportioning of the investigated UHPC mixtures. The w/cm was fixed at 0.20, and the sand-to-cementitious materials ratio was held at 1.0, by volume. HRWA dosage was adjusted to secure initial mini-slump value of 270 ± 10 mm (10.5 ± 0.4 in.), which is necessary to secure self-consolidating characteristics.

4.2. MIXING PROCEDURE AND SAMPLE PREPARATIONS

In order to provide a low temperature condition of 10 ± 1 °C (50 ± 33.8 °F), all solid materials and mixing water were stored in a controlled chamber at 2 °C (35.6 °F) for 24 hr before mixing. Half of the mixing water was replaced with crushed ice, and the ice was introduced into

the mixer 15 min prior to mixing to cool down the mixer pan. For the UHPC at 23 ± 1 °C (73.4 ± 33.8 °F), only the mixing water was cooled down.

A 150-l high-shear concrete mixer with an inclined drum and adjustable vane speed was used. The mixing procedure consisted of mixing the sand and cementitious materials for 2 min at 1 rps. This was followed by adding of 90% of the mixing water with 90% of the HRWR and mixing the material 2 min at 6 rps; (3) the remaining of the liquid was added, and the material was mixed for 4 min at 6 rps; (4) the fibers were introduced gradually over a period of 1 min and all the materials were mixed for 2 min at 10 rps. Specimens were cast in one lift without any mechanical consolidation and covered with wet burlap and a plastic sheet for 24 h. They were demolded and cured in lime-saturated water at 10, 23, and 30 °C (50, 73.4, and 86 °F).

Table 4-1 Physical and chemical characteristics of cementitious materials

Composition	C	FAC	GGBS	SF
SiO_2 (%)	19.72	36.5	36.8	95.5
Al_2O_3 (%)	5.10	24.8	9.2	0.7
Fe_2O_3 (%)	2.76	5.2	0.76	0.3
CaO (%)	64.50	28.1	37.1	0.4
MgO (%)	2.30	5	9.5	0.5
SO_3 (%)	3.25	2.5	0.06	0
Na_2O (%)	0.33	0	0.34	0.4
C_3S (%)	65.23	-	-	-
C_2S (%)	7.33	-	-	-
C_3A (%)	8.85	-	-	-
C_4AF (%)	8.40	-	-	-
Blaine surface area (m^2/kg)	562	465	589	-
Specific gravity	3.15	2.70	2.90	2.2
Loss of ignition (%)	2.6	0.3	5.1	2.6

Note: 1 m^2/kg = 4.88 ft^2/lb

4.3. EXPERIMENTAL PROGRAM

4.3.1. Fresh Properties

Mini-slump flow was conducted in accordance with ASTM C230 using a truncated cone measuring 60 mm in height with upper and lower diameters of 70 and 100 mm (2.7 and 3.9 in.), respectively. The flow time test was measured using a mini V-funnel with an opening of 32 × 32 mm (1.25 × 1.25 in.). UHPC sample of 1.15 liters (0.3 gal) was cast in the funnel. After 30 sec of rest, the bottom outlet was opened, allowing the mortar to flow. The flow time was determined at

the end of the continuous flow. Air content of the UHPC mixtures was determined by the pressure method in accordance with ASTM C 231.

Table 4-2 UHPC mixture proportioning

Code	Reference	G50	G50SF5	FA60	FA60SF5
Cement (kg/m^3)	712	593	548	486	663
Silica fume (kg/m^3)	231	-	42	-	42
Fly ash (kg/m^3)	-	-	-	556	367
GGBS (kg/m^3)	-	546	535	-	-
Sand A (kg/m^3)	-	698	694	715	703
Sand B (kg/m^3)	-	295	304	304	308
Fine sand (kg/m^3)	211	-	-	-	-
Quartz sand (kg/m^3)	1020	-	-	-	-
HRWR* (%)	0.9	1.09	1.42	0.53	0.98
Mixing water (L/m^3)	164	167	182	171	188
Fiber (%)	2	2	2	2	2

*By active mass of HRWA compared to binder mass
Note: 1 kg/m^3 = 1.685 lb/ft^3

4.3.2. Rheological Properties

A co-axial viscometer ConTech 5 was employed to evaluate the rheological properties of the UHPC. The outer and the inner radius are 145 and 100 mm (5.7 and 3.9 in.), respectively, and the height of the vane that is submerged in the mixture is 160 mm (6.2 in.). The torque was measured at the fixed inner cylinder, while the outer cylinder was rotating. The measurement started at 20 min of age and was repeated at 40 and 60 min of elapsed time. The UHPC samples were subjected to pre-shear at a rotational velocity of 0.50 rps during 25 s, followed by a stepwise reduction in rotational velocity until zero. The yield stress and plastic viscosity of the UHPC mixtures were calculated using the Bingham model (Tattersall and Banfill, 1983).

4.3.3. Mechanical Properties

Compressive strength was determined by cubes measuring 50 mm (2 in.), in accordance with ASTM C109. The splitting tensile strength and the modulus of elasticity were evaluated using 100 × 200 mm (3.9 × 7.8 in.) cylinders, in accordance with ASTM C 496 and ASTM C 469, respectively. Three replicates were used for each test.

4.3.4. Shrinkage

Autogenous shrinkage was monitored in accordance with ASTM C 1698. For each mixture, the final setting time was determined in accordance with ASTM C 403, which was used as the starting time for autogenous shrinkage.

Drying shrinkage was evaluated using 25 × 25 × 285 mm (1 × 1 × 11.1 in.) prismatic bars, in accordance with ASTM C 596. After demolding, the specimens were immersed in water for 7 d before exposing them to air drying in a controlled environment with the desired temperature. Three specimens were used for shrinkage test.

4.4. RESULTS AND DISCUSSION

4.4.1. Fresh Properties

4.4.1.1 HRWR demand

Figure 4-1 presents the HRWR demand to obtain a mini-slump flow of 270 ± 10 mm (10.5 ± 0.4 in.) of UHPC at different temperatures. The HRWR demand varied between 0.46% and 1.58% (expressed as percent of the active solid content of HRWR compared to binder mass). The HRWR demand increased in all investigated UHPC mixtures with the increase in temperature from 10 to 30 °C (50 to 86 °F). The FA60 mixture with 0.46% at 10 °C (50 °F) and the G50SF5 mixture with 1.58% at 30 °C (86 °F) exhibited the lowest and highest HRWR dosages, respectively. UHPC made with FA required less HRWR compared to that made with GGBS and the reference mixture where the FA60 mixture had the lowest HRWR demand with 0.46%, 0.53% and 0.77% HRWR at 10, 23, and 30 °C (50, 73.4, and 86 °F), respectively. On the other hand, UHPC made with GGBS necessitated higher dosages compared to other UHPC mixtures. For example, the G50SF5 mixture required the highest HRWR dosages of 1.33%, 1.42%, and 1.58% at 10, 23, and 30 °C (50, 73.4, and 86 °F), respectively. The reference mixture showed the highest variation rates of HRWR demand when temperature increased from 10 to 23 °C (50 to 73.4 °F) and from 23 to 30 °C (73.4 to 86 °F), requiring 0.16% and 0.37% more HRWA, respectively.

The fresh properties, including mini slump flow and mini V-funnel flow time, of the five investigated UHPC mixtures are summarized in Table 4-3 and are discussed below.

4.4.1.2 Mini slump flow

The initial mini-slump flow values of all UHPC mixtures were targeted at 270 ± 10 mm (10.5 ± 0.4 in.) by adjusting the HRWR dosage. This was necessary to secure self-consolidating characteristic of the UHPC mixtures (Meng et al., 2017).

4.4.1.3 Mini V-funnel flow time

As shown in Table 4-3, the mini V-funnel flow time decreased with the increase in temperature varying from 12 to 63 sec. The flow time accelerated as the temperature increased from 10 to 23 °C (50 to 73.4 °F) and 23 to 30 °C (73.4 to 86 °F) by up to 26 and 23 sec, respectively. The FA60 mixture with 12 sec at 30 °C (86 °F) and the G50SF5 mixture with 63 sec at 30 °C (86 °F) exhibited the lowest and highest mini V-funnel flow time.

4.4.1.4 Air content

Results indicated that air content decreased with the increase in temperature varying from 6.2% to 3.2%. The G50SF5 and FA60 mixtures exhibited the highest and lowest values of air volume with 6.2% and 3.2% at 10 and 30 ºC (50 and 86 °F), respectively. The FA60 mixture had the lowest air content values of 5%, 3.5%, and 3.2% at corresponding temperatures of 10, 23, and 30 ºC (50, 73.4, and 86 °F), respectively.

4.4.1.5 Setting time

Figure 4-Figure 4-2 illustrates the initial and final setting times of UHPC mixtures at different temperatures ranging from 1.8 to 11 hr and 5 to 17 hr, respectively. Increasing the temperature from 10 to 30 ºC (50 to 86 °F) accelerated the initial and final setting times by up to 4.5 and 5 hr, respectively. The shortest and longest values of final setting time corresponded to the G50SF5 and FA40SF5 mixtures with 5 hr at 30 ºC (86 °F) and 17 hr at 10 ºC (50 °F), respectively.

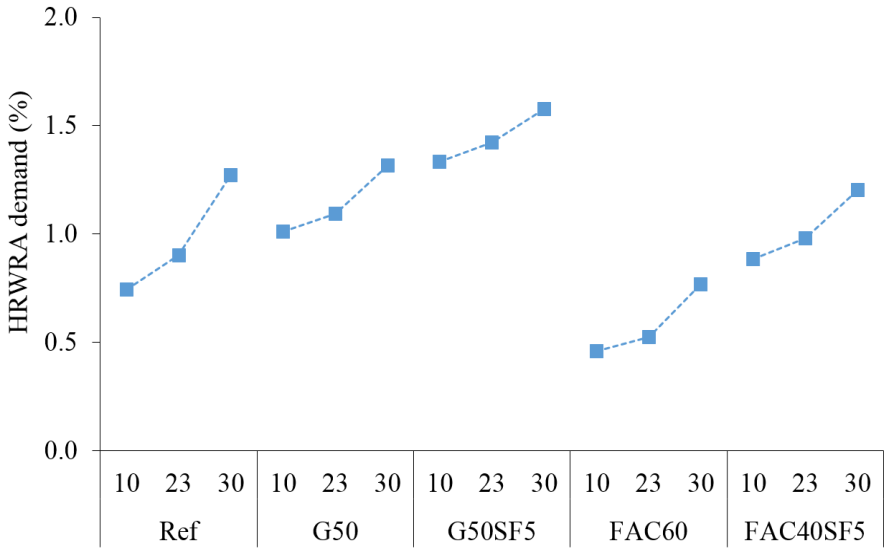

Figure 4-1 HRWR demand for UHPC mixtures at different temperatures

Figure 4-3 and 4-4 illustrate the variations in yield stress and plastic viscosity with three measurement times of 20, 40, and 60 min for the UHPC mixtures at 10, 23, and 30 ºC (50, 73.4, and 86 °F), respectively.

Table 4-3 Fresh properties of four optimized UHPC mixtures at different temperatures

Code	Target temperature (°C)	Measured temperature (°C)	Air content (%)	Mini-slump value (mm)	Mini V-funnel (sec.)
Reference	10	11	6	260	23
	23	24	4.2	260	16
	30	29	3.8	270	13
G50	10	9	5.5	280	41
	23	24	5.6	270	35
	30	29	3.8	280	20
G50SF5	10	11	6.2	260	63
	23	23	5.0	270	37
	30	29	4.2	275	14
FA60	10	9	5.0	260	46
	23	21	3.5	270	30
	30	29	3.2	280	12
FA40SF5	10	9	5.5	260	52
	23	22	4.5	280	39
	30	30	4.3	260	16

Note: 1 mm = 0.039 in., 1°C = 33.8 °F

4.4.2. Rheological Properties

4.4.2.1 Yield stress

Yield stress increased by up to 55% with increasing the temperature from 10 to 30 ºC (50 to 73.4 °F) ranging from 19 to 53 Pa (0.0027 to 0.0077 psi). UHPC made with GGBS exhibited lower yield stress for all three measurement times compared to other mixtures. The G50 mixture had the lowest yield stress values of 19, 21, and 23 Pa (0.0027, 0.003, and 0.0033 psi) for the first (20 min) measurement time at 10, 23, and 30 ºC (50, 73.4, and 86 °F), respectively. On the other hand, the reference mixture exhibited the highest values of 35, 37, and 41 Pa (0.0051, 0.0054, and 0.006 psi) for the same condition, respectively. As shown, yield stress increased over the elapsed time at all temperatures. For example, the FA40SF5 mixture had yield stress values of 36, 41, 45 Pa (0.0052, 0.006, 0.0065 psi) for 20, 40, and 60 min elapsed times, respectively, at 30 ºC (86 °F). UHPC made with GGBS exhibited the lowest variations in the increase rate of yield stress with elapsed time. For example, the G50SF5 mixture had 2 and 3 Pa (0.0003 and 0.00043 psi) further increase in yield stress when elapsed time increased from 20 to 40 min and 40 to 60 min, respectively, at 10 ºC (50 °F). However, these values were 9 and 6 Pa (0.0013 and 0.0009 psi) in the case of the FA60 mixture for the same condition.

4.4.2.2 Plastic viscosity

Plastic viscosity values decreased by up to 45% with the increase in temperature from 10 to 30 ºC (50 to 86 °F) for all investigated UHPC mixtures varying from 15 to 60 Pa.s. UHPC made with GGBS exhibited the higher values of viscosity compared to the reference mixture and UHPC made with FA. For example, the G50SF5 mixture with viscosity values of 60, 48, and 32 Pa.s had the highest values for the first measurement time (20 min) at 10, 23, and 30 ºC, respectively. On the other hand, the FA60 mixture with 24 Pa.s and the reference mixture with 19 and 15 Pa.s showed the lowest viscosity values at 20 min of 10, 23, and 30 ºC, respectively. As shown, plastic viscosity increased over the elapsed time regardless of temperature. For example, the FA60 mixture showed viscosity values of 24, 34, and 42 Pa.s for the first (20 min), second (40 min), and third (60 min) elapsed time.

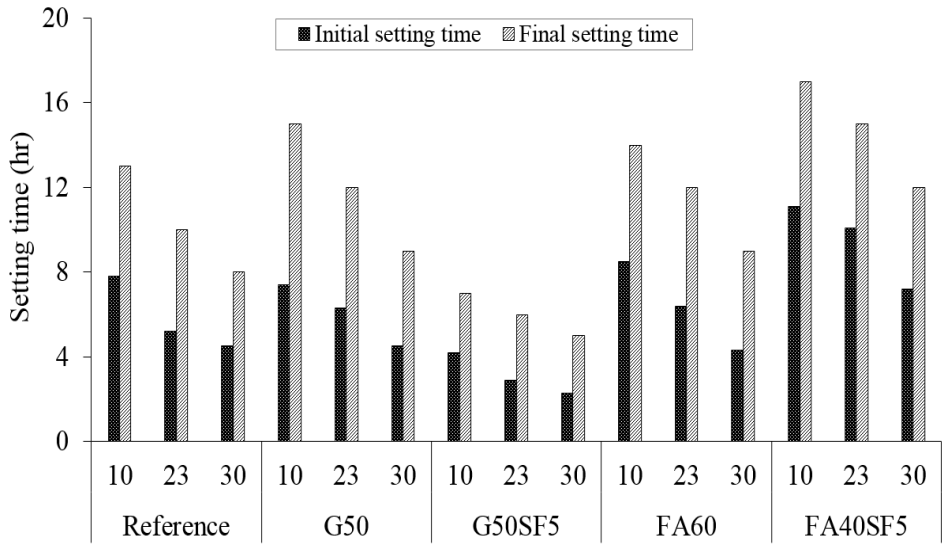

Figure 4-2 Results of setting time

4.4.3. Hardened Properties

Figure 4-5 illustrates the 28-d compressive strength results of the investigated UHPC mixtures at different curing temperatures. The lowest and highest values of the 28-d compressive strengths belonged to the reference mixture at 10 and 30 ºC (50 and 86 °F) with 68 and 142 MPa (9.86 to 20.6 ksi), respectively. Increasing temperature from 10 to 30 ºC (50 to 86 °F) improved the 28-d compressive strength by 65%, 70%, 43%, and 42% for the G50, G50SF5, FA60, and FA40SF5 mixtures, respectively. This is in agreement with the findings from Soliman and Nehdi (Soliman and Nehdi, 2011), who concluded that higher curing temperature resulted in higher compressive strength. Lower compressive strength of the reference mixture at 10 ºC (50 °F) can be attributed to higher air contents which were 1.8% and 2.2% higher than those at 23 ºC and 30 ºC (73.4 and 86 °F). The agglomeration of SF particles can be another possible reason that can reduce its effectiveness (Soliman and Nehdi, 2011). It is reported that the pozzolanic activity of agglomerated SF can be low and the size of such agglomerates can be larger than cement particles, leading to higher porosity and limited fine particle filler effect (Soliman and Nehdi, 2011).

4.4.3.1 Splitting tensile strength

The 28-d splitting tensile strength of the investigated UHPC mixtures at different curing temperatures is presented in Figure 4-6. Results indicated that the tensile strength enhanced with the increase in temperature varying between 8 and 16.5 MPa (1.16 and 2.39 ksi). These lowest and highest values belonged to the reference mixture at 10 ºC (50 °F) and the G50SF5 mixture at 30 ºC (86 °F), respectively.

4.4.3.2 Elastic modulus

Figure 4-7 compares the 28-d MOE results of UHPC mixtures at different curing temperatures. The MOE values enhanced with the increase in temperature for all investigated UHPC mixtures ranging from 41 to 56 GPa (5947 to 8122 ksi). The G50 and reference mixtures exhibited the lowest and highest values of 41 GPa (5947 ksi) at 10 ºC (50 °F) and 56 GPa (8122 ksi) at 30 ºC (86 °F), respectively. The MOE values of UHPC made with GGBS or FA showed by up to 3 and 7 GPa (435 and 1015 ksi) lower values than that of the reference mixture at ambient temperature (23 ºC (73.4 °F)).

4.4.3.3 Flexural strength

Table 4-4 presents the test results of the 28-d flexural properties of the investigated UHPC mixtures at different curing temperatures. The flexural properties enhanced with the increase in temperature. The G50 mixture exhibited the lowest flexural strength with 13 MPa (1.9 ksi) at 10 ºC (50 °F). However, the flexural strengths of the G50 mixture at 23 and 30 °C (73.4 and 86 °F) were close and varied between 21 and 22 MPa (3 and 3.2 ksi).

Results indicate that increasing temperature from 10 to 23 °C (50 to 73.4 °F) had a greater impact on flexural properties than that from 23 to 30 °C (73.4 to 86 °F). For example, the flexural strength improvements were 3, 8, 6, 5, and 3 MPa (435, 1160, 870, 725, and 435 psi) for the reference, G50, G50SF5, FA60, and FA40SF5 mixtures, respectively, with increasing the temperature from 10 to 23 °C (50 to 73.4 °F). However, these enhancements were 1 to 2 MPa (145 to 290 psi) for the increase in temperature from 23 to 30 °C (73.4 to 86 °F). The same trend was observed for first cracking load and toughness values. The G50 mixture exhibited the highest first cracking load, peak load, and toughness (T150) with 25, 35, and 54 kN-mm (219.4, 307.1, and 473.9 lb-in.), respectively, at 30 ºC (86 °F).

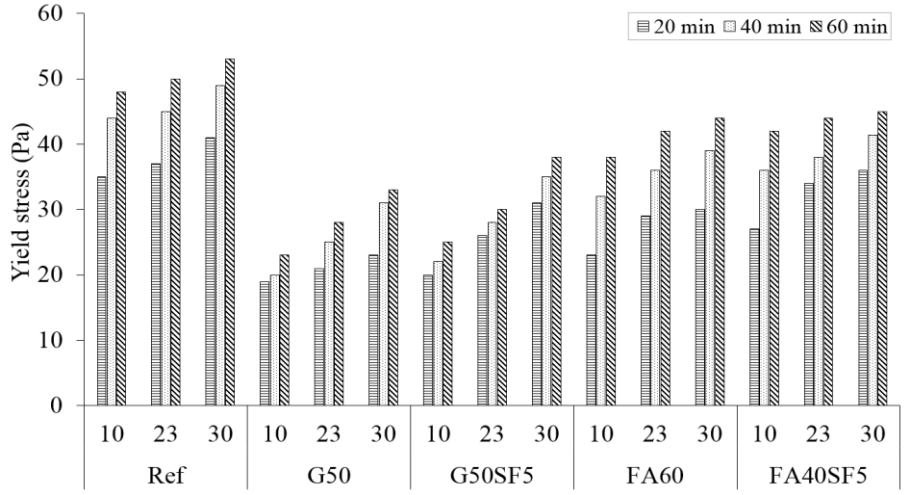

Figure 4-3 Yield stress of UHPC mixtures at various curing temperatures, (Note: 1 Pa = 0.000145 psi)

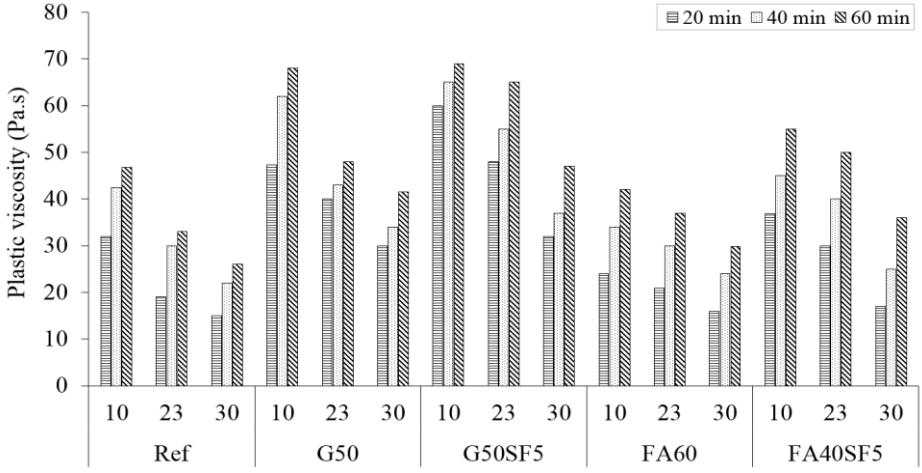

Figure 4-4 Plastic viscosity of UHPC mixtures at various curing temperatures, (Note: 1 Pa.s = 0.000145 psi.s)

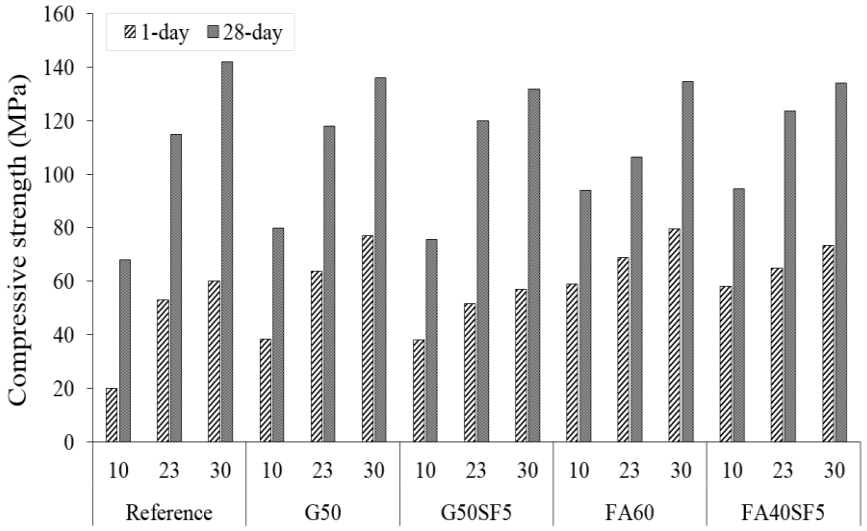

Figure 4-5 Compressive strength of UHPC mixtures at 1 and 28 d at various curing temperatures, (Note: 1 MPa = 145 psi)

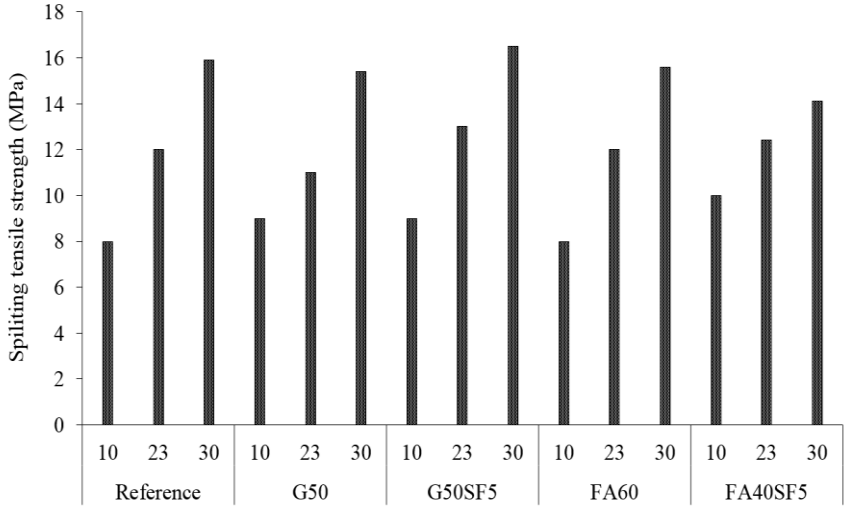

Figure 4-6 Splitting tensile strength of UHPC mixtures at 28 d under various curing temperatures, (Note: 1 MPa = 145 psi)

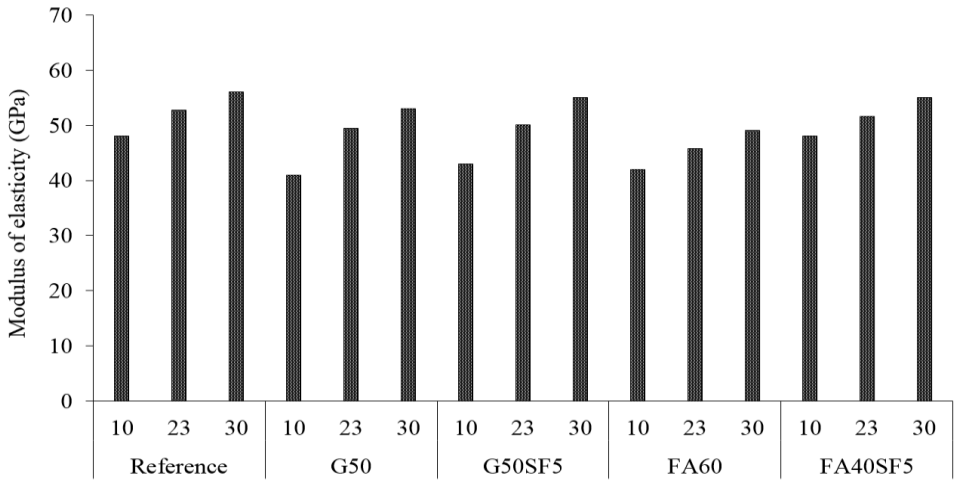

Figure 4-7 Modulus of elasticity of UHPC mixtures at 28 d under different curing temperatures, (Note: 1 GPa = 145 ksi)

Table 4-4 Flexural behavior of UHPC mixtures at different temperatures

Code	Target temperature (°C)	First cracking load (kN)	Peak load (kN)	Flexural strength (MPa)	T150 (kN-mm)
Reference	10	19	19	17	38
	23	22	21	20	40
	30	24	28	21	52
G50	10	15	20	13	35
	23	24	33	21	51
	30	25	35	22	54
G50SF5	10	17	20	14	35
	23	21	29	20	49
	30	25	31	21	52
FA60	10	16	22	15	36
	23	20	29	20	49
	30	22	32	22	54
FA40SF5	10	19	28	19	32
	23	21	31	21	50
	30	22	33	22	53

Note: 1 °C = 33.8 °F, 1 kN = 0.225 kip, 1 MPa = 145 psi, 1 kN-mm = 8.775 lb-in.,

4.4.4. Shrinkage

Figure 4-8 presents the autogenous shrinkage for UHPC mixtures at different curing temperatures. Results indicated that the higher curing temperature resulted in greater shrinkage with faster growth rate, particularly at early ages. This is in good agreement with the reported

results by Soliman and Nehdi (Soliman and Nehdi, 2011). For example, increasing temperature from 10 ºC to 30 ºC (50 to 86 °F) led to increase in autogenous shrinkage by up to 60% and 45% for GGBSs and FACs, respectively. This increase was 35% for the reference mixture. This can be attributed to higher chemical shrinkage due to the acceleration of hydration. As seen, the mixtures at 30 ºC (86 °F) were the first mixtures to set and started to shrink, followed by those mixtures at 23 ºC and 10 ºC (73.4 and 50 °F). This can be due to the development of a strong solid skeleton at high temperatures (Soliman and Nehdi, 2011). Increasing the temperature from 10 ºC to 30 ºC (50 to 73.4 °F) accelerated the shrinkage developments at a high rate during the first 24 h, which can be due to the acceleration of cement hydration, leading to higher chemical shrinkage (Soliman and Nehdi, 2011).

The reference mixture with 25% SF achieved the highest shrinkage development, having ultimate values of 650 με, 730 με, and 870 με at 10 ºC (50 °F), 23 ºC (73.4 °F), and 30 ºC (86 °F), respectively. Incorporation of SF significantly reduced the larger pores while there is no effect on total pore space, resulting in increasing fine pores (Russell and Graybeal, 2013; Yu et al., 2015). This causes an increase in negative pressure of the capillary tubes, which leads to autogenous shrinkage increase. Moreover, silica fume consumes $Ca(OH)_2$ in order to produce C-S-H gel, creating a denser structure (Yu et al., 2015; Neville, 1999). This accelerates the hydration of cement which improves the self-desiccation of the concrete, resulting in increasing the autogenous shrinkage of concrete (Schober and Flatt, 2006; Göller et al., 2009).

A considerable reduction was observed with the replacement of SF with high volume GGBS or FAC. The FAC60 mixture decreased autogenous shrinkage significantly compared to the reference mixture in corresponding temperatures. These reductions were up to 25% and 20% at 10 and 30 ºC (50 and 86 °F). Results showed that an increase in fly ash replacement level from 40% to 60% with the addition of 5% SF decreased the shrinkage development up to 10%. It has been reported that the autogenous shrinkage of concrete decreases with an increase in fly ash amount (Jensen and Hansen, 1999). This can be attributed to the fact that fly ash is not participating in the hydration process with pozzolanic reactions at very early ages and acts as a filler. On the other hand, since it replaces some portion of cement, early-age efficient water-cement ratio increases due to the lower content of cement. This also decreases the heat of hydration. Therefore, it leads to a decrease in early-age self-drying, resulting in a reduction of autogenous shrinkage (Loukili et al., 1999).

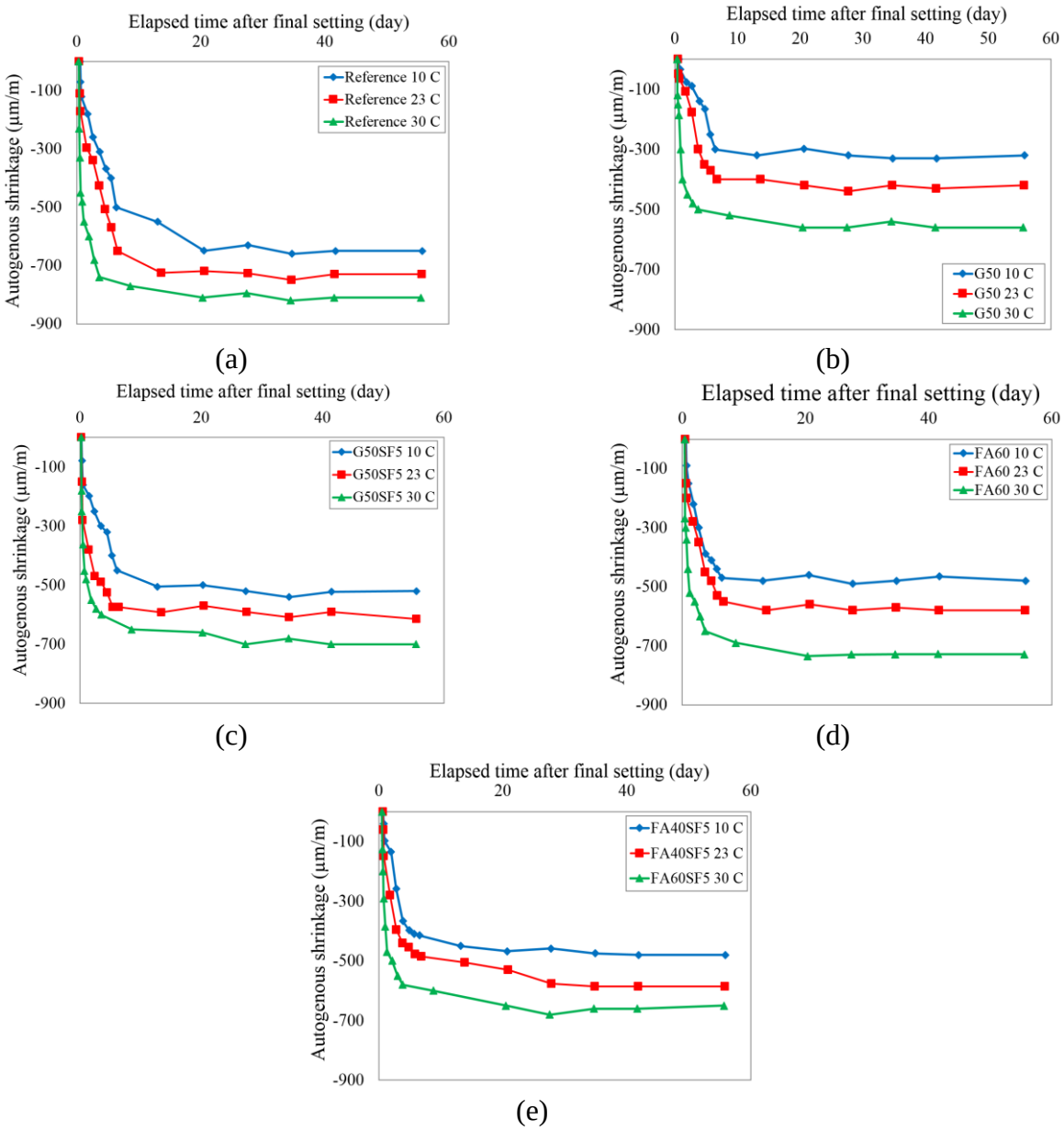

Figure 4-8 Autogenous shrinkage results at different temperatures (µm/m=µƐ)

The G50 mixture had the lowest shrinkage development among all mixtures at corresponding temperatures with ultimate shrinkage values of 350 µε, 420 µε, and -560 µε at 10 ºC (50 °F), 23 ºC (73.4 °F), and 30 ºC (86 °F). The literature shows that the influence of GGBS on the autogenous shrinkage is controversial. However, it has frequently been reported that the fineness and replacement level of GGBS are the main factors in terms of autogenous shrinkage

development (Ortiz et al., 2005). The autogenous shrinkage of concrete reduces with an increase of GGBS amount given the same fineness as cement. However, an increase in autogenous shrinkage is observed with increasing the level of replacement when the fineness of GGBS exceeds 4000 cm^2/g (1952 ft^2/lb) (Ortiz et al., 2005).

The results of drying shrinkage of UHPC mixtures subjected to different mixing and curing temperatures are displayed in Figure 4-9. Results showed that drying shrinkage increased with an increase in temperature by up to 30%, 60%, and 50% for the reference, GGBSs, and FACs mixtures, respectively, as the temperature went up from 10 to 30 ºC (50 to 86 °F). In the case of 30 ºC (86 °F), during the first 8-10 d the development rate reached a smooth trend, and in later ages, the shrinkage values were higher than those of the 10 and 23 ºC (50 and 73.4 °F). Comparing the results at low and high temperatures, it was found that the strain variations were stabilized at 30 ºC (86 °F) sooner than 10 ºC (50 °F). This can be because at high temperature, cement hydration reactions are faster than that at low temperature, resulting in reduction of the internal relative humidity due to increase in evaporation rate (Jianyong and Yan, 2001). The reference mixture had the highest shrinkage development with -756 με, -856 με, and -978 με corresponding to 10 ºC (50 °F), 23 ºC (73.4 °F), and 30 ºC (86°F). SF particles have high specific surface area and very high activity which can expedite the hydration process, resulting in a reduction in internal relative humidity at early and later ages. This can increase the autogenous shrinkage of concrete continuously. In particular, at high temperature, high drying shrinkage of concrete incorporating silica fume is predictable (Lura et al., 2001).

Results showed that the replacement of SF with GGBS or FAC considerably reduced the drying shrinkage. For example, the G50 and G50SF5 mixtures with ultimate shrinkage of 642 and -530 με, reduced the shrinkages up to 25% and 40% compared to the reference mixture, respectively, at 28 d under the environmental temperature of 23 ºC (73.4 °F). At the same condition, the FAC60 and FAC40SF5 mixtures ended up with 35% and 30% reduction in shrinkage. From the results, it can be concluded that increasing FAC replacement level from 40% to 60% decreased the shrinkage up to 10%. Fly ash can delay the cement hydration at early ages, resulting in reduction in the early internal drying speed of concrete. This can lead to reduced early autogenous shrinkage. On the other hand, pastes incorporating fly ash have a lower stiffness at earlier ages, leading to increased possibility of shrinkage. In the case of GGBS, low activity at early age delayed the hydration reaction of cement meaning limited water was

consumed, and in the later ages the hard slag particles constrained the shrinkage of cement (Jianyong and Yan, 2001; Lura et al., 2001).

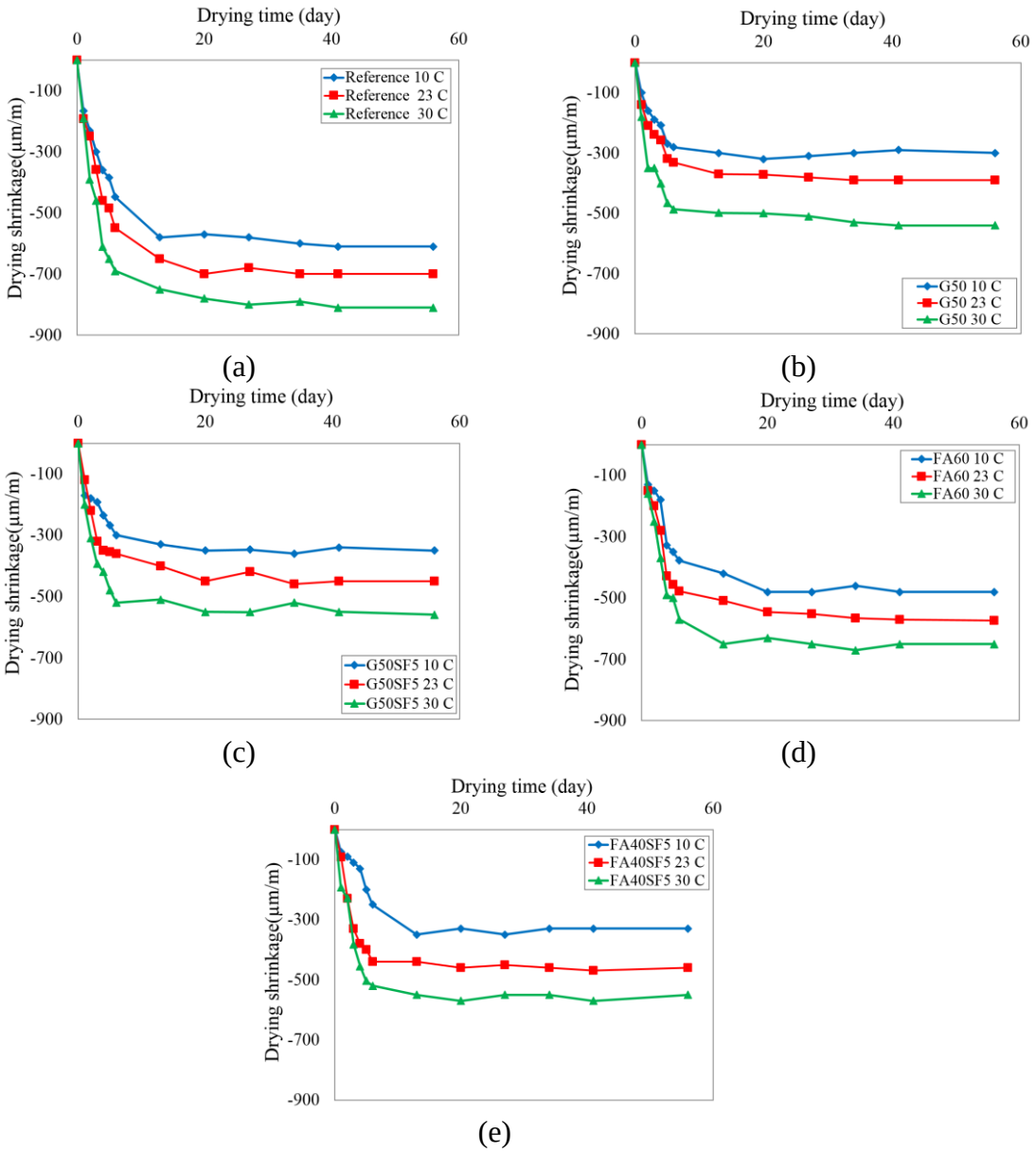

Figure 4-9 Drying shrinkage results at different temperatures (μm/m=με)

4.5. SUMMARY

This chapter investigated the effect of casting and curing temperatures on workability, setting time, mechanical properties as well as autogenous and drying shrinkage of UHPC. The UHPC was mixed and cured at 10, 23, and 30 ºC (50, 73.4, and 86 ºF). Based on the reported studies, the following conclusions can be drawn:

(1) The HRWR demand increased regardless of the investigated UHPC mixture with the increase in temperature. UHPC made with FA required less HRWR content compared to that with GGBS and the reference mixture (25% SF). The FA60 mixture with 0.46% HRWR at 10 °C (50 °F) and G50SF5 mixture with 1.58% HRWR at 30 °C (86 °F) exhibited the lowest and highest HRWR demands, respectively.

(2) Mini V-funnel flow time decreased by up to 45%, with the increase in temperature from 10 to 30 ºC (50 to 86 °F). Increasing the temperature accelerated the initial and final setting times by up to 4.5 and 5 h, respectively. Yield stress increased by up to 55% and plastic viscosity decreased by up to 45% with increasing the temperature from 10 to 30 ºC (50 to 86 °F). UHPC made with GGBS exhibited the highest values of plastic viscosity and the lowest yield stresses compared to the reference mixture and UHPC made with FAC.

(3) Temperature variation can significantly affect the development of mechanical properties of UHPC. Results indicated that mechanical properties of different UHPC mixtures improved with the increase in temperature. Increasing temperature from 10 to 30 ºC (50 to 86 °F) improved the 28-d compressive strength of the G50, G50SF5, FA60, and FA40SF5 mixtures by 65%, 70%, 43%, and 42%, respectively. The flexural toughness (T150) was enhanced by up to 65% with the increase in temperature. All mixtures had their minimum and maximum toughness at 10 and 30 ºC (50 to 86 °F), respectively.

(4) Increasing the temperature from 10 to 30 ºC (50 to 86 °F) led to increasing autogenous and drying shrinkage. UHPC made with GGBS or FA exhibited a reduction in autogenous and drying shrinkage by up to 300 and 350 με, respectively, compared to the reference mixture at 56 d. UHPC made with FAC and GGBS were more robust than the reference mixture made with 25% SF. In general, the FA60 and FA40SF5 mixtures resulted in greater robustness than other UHPC mixtures.

5. COUPLED EFFECT OF SATURATED LIGHTWEIGHT SAND AND SHRINKAGE-MITIGATING ADMIXTURES ON PERFORMANCE OF UHPC

This chapter evaluates the effect of various shrinkage mitigation approaches on performance of UHPC. Such approaches included the use of various contents of CaO-based and MgO-based expansive agents, shrinkage-reducing admixture, and pre-saturated lightweight sand. Workability, compressive strength development, autogenous and drying shrinkage were evaluated for UHPC mixtures subjected to moist curing periods of 1, 3, and 7 d.

5.1. EXPERIMENTAL PROGRAM

5.1.1. Materials

The cementitious materials used in this investigation included a Type III portland cement with a Blaine fineness of 385 m^2/kg (209 yd^2/lb). GGBS with a Blaine fineness of 590 m^2/kg (320 yd^2/lb) was used. A CaO-based expansive agent (EXC) and a MgO-based expansive agent (EXM) were used in powder form. The specific gravity and recommended content of EXC are 3.14 and 3% to 10%, by mass of cementitious materials, respectively. These values are 2.26 and 2% to 7%, respectively, for the EXM. A propylene glycol ether-based shrinkage reducing admixtures (SRA) with a specific gravity of 0.98 was used.

Two natural sands with nominal maximum sizes of 4.75 mm (0.2 in.) (sand A) and 2 mm (0.08 in.) (sand B) and a specific gravity of 2.6 were used. The sands were proportioned at 70:30 mass ratio, which was found to yield the highest packing density for the UHPC mixture (Meng et al., 2017). Pre-saturated light aggregate sand (LWS) with a nominal maximum size of 4.75 mm and a specific gravity of 1.81 was used. The LWS has a 24 hr absorption rate of 17.5%, by dry mass, and a desorption rate of 96.4% as determined according to ASTM C1761. Based on this standard, the minimum required amount of LWS should be 237 kg/m^3 (400 lb/yd^3) to compensate for chemical shrinkage. Such value corresponds to 35% of the total volume of sand for the proposed UHPC mixture.

A polycarboxylate-based high-range water reducer (HRWR) with a solid content of 23% and a specific gravity of 1.05 was employed. The HRWR was used to secure self-consolidating characteristic of the UHPC. The water content in all liquid-based chemical admixtures was accounted to maintain a fixed w/cm for all mixtures. High strength straight steel fibers measuring

13 mm (0.5 in.) in length and 0.2 in (0.008 in.) diameter were incorporated. The aspect ratio and tensile strength of the selected fiber are 40 and 2160 MPa (313 ksi), respectively.

5.1.2. Mixture Proportioning

The 12 investigated UHPC mixtures proportioned with different LWS, EXC, EXM, and SRA contents are presented in Table 5-1. All the mixtures were prepared at a fixed w/cm of 0.20 and fiber content of 2%, by volume of concrete. The EXC at content of 5%, 7.5%, and 10%, by mass of binder, were used, while the EXM contents were 5% and 7%. The SRA dosages used in UHPC were 1.5% and 3%, by volume of water content. Sand A was substituted by LWS at different volumetric replacement ratios of 25%, 40%, and 60%. The HRWR demand was adjusted to secure an initial mini-slump value of 270 ± 10 mm (10.5 ± 0.4 in.), which is necessary to secure self-consolidating characteristic of the UHPC (Meng et al., 2017).

Table 5-1 Mixture proportioning of investigated UHPC mixtures

Mixtures	Cement	GGBS	Sand A	Sand B	LWS	EXC	EXM	SRA	Mixing water	HRWR	Fibers
	(kg/m^3)	(kg/m^3)	(kg/m^3)	(kg/m^3)	(kg/m^3)	(kg/m^3)	(kg/m^3)	(L/m^3)	(L/m^3)	(%)	(%)
G50	593	546	704	298	-	-	-	-	235	2.02	2
LWS60	593	546	103	298	405	-	-	-	237	1.14	2
EXC7.5	571	526	704	298	-	44	-	-	250	2.37	2
EXC7.5LWS25	571	526	454	298	169	44	-	-	230	1.23	2
EXC7.5LWS40	571	526	303	298	270	44	-	-	235	1.14	2
EXC7.5LWS60	571	526	103	298	405	44	-	-	238	1.05	2
EXC5LWS60	578	532	103	298	405	30	-	-	236	0.97	2
EXC10LWS60	563	519	103	298	405	59	-	-	240	1.05	2
EXM5LWS60	572	529	103	298	405	-	29	-	242	1.14	2
EXM7LWS60	563	522	103	298	405	-	40	-	252	1.40	2
SRA1.5LWS60	593	546	103	298	405	-	-	17	213	1.14	2
SRA3LWS60	593	546	103	298	405	-	-	34	206	1.14	2

Note: $1 kg/m^3 = 1.685 lb/yd^3$, $1 L/m^3 = 0.202 gal/yd^3$

A 12-L (3.168 gal) Hobart mixer was used to prepare the UHPC at room temperature (23 ± 2 °C (73.4 ± 35.6 °F)). The mixing procedure consisted of four steps: (1) dry cementitious materials and sand were added and mixed for 2 min at 1 rps; (2) 90% of the mixing water with 90% of the HRWR were introduced, and the material was mixed for 3 min more at 2 rps; (3) the remaining of water and HRWR were added, and the material was mixed for 7 min at 2 rps; (4)

steel fibers were added gradually over 1 min, and then the material was mixed for 2 min at 10 rps.

5.1.3. Testing Program

The mini-slump flow and mini V-funnel flow time tests were used to evaluate the flowability of the fresh UHPC at 10 and 70 min of age. The V-funnel flow time can also be considered as an indication of plastic viscosity (Erdem et al., 2009). Between 10 and 70 min, the UHPC mixture was left in the mixer and was covered by plastic sheeting to avoid any water evaporation. The UHPC was then remixed for 2 min before testing at 70 min.

For the mini-slump test, a truncated cone measuring 60 mm (2.3 in.) in height with upper and lower diameter of 70 and 100 mm (2.7 and 3.9 in.), respectively, was used. The UHPC was cast in the mini-cone in a single lift without any mechanical consolidation. The cone was lifted after 30 sec to determine the mean spread diameter at the end of the flow. The opening of the V-funnel measures 32 × 32 mm (1.25 × 1.25 in.), and the sample volume is 1.15 L (0.3 gal). The bottom outlet was opened 30 sec after casting the UHPC. The flow time was determined at the end of the continuous flow. All tested mixtures exhibited continuous flow.

Cubic samples measuring 50 mm (2 in.) were used to determine compressive strength at 7, 28, 56, and 91 d. Three specimens were employed for each test. The specimens were initially covered with wet burlap and plastic sheet. They were demolded at 24 ± 1 h and then subjected to different initial curing times of 0, 2, and 6 d, or continuous in lime-saturated water at 23 ± 2 °C (73.4 ± 33.8 °F). These curing conditions are referred to as air drying (AD), 3 d of initial moist curing (3MC), 7 d of moist curing (7MC), and continuous moist curing (MC), respectively.

Autogenous shrinkage was measured using three replicated samples. The UHPC was cast in rigid corrugated polyethylene tubes that were capped at both ends to prevent any loss of moisture. Linear deformations were recorded right at the final setting time using a digital comparator with a linear variable differential transformer (LVDT). The samples were kept in a controlled environmental chamber at 23 ± 2 °C (73.4 ± 33.8 °F) and 50% ± 4% RH throughout the test period. The initial and final setting times were assessed by the penetration test according to ASTM C 403. Drying shrinkage was determined according to ASTM C 596 at 23 ± 2 ºC (73.4 ± 33.8 °F) and 50% ± 4% RH. Three prismatic specimens with dimensions of 285 × 25 × 25 mm (11 × 1 × 1 in.) were prepared for each mixture. The samples were demolded after one day and

subjected to the AD, 3MC, and 7MC curing conditions. The drying shrinkage was measured over a period of 91 d.

5.2. RESULTS AND DISCUSSION

5.2.1. Fresh Properties

Table 5-2 summarizes the fresh properties of the 12 investigated UHPC mixtures. The dosage of the HRWR required to secure mini-slump flow of 270 ± 10 mm (10.5 ± 3.9 in.) ranged between 0.97% and 2.37%. This was expressed as a percentage of the active solid content of the HRWR to binder mass. The EXC5LW60 (i.e., 5%EXC + 60% LWS) and EXC7.5 mixtures obtained the lowest and highest HRWR demands, respectively. The majority of the mixtures had HRWR demand of 0.96% to 1.40%, while the EXC7.5 and G50 (i.e., reference) mixtures had high HRWR demand of 2.37% and 2.02%, respectively. Compared to the EXC7.5 mixture, the incorporation of 25% to 60% of LWS resulted in a considerable decrease in HRWR demand (1.23% to 1.05%). The mini-slump values at 70 min ranged between 230 and 265 mm (9 and 10 in.). The loss in mini-slump over 60 min was therefore limited to 15 to 40 mm (0.6 to 1.56 in.). The G50 and SRA1.5LWS60 (i.e., 1.5% SRA + 60% LWS) mixtures exhibited the lowest and highest 70 min mini-slump flow values of 230 and 265 mm (9 and 10 in.), respectively. The use of 60% LWS with EXC, EXM, and SRA had a positive effect on reducing mini-slump loss.

Table 5-2 Fresh properties and compressive strength of UHPC mixtures

Test		G50	LWS60	EXC 7.5	LWS+EXC7.5			EXC+LWS 60		EXM+LWS60		SRA+LWS60	
					25	40	60	5	10	5	7	1.5	3
Mini-slump flow (mm)	10 min	270	260	280	260	280	275	275	265	270	265	280	260
	70 min	230	240	240	230	255	260	260	235	245	235	265	245
Mini V-funnel (sec)	10 min	19	16	21	20	18	17	18	23	17	20	18	20
	70 min	32	23	34	29	25	21	24	32	23	27	25	29
Air content (%)		4.8	3.1	4.5	3.3	3.7	4	3.8	4.3	3.5	4	3.4	3.8
Initial setting (h)		11	5	9	3.5	4	4.5	5	4	5.5	5	6	7
Final setting (h)		17.5	9.2	16	6	7	8	9.5	7	11	9	10.5	11.8

Note: 1 mm = 0.039 in.

The mini V-funnel flow times of all UHPC mixtures varied from 16 to 23 sec at 10 min and 21 to 34 sec at 70 min. The LW60 and EXC10LW60 mixtures exhibited the lowest and highest initial V-funnel values of 16 and 23 sec, respectively. On the other hand, the fastest and slowest flow times after 70 min belonged to the EXC7.5LWS60 and EXC7.5 mixtures, which were 21 and 34 sec, respectively.

The use of LWS decreased the loss in V-funnel time; the mixture made with a combination of 7.5% EXC and LWS at contents of 25%, 40%, and 60% had V-funnel flow time losses of 9, 7, and 4 sec, respectively. Increasing the replacement level of EXC (5%, 7.5%, and 10%), EXM (5% and 7%), and SRA (1.5% and 3%) slightly increased (10% to 25%) the mini V-funnel at 10 and 70 min but had no significant effect on the loss of V-funnel time. The air content of the UHPC mixtures varied between 3.1% and 4.8%, which corresponded to the LWS60 and G50 mixtures, respectively. The initial setting times varied between 3.5 and 11 hr and the final setting times between 6 and 17.5 hr. The G50 and EXC7.5LWS25 mixtures had the longest and shortest setting times, respectively. The combined use of EXC, EXM, or SRA with LWS significantly shortened the setting time. For example, the initial and final setting times of the EXC7.5LW25 were 3.5 and 6 hr compared to 9 and 16 hr, respectively, for the EXC7.5 mixture. This significant acceleration of setting can be due to the sharp drop in HRWR demand when 25% LWS was incorporated. The increase of the EXC content from 5% to 10% and the EXM dosage from 5% to 7% delayed the setting time by 2.5 and 2 hr, respectively. The increase of the SRA from 1.5% to 3% resulted in a slight acceleration in setting time by 1 hr.

5.2.2. Shrinkage

5.2.2.1 Autogenous Shrinkage

Figure 5-1 illustrates the autogenous shrinkage of UHPC mixtures made with different LWC, EXC, EXM, and SRA dosages. The incorporation of LWS at replacement levels of 25%, 40%, and 60%, by volume of sand, combined with 7.5% EXC resulted in considerable decrease in autogenous shrinkage when compared to the reference G50 mixture. As illustrated in Figure 5-1(a), the expansion increased with the LWS content. The UHPC mixtures made with 25%, 40%, and 60% LWS replacements exhibited maximum expansions of 80, 300, and 375 με, respectively, at 7 d. Given the higher relative humidity associated with greater use of LWS (Meng and Khayat, 2017), greater expansion was observed from the use of 7.5% CaO-based EX.

Following the peak values, the deformation decreased gradually until started to exhibit net shrinkage. For example, the EXC7.5LWS60 mixture had a net expansion of 5 με after 91 d compared to 296 με for the EXC7.5LWS25 mixture.

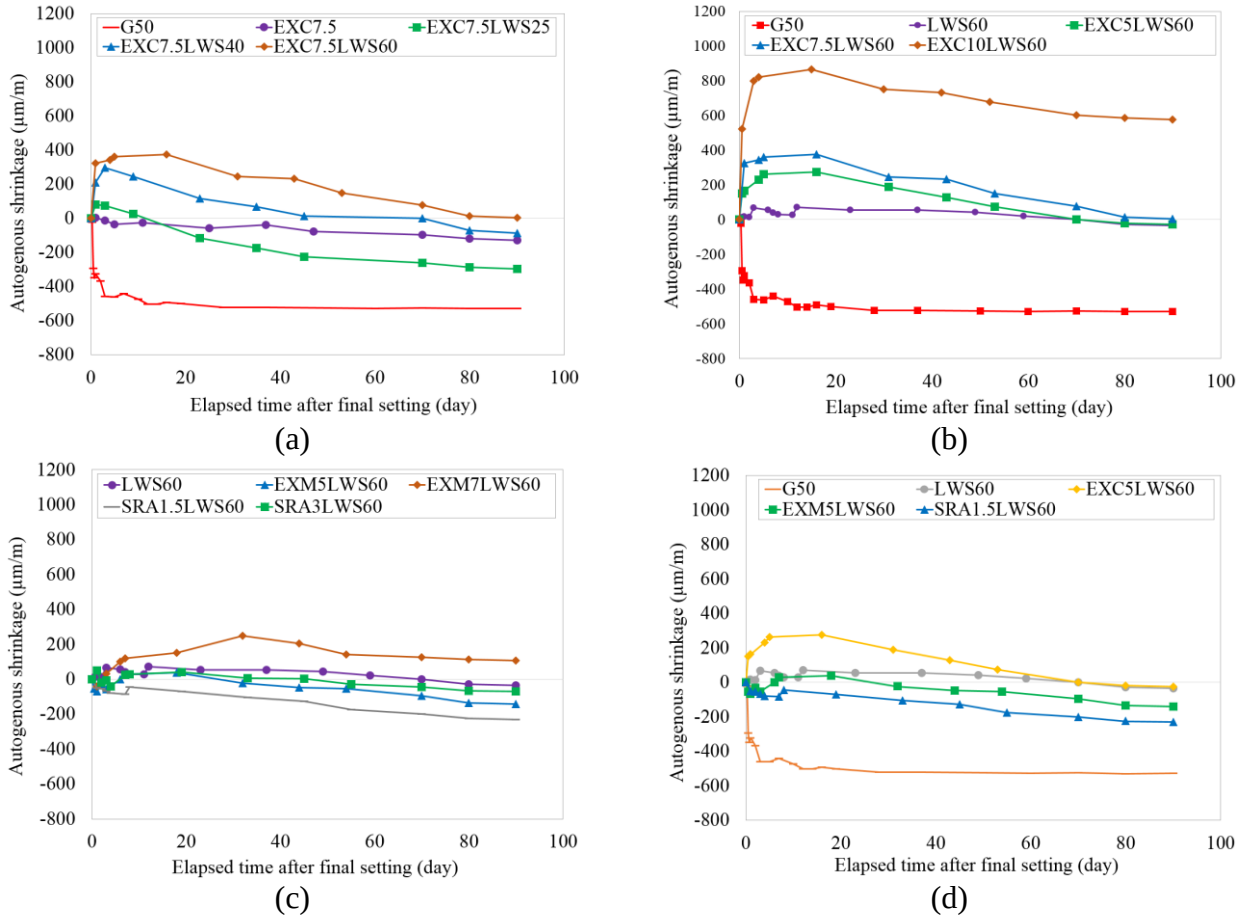

Figure 5-1 Variations in autogenous shrinkage for UHPC mixtures with different: (a) LWS contents; (b) EXC dosages; (c) EXM and SRA dosages; (d) shrinkage mitigating strategies at the low dosages (μm/m=με)

The combined use of different EXC replacements coupled with 60% LWS exhibited a significant effect on autogenous shrinkage. As shown in Figure 5-1(b), the use of the EXC developed the substantial expansion of 865 με at 15 d in the case of the EXC10LWS60 mixture. This was the highest expansion value among the investigated mixtures. The expansion increased with the EXC replacement level with the EXC5, EXC7.5, and EXC10 mixtures exhibiting 275, 375, and 865 με, respectively. Following the peak values, the shrinkage gradually increased and leveled off after 80 d; the EXC5LWS60 and EXC7.5LWS60 mixtures had 0 to 5 με and the EXC10LWS60 mixture had an expansion of 580 με.

As shown in Figure 5-1(c), the incorporation of 5% EXM coupled with 60% LWS had limited effect on the autogenous shrinkage of UHPC. Its shrinkage ended up at 140 με compared to 35 με shrinkage of the LWS60 mixture after 91 d. On the other hand, a greater dosage of 7% EXM with 60% LWS led to an expansion of 250 με at 28 d. Compared to the LWS60 mixture, the incorporation of SRA did not further reduce autogenous shrinkage, which may be due to the low capillary water in the UHPC system.

Figure 5-1(d) compares the autogenous shrinkage of UHPC mixtures made with the lower contents of the EXC, EXM, and SRA to those of the G50 and LWS60 mixtures. The reference G50 mixture had shrinkage of 528 με at 91 d; the other mixtures had 5 to 230 με at 91 d and the EXC5LWS60 mixture exhibited the highest expansion at early age (270 με).

5.2.2.2 Total shrinkage

Drying shrinkage was initiated following either 1, 3, and 7 d moist curing, which were designated as AD, 3MC, and 7MC, respectively. Drying shrinkage was monitored for 91 d, and the majority of the shrinkage occurred by 28 d. The total shrinkage is considered here as the sum of drying shrinkage at any given age and the autogenous shrinkage at the time of demolding. The total shrinkage results at different ages and curing conditions are reported in Table 5-3.

Table 5-3 Results for total shrinkage* of UHPC under different curing conditions (μm/m=με)

Mixture	1 d			3 d			7 d			28 d			91 d		
	AD	3MC	7MC	AD	3MC	7MC	AD	3MC	7MC	AD	3MC	7MC	AD	3MC	7MC
G50	-324	-324	-324	-536	-200	-208	-700	-632	-132	-782	-780	-728	-810	-820	-730
LWS60	18	18	18	-322	178	113	-598	-438	142	-780	-698	-580	-830	-750	-630
EXC7.5	3	3	3	-193	217	251	-420	-305	343	-517	-413	-350	-580	-465	-410
EXC7.5LWS25	81	81	81	-251	220	193	-368	-256	301	-623	-519	-460	-680	-575	-470
EXC7.5LWS40	211	239	239	-121	383	351	-225	-86	421	-430	-333	-289	-465	-370	-350
EXC7.5LWS60	239	245	245	-141	519	487	-377	-189	529	-513	-400	-273	-535	-453	-321
EXC5LWS60	165	165	165	-231	365	309	-455	-295	370	-570	-500	-371	-600	-551	-415
EXC10LWS60	522	522	522	122	862	800	2	162	910	-94	-26	254	-110	-30	105
EXM5LWS60	-68	-68	-68	-410	84	45	-600	-438	92	-730	-690	-560	-815	-750	-600
EXM7LWS60	-40	-40	-40	-310	152	110	-530	-330	175	-690	-528	-480	-756	-610	-520
SRA1.5LWS60	-50	-50	-50	-234	-10	6	-390	-310	46	-565	-550	-468	-680	-750	-550
SRA3LWS60	50	50	50	122	102	98	-222	-110	126	-318	-280	-250	-455	-366	-310

*Negative and positive values denote shrinkage and expansion, respectively.

The initial expansion observed during moist curing increased with LWS replacement level, regardless of the curing condition. The EXC7.5LWS60, EXC7.5LWS40, and

EXC7.5LWS25 mixtures exhibited initial expansions of 240, 210, and 80 με, respectively, in the case of the AD condition. The reference EXC7.5 mixture that had no residual shrinkage of early age. The maximum total shrinkage values of 25% and 60% LWS replacements were 580 and 465 με, respectively. The increase in moist-curing from 3 to 7 d had slight enhancement of initial expansion at early age. For example, the EXC7.5LWS60 mixture had initial expansion value of 520 με at the end of 3 d (3MC condition). Such value was 530 με at the end of 7 d for the 7MC condition. The increase of EXC dosage led to a significant reduction in shrinkage compared to the LWS60 mixture, especially for 10% EXC where the total shrinkage dropped from 535 to 110 με for the AD condition. This reduction of the total shrinkage was even enhanced with moist curing. For example, the EXC10LWS60 mixture achieved the highest initial expansion of 900 με in the 7MC condition ending up with a net expansion of 105 με after 91 d, compared to initial expansion of 520 με and total shrinkage of 110 με at 91 d when no moist curing was applied.

The shrinkage mitigating performance of the UHPC mixtures containing EXM 60% LWS improved with moist curing duration where a reduction of shrinkage by up to 30% at the end of 91 d of the 7MC condition was observed. The use of SRA in combination with 60% LWS was found to be effective in reducing the total shrinkage. For UHPC that had curing condition of AD, the incorporation of 1.5% and 3% SRA with 60% LWS led to the total shrinkage values of 680 and 450 με, respectively, compared to the LWS60 mixture with 830 με at 91 d. The initial expansion during moist curing period and shrinkage reduction after air drying slightly increased with moist curing. For example, the SRA3LWS60 mixture ended up with total shrinkage of 310 με with the 7MC condition compared to 455 με for the mixture without any moist curing (AD).

The variation of total shrinkage with time for the UHPC mixtures containing EXC in combination with 60% LWS after different curing conditions is illustrated in Figure 5-2. Applying 3 d of moist curing is shown to significantly increase the initial expansion. However, no significant improvement of initial expansion was observed after extending the moist curing period from 3 to 7 d. The EXC10LWS60 mixture exhibited a maximum initial expansion of 520, 870, and 910 με for curing conditions of AD, 3MC, and 7MC, respectively. The total shrinkage variations became stabilized after 28 d, regardless of curing condition. The same trend was observed for the EXC5LWS60 mixture, as shown in Figure 5-2(d). An increase in initial expansion from 165 to 365 με was observed for the mixture subjected to 3 d of initial moist

curing compared to AD. However, no significant additional expansion was exhibited for 7 d of moist curing.

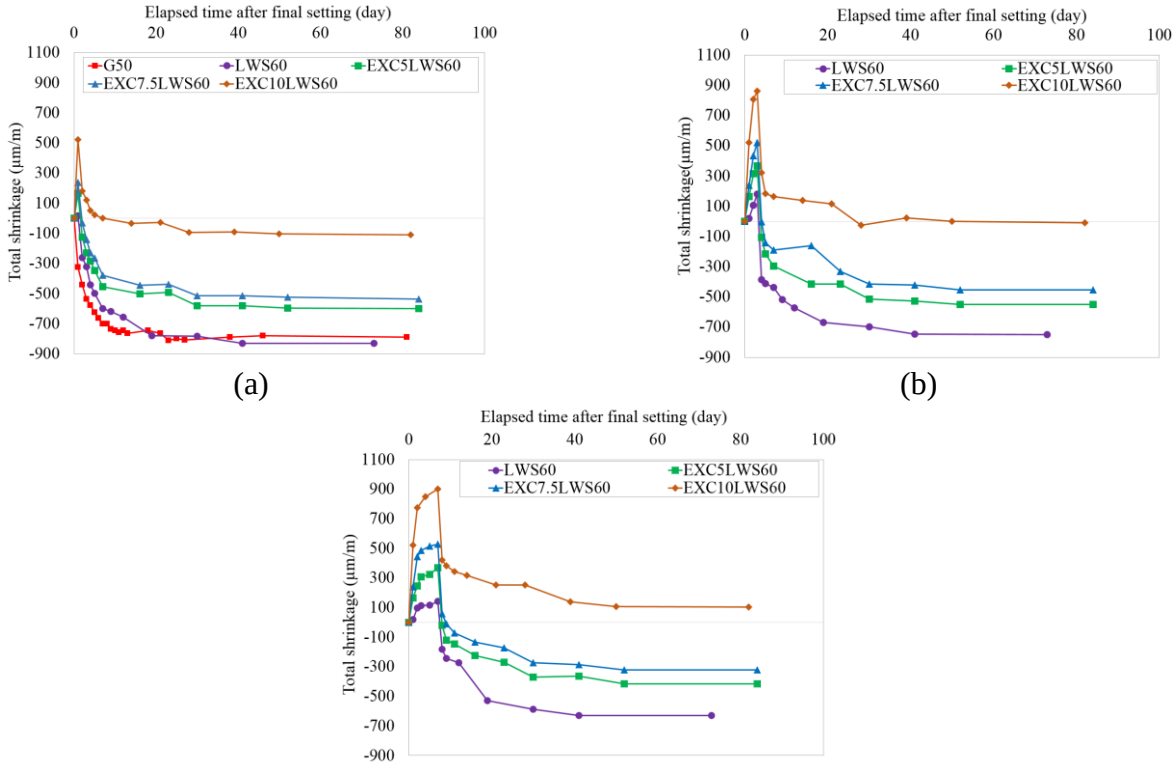

Figure 5-2 Variations in total shrinkage of UHPC mixtures with 60% LWS and different EXC contents and initial moist curing periods: (a) 1 d; (b) 3 d; and (c) 7 d of curing condition (μm/m=με)

Figure 5-3 compares the total shrinkage of the tested UHPC mixtures at 91 d for samples subjected to 1, 3, and 7 d of initial moist curing. All mixtures exhibited lower shrinkage with the increase of moist curing duration. Unlike UHPC mixtures of 60% LWS and other EXs, the G50 reference mixture had greater shrinkage values regardless of the moist curing regime. The LWS60 mixture with no EX had an initial expansion of 180 με at the end of 3 d. As expected, the increase of replacement level of LWS from 25% to 60%, EXC dosage from 5% to 10%, EXM content from 5% to 7%, and SRA concentration from 1.5% to 3% resulted in greater initial expansion during the moist curing period and lower total shrinkage upon drying. The EXC10LWS60 mixture had the best performance in terms of total shrinkage reduction where it obtained the highest expansion of 850 and 910 με at 3 and 7 d of the 3MC and 7MC conditions,

respectively. It was also the only UHPC mixture with the expansion of 110 με at 91 d of the 7MC condition.

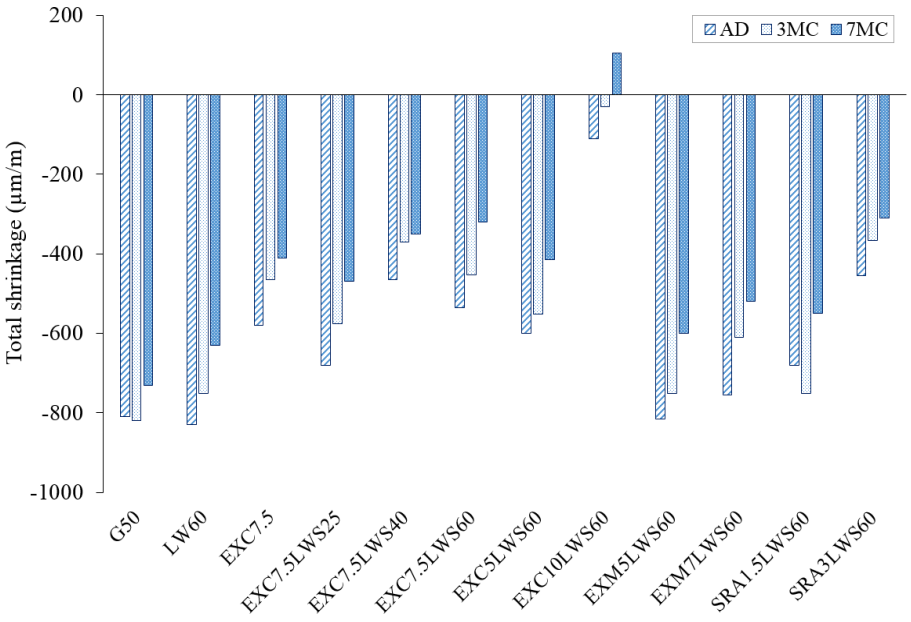

Figure 5-3 Total shrinkage results of UHPC mixtures at 1 d of AD, 3 d of 3MC, 7 d of 7MC, and 91 d of each curing regime, respectively (μm/m=με)

5.2.3. Compressive Strength

Table 5-4 presents the compressive strength of the 12 investigated mixtures subjected to different curing conditions. The coefficient of variation (COV) of the strength results ranged between 0.2% and 5.5%, which indicates good reproducibility of the test results. The lowest 91 d compressive strength was 87 MPa (12.6 ksi) for the G50 mixture that was air-cured (AD). The LW60 mixture subjected to 7 d of moist curing (7MC) had the highest compressive strength of 148 MPa (21.5 ksi).

As shown in Figure 5-4(a), regardless of the moist curing regime, the use of LWS showed a clear benefit in enhancing compressive strength. The mixtures with LWS had greater compressive strength than the G50 and EXC7.5 mixtures without LWS. The latter mixture exhibited lower compressive strength than the G50 mixture. The use of LWS with 7.5% EXC enhanced compressive strength by up to 45% compared to the EXC7.5 mixture without any LWS. Higher LWS replacements led to slightly greater compressive strength. The use of 25% LWS increased compressive strength by 10% to 30% compared to the reference EXC7.5 mixture. Further increase in LWS had limited effect on compressive strength (less than 10%).

The enhancement of compressive strength with the inclusion of the LWS is attributed to its internal curing function, given the very low w/cm of the tested material. Similar observations were reported by Meng and Khayat (2017) where the use of LWS up to 75% in UHPC with 0.20 w/cm was shown to increase the degree of hydration and mechanical properties.

Table 5-4 Compressive strength results for investigated UHPC mixtures

Test		G50	LWS60	EXC7.5	LWS?+EXC7.5			EXC?+LWS60		EXM?+LWS60		SRA?+LWS60	
					25	40	60	5	10	5	7	1.5	3
Comp. str.-AD (MPa)	7	66 (1.5*)	99 (2.3)	66 (2.6)	84 (2.6)	87 (2.3)	96 (2.4)	98 (3.2)	88 (4.4)	85 (2.7)	77 (2.8)	80 (1.8)	71 (3.4)
	28	80 (1.8)	120 (1.7)	83 (5.0)	104 (1.0)	108 (3.3)	110 (3.3)	115 (2.6)	108 (4.4)	102 (4.8)	98 (4.2)	123 (3.0)	118 (1.6)
	56	85 (3.6)	127 (4.4)	88 (3.8)	111 (1.2)	114 (4.6)	119 (3.7)	124 (2.1)	118 (4.1)	110 (4.7)	104 (1.6)	128 (2.4)	123 (2.6)
	91	87 (2.2)	130 (1.8)	90 (0.2)	115 (0.9)	118 (1.5)	122 (4.1)	129 (0.8)	120 (5.2)	114 (3.2)	107 (1.7)	131 (1.1)	127 (0.6)
Comp. str.-3MC (MPa)	7	77 (0.8)	112 (1.6)	68 (3.5)	89 (3.8)	93 (0.9)	102 (0.5)	102 (3.6)	92 (2.3)	90 (3.2)	79 (2.8)	83 (1.9)	74 (3.1)
	28	96 (1.5)	132 (2.7)	93 (3.5)	112 (2.2)	115 (4.4)	118 (2.9)	120 (2.4)	107 (2.4)	112 (5.2)	107 (2.2)	125 (2.7)	122 (0.6)
	56	103 (0.4)	139 (2.5)	101 (0.9)	118 (4.6)	120 (0.4)	128 (0.7)	128 (1.5)	122 (3.1)	117 (1.5)	112 (4.5)	131 (3.4)	126 (4.7)
	91	105 (3.2)	142 (0.8)	104 (4.2)	122 (2.2)	124 (1.5)	131 (3.4)	134 (1.1)	126 (3.1)	125 (1.0)	119 (1.8)	135 (3.3)	129 (1.1)
Comp. str.-7MC (MPa)	7	83 (3.5)	119 (1.4)	72 (3.0)	92 (3.7)	97 (1.0)	104 (1.8)	107 (3.0)	93 (3.2)	94 (4.6)	80 (4.2)	86 (2.3)	79 (1.9)
	28	106 (2.2)	142 (4.6)	97 (1.9)	117 (3.9)	120 (5.5)	123 (2.3)	126 (0.8)	111 (2.0)	119 (1.3)	111 (2.7)	127 (1.9)	124 (2.4)
	56	112 (3.0)	146 (1.3)	105 (4.6)	126 (2.9)	129 (0.6)	131 (1.0)	135 (3.4)	126 (3.9)	124 (0.6)	118 (4.6)	134 (1.7)	131 (1.3)
	91	115 (1.7)	148 (2.0)	110 (2.3)	129 (1.1)	132 (1.1)	136 (0.6)	140 (0.9)	130 (3.3)	128 (3.0)	122 (1.1)	138 (3.6)	133 (1.4)
Comp. str.-MC (MPa)	28	108 (2.0)	129 (2.0)	98 (3.4)	109 (3.6)	108 (4.2)	111 (3.7)	117 (4.4)	109 (4.6)	107 (2.4)	98 (3.6)	118 (1.9)	115 (3.7)
	56	115 (1.3)	139 (4.6)	109 (2)	114 (1.2)	117 (3.6)	126 (2.3)	131 (3.6)	126 (1.2)	125 (2.0)	103 (4.0)	128 (2.4)	130 (4.7)
	91	120 (0.6)	143 (3.1)	112 (2.2)	120 (2.4)	124 (1.2)	130 (0.5)	133 (2.1)	127 (1.8)	129 (3.3)	115 (2.9)	130 (5.1)	132 (3.9)

* C.O.V. (%)

Note: 1 MPa = 145 psi

Compared to the LWS60 mixture, the combined use of either EXC, EXM, or SRA with 60% LWS decreased the compressive strength by up to 30%, 40%, and 40%, respectively. Strength loss increased with the increase of dosage of the shrinkage mitigating admixture. As shown in Figure 5-4(b), for the UHPC mixtures made with different EXC contents with 60%

LWS, increasing the replacement level of the EXC (5% to 10%) resulted in compressive strength loss from 140 to 130 MPa (20.3 to 18.9 ksi). The same trend was observed for the EXM (5% to 7%), and the SRA (1.5% to 3%) where shrinkage drop was from 128 to 122 MPa (18.6 to 17.7 ksi), and 138 to 133 MPa (20.0 to 19.3 ksi), respectively, at 91 d for the 7MC condition.

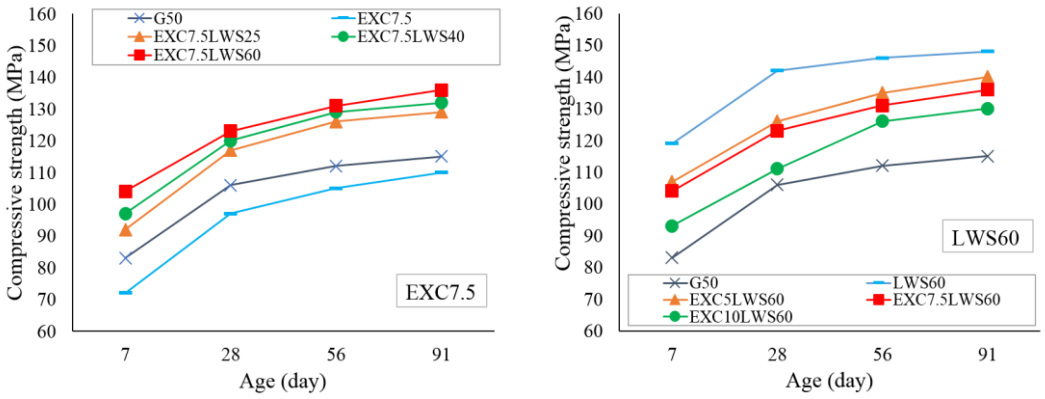

Figure 5-4 Variations of compressive strength of investigated UHPC over age at 7MC curing condition: (a) LWS contents; (b) EXC dosages, (Note: 1 MPa = 145 psi)

The impact factor of the EX on mechanical properties of the concrete relies on the effect of the expansion volume generated in the microstructure (Higuchi et al., 2014). The expansion can refine the microstructure, thus resulting in a decreased size and volume of the total porosity and enhanced mechanical properties. However, excessive expansion can cause cracking of the concrete, particularly at the interface between aggregate and cementitious matrix (Higuchi et al., 2014).

As indicated in Figure 5-5, the increase in the period of moist curing from 1 to 3 and 7 d had a significant effect on the 91 d compressive strength of UHPC, especially when no LWS was used. The two reference mixtures, G50 and EXC7.5, showed a consistent increase in compressive strength with the duration of moist curing. The compressive strengths of the G50 and EXC7.5 mixtures increased from 87 and 90 MPa (12.6 and 13.1 ksi) under air dried (AD) condition to 115 and 110 MPa under 7MC curing condition (16.7 and 15.9 ksi), respectively,. These mixtures exhibited a slight increase in compressive strength at 91 d under continuously moist cured, which were 120 and 112 MPa (17.4 and 16.2 ksi), respectively.

On the other hand, the benefit of moist curing condition was limited in UHPC with LWS. Figure 5-5 illustrates that the compressive strength of the EXC10LWS60 mixture of 91 d for curing conditions of the AD and 7MC were 122 and 136 MPa (17.6 and 19.7 ksi), respectively. Further increase in moist curing (MC) led to lower 91 d compressive strength. For example, mixtures containing the 7.5% EXC and 60% LWS had approximately 10% lower at 91 d than concrete that subjected to 7 d of moist curing followed by air drying. This can be due to the relatively lower relative humidity of the 7 MC concrete at the time of testing (91 d) than that of the MC specimens, which can increase strength.

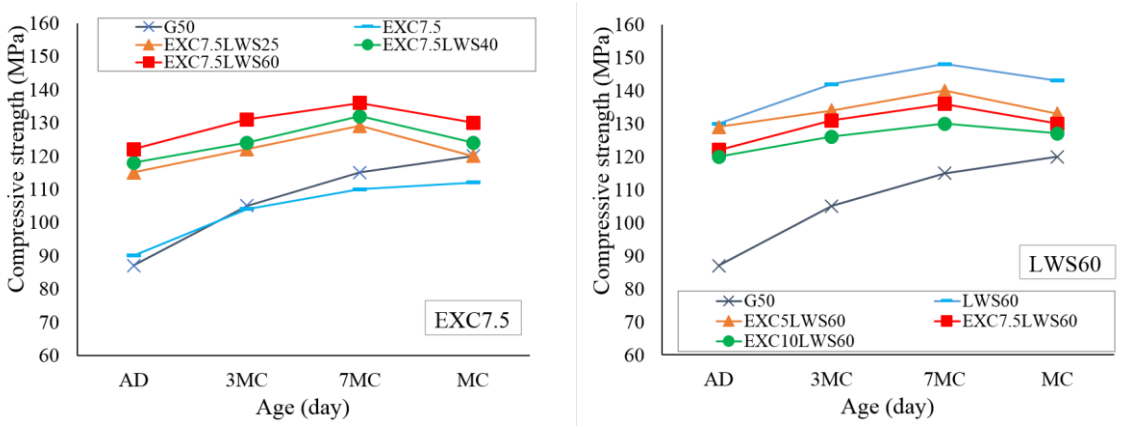

Figure 5-5 Variations of compressive strength of the investigated UHPC mixtures over different curing conditions at 91 d: (a) LWS contents; (b) EXC dosages, (Note: 1 MPa = 145 psi)

Regardless of the shrinkage-mitigating admixture, the highest compressive strength was obtained for the EXC5LW60 mixture, which was 140 MPa (20.3 ksi) when subjected to 7 d of moist-curing (7MC). The compressive strengths of UHPC mixtures made with combinations of EXC, EXM, or SRA with 60% LWS were greater than that of the G50 mixture but lower than that of the LWS60 mixture, regardless of the curing condition. The same trend occurred for mixtures containing EXC, EXM, or SRA combined with 60% LWS where extending moist curing period up to 7 d enhanced compressive strength. However, the 91 d compressive strengths of all UHPC mixtures, except the reference G50 mixture, were lower than those subjected to 7 d of moist curing followed by air drying, as shown in Figure 5-5(a) and (b). For example, the 91 d compressive strength of the EXC10LWS60 mixture increased from 120 MPa (17.4 ksi) in the

AD condition to 126 and 130 MPa (18.3 and 18.9 ksi) at the 3MC and 7MC conditions, respectively, but dropped to 126 MPa (18.3 ksi) with the MC curing condition.

5.3. SUMMARY

This chapter investigated the effect of LWS, SRA, EXC, and EXM on compressive strength, autogenous and drying shrinkage of UHPC. Based on the results, the following conclusions can be drawn:

(1) The incorporation of 25% to 60% pre-saturated LWS resulted in considerable decrease in HRWR demand (1.23% to 1.05%) compared to the EXC7.5 mixture (2.3%) required to secure self-consolidating characteristics. The EXC5LW60 and EXC7.5 mixtures exhibited the lowest and highest values of HRWR demand, respectively. The content of LWS necessary to compensate chemical shrinkage for the investigated UHPC was 35%, by volume of sand.

(2) The combined use of 60% LWS and EXC, EXM, or SRA had a positive effect on reducing mini-slump flow and mini V-funnel losses with time. The fastest and slowest flow times after 70 min were obtained in the EXC7.5LWS60 and EXC7.5 mixtures. The combined use of EXC, EXM, or SRA with LWS significantly shortened the final setting times. The reference G50 mixture had final setting time of 17.5 h and decreased to 6-8 h for the mixtures with LWS and 7.5% EXC.

(3) The coupled effect of incorporating EXC with 60% LWS resulted in a significant effect on controlling autogenous shrinkage of UHPC. The EXC10LWS60 mixture had the highest expansion of 865 με and exhibited expansion value of 580 με at 91 d compared to the reference G50 mixture that had a shrinkage of 530 at 91 d.

(4) The coupled effect of LWS and EXC for different curing conditions indicate that increasing LWS and EXC replacement levels along with extending moist curing significantly improved expansion during moist curing period and reduced total shrinkage thereafter. The EXC10LWS60 mixture had the best performance in terms of total shrinkage (expansion of 110 με at 91 d) following 7 d of moist curing. The use of SRA or EXM in combination with 60% LWS was effective in reducing total shrinkage by up to 30%.

(5) The increase in the period of moist curing from 1 to 3 and 7 d had a significant effect on the 91 d compressive strength of UHPC. Such increase was by up to 35% for UHPC with no LWS and 15% for that with 60% LWS.

(6) The combined use of either EXC, EXM, or SRA with 60% LWS decreased 91 d compressive strength under 7MC ranging from 8 to 20 MPa (1.2 to 2.9 ksi) compared to 60% LWS. Further increase in EXC content from 5% to 10%, EXM from 5% to 7%, and SRA from 1.5% to 3% in mixtures subjected to 7 d of moist curing resulted in 91 d compressive losses of 10, 6, and 5 MPa (1.5, 0.9, and 0.7 ksi), respectively.

6. PERFORMANCE OF UHPC AS BONDED OVERLAYS

The main purpose of the work presented in this chapter is to verify the feasibility of using UHPC as thin bonded concrete overlay. Optimized UHPC mixtures that were developed to secure superior workability, cracking resistance, bonding performance, along with strength and durability were used as bonded overlays. In total, 16 slabs made of different mixture proportions were constructed to compare the performance UHPC overlays of different thicknesses to that of latex-modified concrete and conventional portland cement concrete.

6.1. PREPARATION OF SUBSTRATE

A total of 16 substrate slabs were cast outdoor using a conventional concrete (CC) delivered by a local ready mix concrete supplier. The slabs measured 2 × 1.5 m (21.5 × 16.1 ft) with a depth of 150 mm (5.9 in.). The CC mixture for the slabs was designed according to the typical MoDOT mixture design for bridge decks. All slabs were reinforced with two mats of longitudinal #4 bars (nominal diameter of 12.7 mm = 0.5 in.). The mats were placed at the top and bottom parts of the slabs with bar space of 250 mm (9.8 in.). The top and bottom rebar mats were located 25 and 50 mm (0.98 and 2 in.) from the top and bottom of the concrete, respectively. The slabs were demolded after 24 hr and then moisture cured for 14 d using wet burlap and a plastic sheet. They were then allowed to air dry outdoor for about 12 months prior to applying the overlays. Figure 6-1 shows the prepared substrate concrete slabs exposed to air drying.

Figure 6-1 Concrete pavement sections as substrate

6.2. SURFACE PREPARATION

Proper substrate surface preparation prior to application of overlay materials is of critical importance to a long-lasting bond between the existing concrete substrate and the overlay material. A chemical surface retarder was used to provide an aggregate exposed surface on the substrate concrete. The retarder was uniformly applied with a low-pressure pump-up type garden sprayer onto the surface of the concrete immediately after final finishing. The retarded mortar was flushed off with a stream of water and removed by scrubbing with a stiff brush 24 hr after application to expose the aggregate. The final prepared surface is shown in Figure 6-2.

Figure 6-2 Substrate surface preparation

6.3. INSTRUMENTATION PLAN

The substrate slabs were fully instrumented with strain gauges, relative humidity sensors, and thermocouples after adequate air drying. The instrumentation plan aimed to monitor the concrete shrinkage deformation, humidity and temperature variations at the interface layer over time after applying the optimized overlay materials.

The embedment type of strain gauges manufactured by KYOWA (120-120-H2-11) was used to measure the shrinkage deformations. Figure 6-3 shows the embedment strain gauge. The sensors are designed with the outer body of 120 mm (4.7 in.) sensing grid with an effective gauge length of 75 mm (2.9 in.). The sensor consists of a 75 mm (2.9 in.) 120 ohm (Ω) foil strain gauge (nickelchromium alloy on polymide backing). The gauges feature a specially treated

surface with a honeycomb pattern, providing an adequate bond to concrete. They provide suitable waterproofness and elastic modulus to be able to embed in fresh mortar or concrete to measure the internal stress.

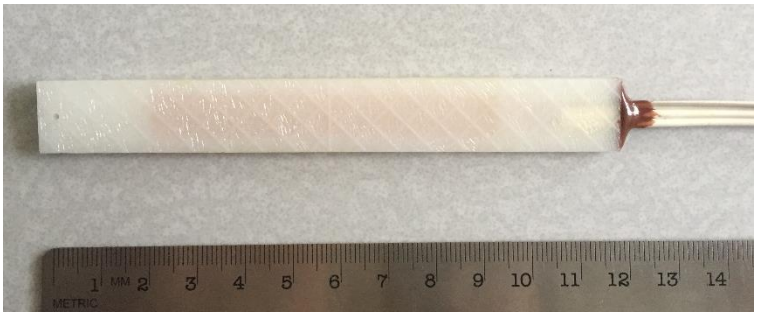

Figure 6-3 Embedded strain gauge for monitoring shrinkage deformation

Type T 20 gauge wires produced by Coleparmer (UX-08542-24) were used as thermocouples. These thermocouples are functional between -250 and +250 °C (-418 and +418 °F) as they consist of copper and constantan wires. The ends of the solid thermocouple wires were twisted and then soldered in order to make an adequate electrical connection.

The capacitive relative humidity sensors manufactured by Sparkfun (HIH-4030), measuring 6 × 20 mm (0.2 × 0.8 in.), were used to measure the RH at the interface layer. The accuracy of the sensors is ± 2% RH between 10% and 90% RH, and range up to ± 4% at 100% RH, as reported by the manufacturer. Each RH sensor was encased in a 12 mm (0.468 in.) PVC tube with covered ends to be able to be embedded inside concrete because the sensors were not waterproof. The end intended to be positioned inside concrete at the interface layer was covered with Gore-tex to allow humidity transmission while preventing the penetration of concrete inside the pipe. The RH sensor, used for embedding in concrete, is shown in Figure 6-4.

Figure 6-5 demonstrates the instrumentation layout. Each slab was instrumented at three different measurement locations of A, B, and C. As shown in Figure 6-6, three sensors, including embedded concrete strain gauge, relative humidity sensor, and thermocouple were installed at the interface layer of each measurement location to monitor the concrete strain, RH, and temperature, respectively.

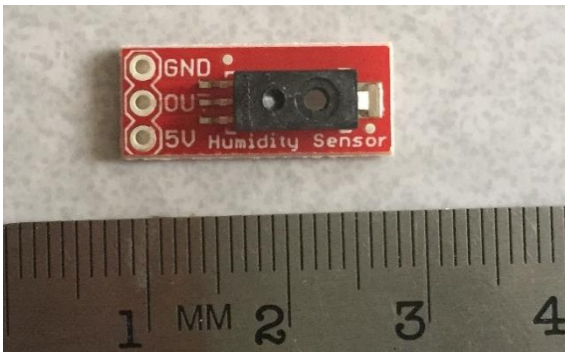

Figure 6-4 Relative humidity sensor

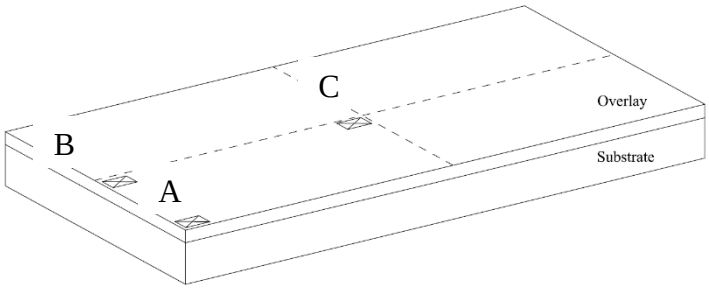

(a)

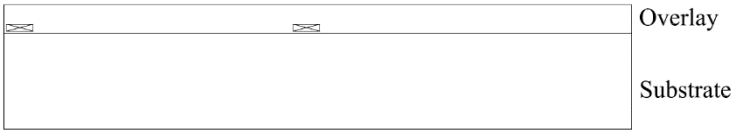

(b)

Figure 6-5 Sensor locations: (a) overall view; (b) lateral view of experimental pavement section

Figure 6-6 Embedded sensors of strain, temperature, and RH at each measurement location

All variations were recorded using Campbell Scientific data acquisition hardware and software, as shown in Figure 6-7. Lead wires from the strain gauges were routed through an AM16-32 multiplexer, using a separate completion module for each gauge on the multiplexer. The data logger used was a Campbell Scientific CR1000. The thermocouple wires were routed through an AM25T multiplexer, which has an internal RTD (resistance temperature detector) to measure the cold junction temperature required to compute the temperature at the soldered end of the thermocouple. The multiplexer was controlled by the CR1000 data logger.

Figure 6-7 Data acquisition system

Table 6-1 presents the investigated concrete overlay characteristics. In total, 11 stabs with UHPC overlay, three slabs with latex-modified concrete (LMC) overlay, and two reference concrete overlays cast at three thicknesses of 25, 38, and 50 mm (1, 1.5, and 2 in.) were cast. The UHPC mixtures had steel fiber volumes of 2% and 3.25%.

Table 6-1 Cast slabs characteristics

Slab No.	Overlay type	Mixture characteristics	Thickness (mm)	Steel fiber volume (%)
1	UHPC 1	EXC 10% - LWS 60%	25	2
2	UHPC 1	EXC 10% - LWS 60%	38	2
3	UHPC 1	EXC 10% - LWS 60%	50	2
4	UHPC 1	EXC 10% - LWS 60%	38 (Repeat)	2
5	UHPC 2	EXC 10% - LWS 60%	25	3.25
6	UHPC 2	EXC 10% - LWS 60%	38	3.25
7	UHPC 2	EXC 10% - LWS 60%	50	3.25
8	UHPC 3	EXC 5% - LWS 60%	38	2
9	UHPC 3	EXC 5% - LWS 60%	25	2
10	UHPC 4	EXC 0% - LWS 60%	38	2
11	UHPC 5	EXC 0% - LWS 0%	38	2
12	Latex modified concrete	MoDOT section 505.20	25	0
13	Latex modified concrete	MoDOT section 505.20	38	0
14	Latex modified concrete	MoDOT section 505.20	50	0
15	Reference	MoDOT modified B-2	38	0
16	Reference	MoDOT modified B-2	50	0

Note: 1 mm = 0.039 in.

The mixing, placement, and finishing of the various overlay materials are presented in Figure 6-8. Immediately after casting, all slabs were stored indoor. The top surface of each overlay was covered with wet burlap and plastic sheet. The wet cover for the UHPC, LMC, and reference mixtures was maintained until 7, 2, and 3 d, respectively, to provide sufficient moisture conditions. The wet curing durations for LMC and reference mixtures were according to MoDOT recommendations for bridge deck concrete wearing surface (Section 505). Following the moist curing period, the burlaps and plastic sheets were removed, and the slabs were exposed to air drying indoor, as shown in Figures 6-9 and 6-10. The lateral sides of the overlays were sealed to allow temperature and RH transmission to happen only from top surfaces.







Figure 6-8 Preparation and casting of UHPC overlay

Figure 6-9 Prepared slabs were stored indoor

Figure 6-10 Composite slabs with sensors at three different locations

6.4. SHRINKAGE, RH, AND TEMPERATURE MEASUREMENTS

Figure 6-11 presents the results of total shrinkage deformation at the interface layer of different measurement stations in the investigated slabs. Negative and positive values in this figure correspond to shrinkage and expansion of the overlay mixture, respectively. As mentioned earlier, the UHPC, LMC and reference overlays were subjected to wet curing using wet burlap and a plastic sheet for 2, 3, and 7 d before exposure to air drying. The results of shrinkage

deformation were shown to be a function of the UHPC mixture design, location, and overlay thickness, as discussed below.

6.4.1. Effect of Overlay Type

Figure 6-11 shows the total shrinkage variations over time at location A of concrete overlays measuring 38 mm (1.5 in.) in thickness for overlays made with UHPC (EXC10LWS60, EXC5LWS60, LWS60, and G50), LMC, and reference concrete. The results indicate that the incorporation of EXC at replacement levels of 5% and 10%, combined with 60% LWS resulted in considerable decreased the total shrinkage. The expansion increased with the EXC content, where the EXC10LWS60 mixture developed a substantial expansion of 637 με at 7 d. This was the highest expansion among the investigated mixtures, followed by the EXC5LWS60 and LWS60 mixtures with 200 and 120 με at 7 d, respectively. Following expansion peak values, the expansion gradually decreased; the EXC10LWS60 and EXC5LWS60 mixtures had 469 to 95 με at 195 and 175 d, and the LWS60 mixture still exhibited a small expansion of 5 με at 185 d. The G50 mixture without EXC and LWS exhibited the highest total shrinkage value of 105 με at 175 d. The reference and LMC mixtures showed total shrinkage values of 45 and 65 με at 120 and 165 d, respectively, after a slight initial expansion.

6.4.2. Effect of Overlay Thickness

Figure 6-12 presents the total shrinkage deformation of the EXC10LWS60 mixture with different thicknesses of 25, 38, and 50 mm (1, 1.5, and 2 in.) at location A. Results indicated that the initial expansion increased with the decrease of overlay thickness. The UHPC overlay mixture made with 10% EXC combined with 60% LWS with 25 mm (1 in.) in thickness exhibited the highest expansion of 850 με at 7 d. The same mixture with 38 and 50 mm thickness (1.5 and 2 in.) showed 660 and 485 με maximum initial expansions at 7 d, respectively. Following the peak values, the initial expansion gradually decreased. However, the EXC10LWS60 mixture with thicknesses of 25, 38, and 50 mm (1, 1.5, and 2 in.) still exhibited an expansion of 740, 480, 380 με after 190, 195, and 205 d, respectively.

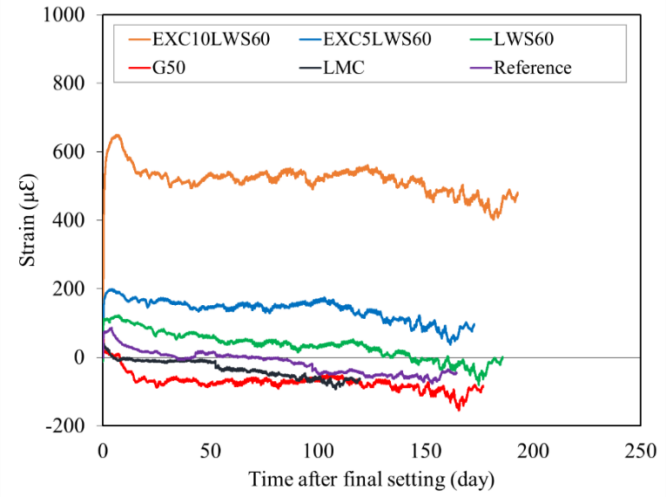

Figure 6-11 Total shrinkage deformation of various investigated overlay types with 38 mm thickness at location A, (Note: 1 mm = 0.039 in.)

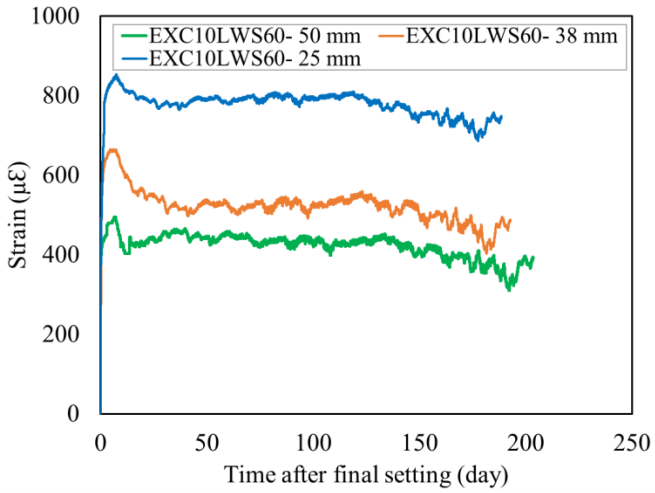

Figure 6-12 Total shrinkage deformation of the EXC10LWS60 mixture with different thicknesses of 25, 38, and 50 mm at location A, (Note: 1 mm = 0.039 in.)

6.4.3. Effect of Steel Fiber Content

As indicated earlier, the EXC10LWS60 UHPC overlay made with two steel fiber contents of 2% and 3.25%, by volume, was used to evaluate the effect of steel fiber volume in the bonded overlay performance. Figure 6-13 shows the total shrinkage deformation of the EXC10LWS60 mixture with steel fiber volumes of 2% and 3.25%, with overly thickness of 38 mm (1.5 in.) at location A. Results indicated that the higher volume of steel fiber resulted in lower expansion. Both mixtures with 2% and 3.25% steel fiber volume exhibited a similar general behavior in terms of deformation variations. However, the mixture made with 2% steel

fiber volume had the higher initial expansion value of 640 με compared to that of 3.25% with 490 με, both at 7 d. Following the maximum initial expansion value, the mixtures with 2% and 3.25% leveled off with an expansion of 480 and 380 με at 195 and 135 d.

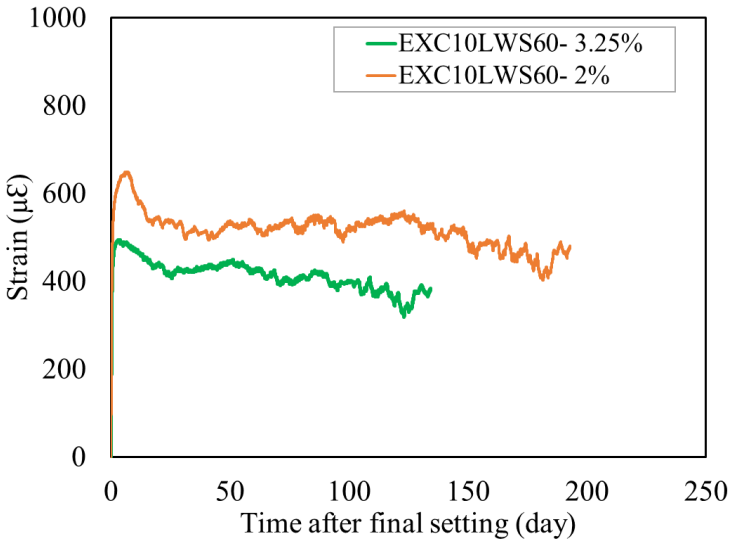

Figure 6-13 Total shrinkage deformation of the EXC10LWS60 mixture with steel fiber volumes of 2% and 3.25%, with overlay thickness of 38 mm at location A

6.4.4. Temperature and Relative Humidity Variations

As mentioned earlier, all four lateral sides of the overlays were sealed to allow temperature and RH transmission to happen only at the top surface of the slabs. As a result, no significant difference was observed in temperature and RH variations among different measurement locations of A, B, and C. All mixtures exhibited a saturated condition (100% RH) during the wet curing period. The RH gradually dropped right after exposing the slabs to air drying. RH variations reached to a stabilized range of 65% - 80%, depending on the overlay mixture type and thickness. Figure 6-14 presents the RH variations of the EXC10LWS60 mixture with overlay thickness of 38 mm (1.5 in.) at measurement locations of A, B, and C.

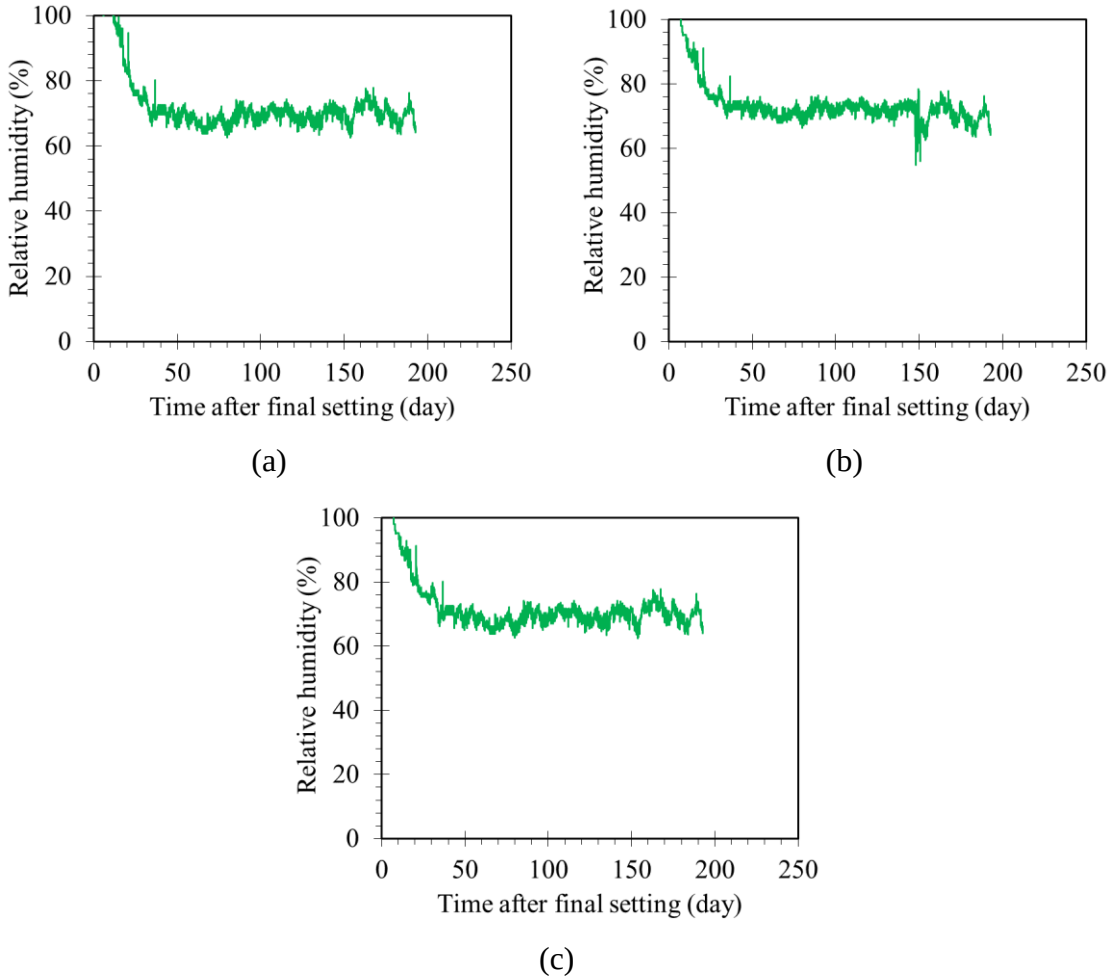

Figure 6-14 RH variations of the EXC10LWS60 mixture with overlay thickness of 38 mm at locations: (a) A; (b) B; (c) C

Temperature variations showed a high temperature after the first 24 h of casting by up to 40 °C (104 °F) for all of the investigated mixtures. However, after 24 h, the temperature gradually reached nearly ambient temperature.

Figure 6-15 presents the temperature variations of the EXC10LWS60 mixture with overlay thickness of 38 mm (1.5 in.) at measurement locations of A, B, and C. The temperature kept fluctuation around 20 °C, regardless of locations and time.

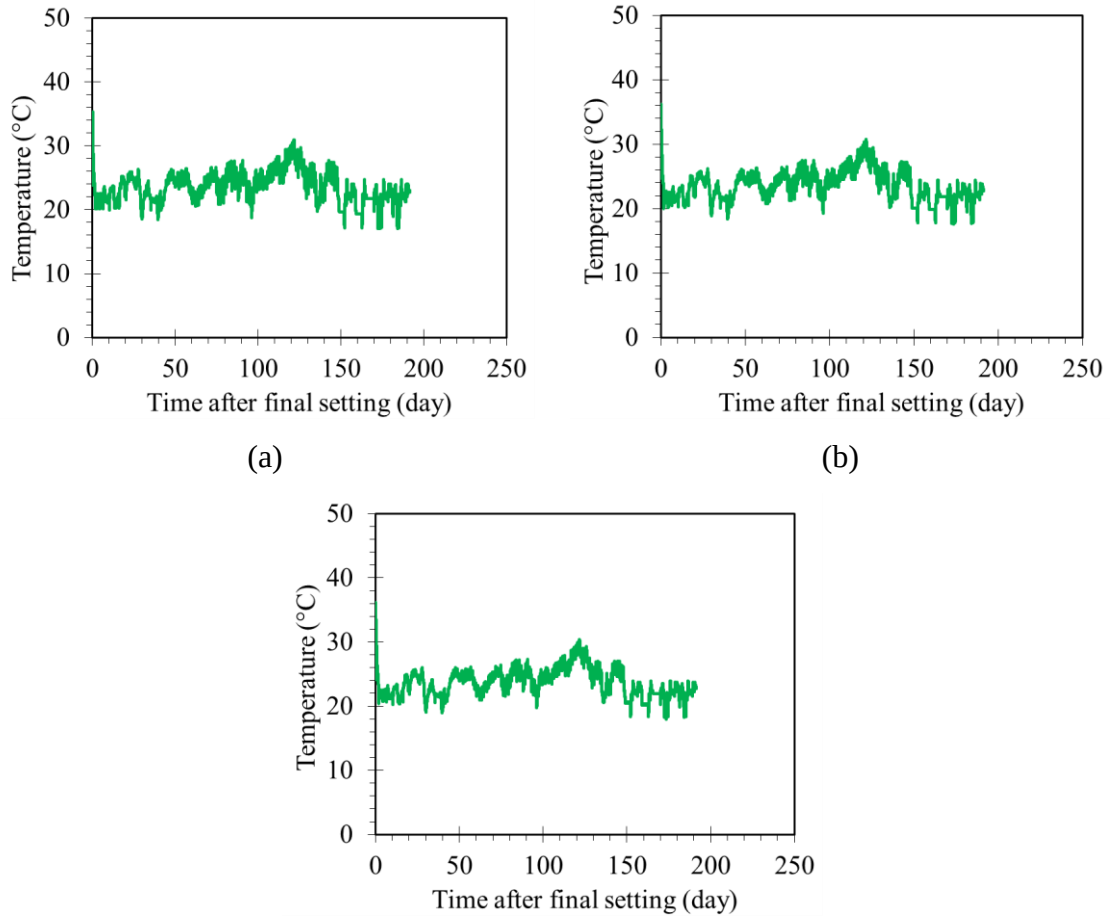

Figure 6-15 Temperature variations of the EXC10LWS60 mixture with overlay thickness of 38 mm at locations: (a) A; (b) B; (c) C, (Note: 1 °C = 33.8 °F, 1 mm = 0.039 in.)

6.4.5. Overall Performance

Visual and microscopic inspections of UHPC overlays at the surface and interface layer showed no signs of cracking and debonding after more than 200 d of casting.

6.5. SUMMARY

In this chapter, 16 slabs made of different mixture proportions were constructed to compare the performance of UHPC overlay materials to those of LMC and conventional portland cement concrete overlays. Based on the results, the following conclusions can be drawn:

(1) The results of shrinkage deformation were shown to be a function of concrete mixture design, location, and UHPC overlay thickness.

(2) The incorporation of EXC at replacement levels of 5% and 10%, combined with 60% LWS resulted in considerable decrease in total shrinkage. The UHPC overlay mixture made with 10% EXC combined with 60% LWS with 25 mm (1 in.) in thickness exhibited the highest expansion of 850 με at 7 d. The same mixture with 38 (1.5 in.) and 50 mm (2 in.) showed 660, and 485 με maximum initial expansions at 7 d, respectively.

(3) Temperature variations showed a high temperature during the first 24 h of casting by up to 40 °C (104 °F) for all of the investigated mixtures. However, after 24 h, the temperature gradually reached close to the ambient temperature varying between 20 to 50 °C (68 to 122 °F). All mixtures exhibited a saturated condition (100% RH) during the wet curing period. The RH gradually dropped right after exposing the slabs to air drying. RH variations reached stabilized range of 65% to 80%, depending on the overlay mixture type and thickness. Visual and microscopic inspections of UHPC overlays at the surface and interface layer showed no signs of cracking and debonding after more than 200 d of casting.

(4) UHPC made with 50% GGBS, 5% to 10% EXC, and 60% LWS reinforced with 2% steel fiber (by volume), is recommended for field implementation. A clean aggregate exposed surface on the substrate concrete is of critical importance to a long-lasting bond, which can be attained by hydrodemolition method. It is recommended to apply at least 7 d moist curing (wet burlap covered by a plastic sheet) immediately after UHPC casting.

7. LIFE CYCLE COST ANALYSIS OF UHPC OVERLAY

Life cycle cost analysis (LCCA) is an engineering economic analysis tool that can allow transportation officials to quantify the differential costs of alternative investment options for a given project. In this chapter, LCCA was determined for selected concrete mixtures with different mixture compositions and performance characteristics.

7.1. MATERIAL UNIT COST

Table 7-1 lists mixture proportions and cost estimation of three selected mixtures investigated in this research, including UHPC (EXC10LWS60), LMC, and MoDOT Reference mixtures. The cost of LMC and UHPC overlays have a wide range of values due to different mixtures, that might even be inconsistent in many cases (Alhassan and Ashur, 2014). For the LCCA case study, triangular distributions were used for the probabilistic approach based on information provided by the FHWA (Harber et al., 2017). Mean or most likely values were used for the deterministic approach.

Table 7-1 Mixture proportions and cost estimation of overlay mixtures ($/m^3)

	MoDOT reference concrete mixture	Cost ($)	Latex-modified Concrete (LMC)	Cost ($)	UHPC	Cost ($)
Type I/II Cement (kg/m^3)	280	40	390	56	-	-
Type III Cement (kg/m^3)	-	-	-	-	534	71
Class C Fly ash (kg/m^3)	95	5	-	-	-	-
Slag (kg/m^3)	-	-	-	-	491	52
River Sand (kg/m^3)	930	10	940	10	102	1
Masonry Sand (kg/m^3)	-	-	-	-	295	3
Coarse Agg. (kg/m^3)	930	10	740	8	-	-
Lightweight sand (kg/m^3)	-	-	-	-	406	37.6
CaO-based expansive agent (kg/m^3)	-	-	-	-	118	28.2
Latex (kg/m^3)	-	-	121	320	-	-
HRWR (l/kg^3)	1.25	6.5	-	-	46	177
AEA (ml/kg^3)	28	0.5	-	-	-	-
Water (kg/m^3)	150	-	80	-	150	-
Steel fiber (kg/m^3)	-	-	-	-	147	648
Total cost ($/m^3)		$72		$394		$1017.8

Note: 1 kg/m^3 = 1.686 lb/yd^3, 1 l/kg^3 = 0.0247 gal/lb^3, 1 $/m^3 = 35.3 $/ft^3

7.2. VOLUME REDUCTION

Despite the high unit cost of UHPC, many studies have shown that less quantity may be needed to achieve the same performance compared with conventional material. For example, Joe and Moustafa (2016) reported that 30% to 75% less material can be used in bridge piers if UHPC was used instead of conventional concrete (CC). This means that the high unit cost of typical UHPC mixtures may be outweighed by the overall reduction in the required concrete quantities. In addition, less volume of material may increase ease of construction and the speed of construction.

For overlay applications, a thin UHPC layer can provide both enhanced durability and increased strength with minimal applied dead load (Harber et al., 2017). Typical rigid concrete overlay thickness ranges between 63 and 153 mm (2.5 and 6 in.), while the thickness of UHPC overlays are reported between 25 and 50 mm (1 and 2 in.) (Harber et al., 2017; Krauss et al., 2009; Brühwiler, 2012). A recent study of FHWA (Harber et al., 2017) lists the approximate construction unit cost ranges for a common bridge deck overlay and UHPC overlay (Table 7-2). It is important to note that the cost estimates for the two UHPC case studies reported in the United States reflect material costs only, whereas the UHPC unit costs of the case studies in the Chillon Viaduct (Switzerland) include both material and installation costs.

Table 7-2 Approximate cost ranges of bridge deck overlay solutions (Harber et al., 2017)

Overlay Type	Overlay Thickness—in.(mm)	Cost—$/ft² ($/m²)
High-performance concrete*	1–5 (25–127)	17–25 (183–269)
Low slump concrete*	1.5–4 (38–102)	13–19 (140–204)
Latex-modified concrete*	1–5 (25–127)	18–39 (193–419)
Asphalt with a Membrane*	1.5–4 (38–102)	3–8 (32–86)
Polymer-based*	0.13–6 (3–152)	10 –17 (107–183)
Nonproprietary UHPC	1–2 (25–52)	3–6 (32–64)†
Proprietary UHPC		9–18 (97–184)‡
Rehabilitation of the Chillon Viaduct (Switzerland)		
Proprietary UHPC Overlay	1.6 (40)**	20 (215)**
Other Rehabilitation Solutions		
Deck Replacement*	—	43 - 53 (462–570)

*Data collected from Krauss et al. (2009); The costs shown reflect average values from low and high ranges.
**Data collected from Brühwiler et al. (2015); Price reflects cost of material and installation.
†Price reflects material cost only; Assumes UHPC CY cost of $1,000.
‡Price reflects material cost only; Assumes UHPC CY cost of $3,000.
—Not applicable.

7.3. FAST CONSTRUCTION AND PUBLIC TIME-SAVING

The LCCA can take various external costs into account, such as the value of public time-savings as part of user costs. Such considerations are important, especially for large-scale construction projects that demand accelerated construction methods to achieve minimum traffic disruption. UHPC has been proved in both laboratory tests and field to increase the speed of construction (McDonagh, 2016; Rallabhandhi, 2016). It was successfully employed by New York State and Iowa State Departments of Transportation (IDOT) in many bridges as various components and proved to help with accelerated bridge construction (Rallabhandhi, 2016). The following case study will mainly consider UHPC benefits from the aspects of volume reduction and accelerated construction.

7.4. LCCA CASE STUDY FOR UHPC

This section illustrates the application of the LCCA approach to evaluating the selected mixtures. Hypothetical LCCA examples for a UHPC bridge deck overlay are built using the improvement rate approach (Ozbay, 2016). In this case study, three materials including conventional portland cement concrete (PCC), LMC, and UHPC (EXC10LWS60) are compared. The structural and traffic data were obtained from one of the I-80 highway sections in New Jersey located about 1 mile east of Passaic River, for demonstration purposes only. A third order polynomial regression equation was estimated based on the NBI database to represent the deterioration of the bridge deck (Lou et al., 2016), as shown in Figure 7-1. This deterioration model is built based on real historical data.

$$CR = M_0 + M_1 x + M_2 x^2 + M_3 x^3 \quad \text{(Eq. 7.1)}$$

where CR is the conditional rating, M_0, M_1, M_2, and M_3 are coefficients. (M_0 = 8.457, M_1 = -0.27901, M_2 = 0,013952, M_3 = -0.000314).

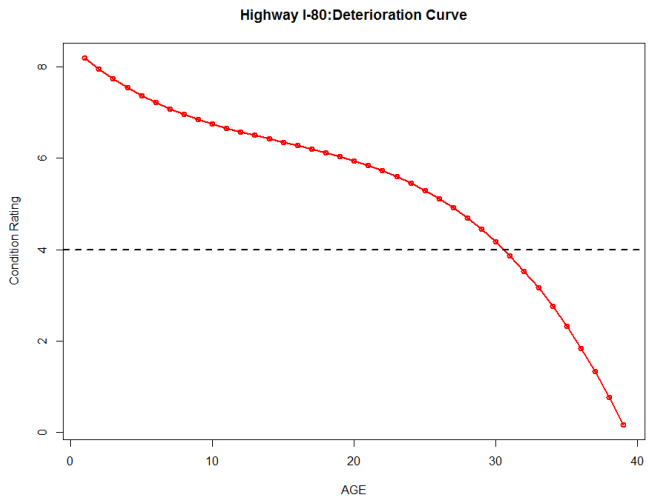

Figure 7-1 Deterioration curve of bridges on Highway I-80 (Lou et al., 2016)

The following assumptions are made based on the laboratory investigations in this study and previous UHPC field implementations in the United States and Europe.

- Given the significant improvement of mechanical properties, shrinkage mitigation, cracking resistance, and durability properties, the optimized UHPC is expected to require minimal maintenance during its service life and have a longer service life. UHPC has an estimate of 70% possibility of 60% improvement in terms of service life and 30% possibility of 40% improvement in terms of service life. The improvement rate is applied to the whole bridge deck deterioration curve (conditional rating 9 to 0).
- UHPC installation cost is assumed to be similar to that of the LMC (Krauss et al., 2009).
- Mean values or most likely values of the input parameters are used in the deterministic approach.
- Construction time saving of 10% to 30% is assumed for UHPC overlay compared to the conventional PCC overlay. UHPC is considered to have the same construction rate as LMC.
- Maintenance cost is not considered in this case study as it is assumed to be minimal for both LMC and UHPC.
- Agency and user costs are evaluated.

- As public time-saving is one of the major considerations, the user cost factor is set to 0.5.
- The above values/assumptions will be further evaluated once field implementation data becomes available.

Table 7-3 lists the input data for the LCCA example.

Table 7-3 LCCA case study input data

I. Analysis Options	**Conventional PCC**	**LMC**	**UHPC**
1. Service Life (years)	15 [Rallabhandhi, 2016]	14-29 [Rallabhandhi, 2016]	21-24*
2. Analysis Period (years)	75	75	75
3. Discount Rate (%)	3.0%	3.0%	3.0%
4. Thickness (in.)	2.5-6 [Krauss et al., 2009]	1-5 [Harber et al., 2017]	1-2 [Harber et al., 2017]
5. Construction Unit Cost ($/ft^2)	12.65 [RS Means, 2013]	18-39 [Harber et al., 2017]	15-30 [Harber et al., 2017]**
II. Traffic Data			
Average Daily Traffic (veh/day)	114,739		
Trucks as percentage of ADT (%)	1.55%		
Annual Growth Rate of Traffic (%)	0.5%		
Lanes opened under normal condition	Inbound (4), outbound (5)		
Value of time ($/hr)	11.58 (Passenger car), 20.43 (Truck)		
III. Work Zone Input			
Re-overlay Schedule	Every 15 years	Every 14-29 years	Every 21-24 years
Re-overlay Duration (d)	7	5-6	5-6
Free Flow Speed (mph)	70	70	70
Work Zone Speed (mph)	30	30	30

*Estimated based on improvement rate provided in previous chapters

**Estimated based on material unit price of UHPC ($3000/CY) and thickness of 25-50 mm. Installation fee is estimated as certain percentage of the entire construction unit cost (Sprinkel, 2011).

Three data sources were reviewed in terms of the construction unit cost of UHPC.

1) $9-18/ft^2 (based on $3000/ yd^3 UHPC, material cost only, US, Table 7-2)
2) $20/ft^2 (material cost and installation cost, Switzerland, Table 7-2)
3) $5/ft^2 (based on $1017.8/m^3 2" UHPC, material cost only, US, Table 7-1)

The Switzerland case (second option) is the only one that includes installation cost. However, due to relatively wider application of UHPC in Switzerland compare to that in the United States, both the material cost and installation cost may not be representative when apply to US UHPC applications. In addition, since the third option laboratory estimation ($5/ft^2) is lower than the values in the other two data sources, as a conservative approach, the first option $9-18/ft^2 (material cost only) is used in the following case study with an assumption that the installation fee will be estimated as certain percentage of the entire construction unit cost. The final estimated UHPC construction unit cost is $15-30/ft^2. The detailed calculation is as follow:

Step 1: Material cost:

$3000/yd^3 = 3000/27 = $111.11/ft^3 (1 cubic yard = 27 cubic feet)

1) For 1'' UHPC:

1 inch = 1/12 feet = 0.083 feet

111.11×0.083 = $9.26 /ft^2

2) For 2" UHPC:

2 inches =2/12 feet = 0.167 feet

111.11×0.167 = $18.52 /ft^2

Step 2. Since no commercial information about the installation fee and all other costs are available at this moment in US, installation fee and all other costs are assumed to be 40% of the entire construction unit cost. Therefore, the construction unit cost can be estimated as below:

1'' UHPC construction unit cost = 9.26 / (1-0.4) ≈ $15/ft^2

2'' UHPC construction unit cost = 18.52 / (1-0.4) ≈ $30/ft^2

7.5. DETERMINISTIC LCCA RESULTS

As a conservative approach, a lower bound of the LMC construction unit cost ($18/ft^2) and a mean service life (21.5 years) are used in the deterministic approach. A material cost of $15/ft^2 with a service life of 21 years and $30/ft^2 with a service life of 24 years are assumed for 1 in. UHPC and 2 in. UHPC overlay, respectively.

Figure 7-2 presents the deterministic results for PCC, LMC, 25 mm (1 in.) UHPC, and 50 mm (2 in.) UHPC overlays. While PCC overlay has the lowest agency cost due to its relatively

lower unit price, its user cost can be up to 40% to 50% higher compared to that of LMC and UHPC overlays. Similarly, 2 in. UHPC overlay has the lowest user cost. However, its agency cost is the highest among all four alternatives. On the other hand, the deterministic results indicate that both the LMC and 1 in. UHPC overlays are better options in terms of their total life-cycle costs. Since the difference of agency, user and total life cycle costs (with a user cost factor of 0.5) between the LMC and 1 in. UHPC overlay are within ±10%, these two alternatives can be considered similar or equivalent. However, the deterministic approach has many oversimplified assumptions and does not consider the uncertainty of the input parameters. Therefore, the probabilistic approach is also applied in the next section to provide additional insights that will allow the decision makers to quantify parametric variation and uncertainty with the ultimate objective of choosing the best alternative.

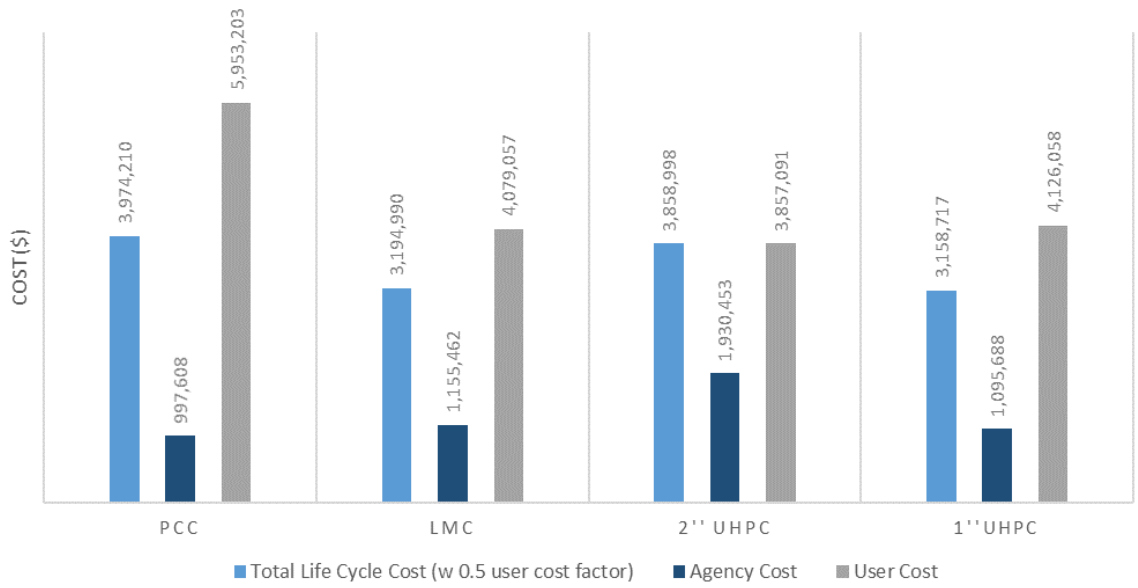

Figure 7-2 Deterministic LCCA results for PCC, LMC, 1 in. UHPC, and 2 in. UHPC overlays

7.6. PROBABILISTIC LCCA RESULTS

From the deterministic results, the PCC and 2 in. UHPC overlays have higher values in terms of total life cycle cost when compare to LMC and 1 in. UHPC overlay. However, difference between LMC and 1 in. UHPC overlay total life cycle cost are relatively small (within ±10%). Therefore, further investigation on these two alternatives are conducted using probabilistic approach. The effect of uncertainties for the two input parameters namely, service life and construction unit cost were tested using probabilistic distributions for LMC and 1 in.

UHPC overlay alternatives. Due to the limited available data, hypothetical triangular distributions were used as the best guess of the probabilistic distribution of these two parameters.

7.6.1. Service life

LMC is assumed to have a triangular distribution for its service life with a minimum, most likely, and maximum values of 14, 21.5, and 29, respectively. The 1 in. UHPC is assumed to have a triangular distribution for its service life with a minimum, most likely, and maximum values of 21, 22.5, and 24, respectively. The lower and upper bound values are based on the recent 2017 UHPC overlay studied by FHWA (Harber et al., 2017). All other input parameters are fixed.

Figure 7-3 shows the probability density function (PDF) and cumulative distribution functions (CDF) of the two alternatives in terms of agency, user, and total life-cycle costs. After randomly sampling from these probability distributions using Monte Carlo simulation (50,000 runs), the final life cycle cost analysis is obtained. Results (Figure 7-3(c)) indicate that the Alternative B, namely 1 in. UHPC, is slightly less expensive (3.60 million dollars) compared with the Alternative A, namely, LMC (3.62 million dollars) in terms of their mean values. In contrast, if only the mean value of agency cost is considered, LMC is less expensive than UHPC (1.46 million dollars compared with 1.54 million dollars). However, as both the differences are less than 10%, LMC and UHPC should be treated as similar or equivalent alternatives in this case. In Figure 7-3(b) and (c), the "gaps" in LMC PDF and step effect in its CDF are due to the changes in the number of re-overlay activities due to differences in service life values. For example, LMC with a service life of 14 years will have five re-overlay activities during the 75-year analysis period. LMC with a service life of 29 years will have only two re-overlay activities during the 75-year analysis period. Since user costs occur only during rehabilitation/replacement in our LCCA approach, the four possible "numbers of re-overlay" from 2 to 5 (as LMC service life ranges from 14 to 29 years) resulted in four spikes in the PDF graph. Moreover, under the current assumptions of the input parameters, the life cycle cost of 1 in. UHPC overlay are less uncertain (narrow distribution) with standard deviation of 0.07 million dollars compared to that of LMC (0.64 million dollars). The CDF in Figure7-3(a), (b), and (c) can also help the decision makers to identify the likely range of the NPV. For instance, according to Figure 7-3(b), there is

an 80% chance that the user cost of UHPC will be less than 4.1 million dollars, while there is only a 40% chance that the user cost of LMC will be less than 4.1 million dollars.

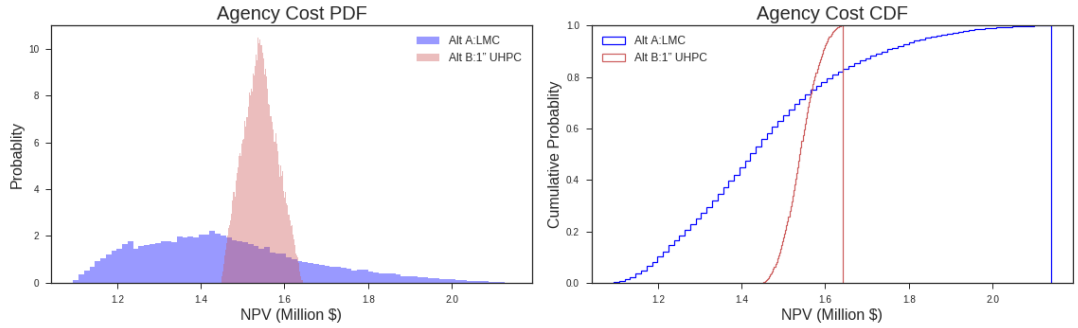

(a) PDFs and CDFs of agency costs

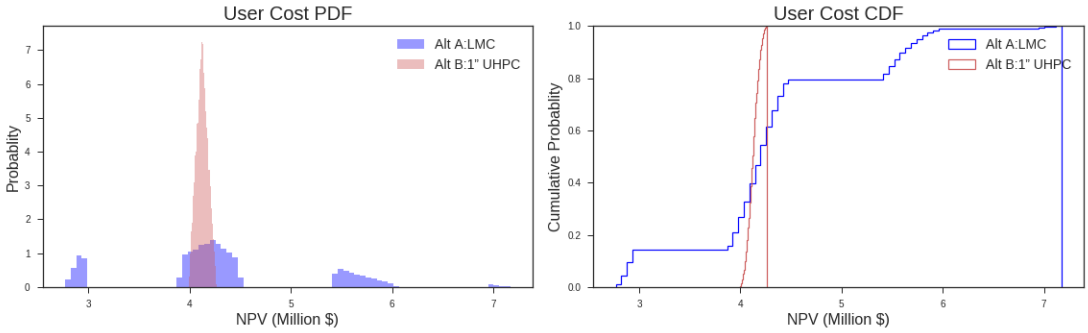

(b) PDFs and CDFs of user costs

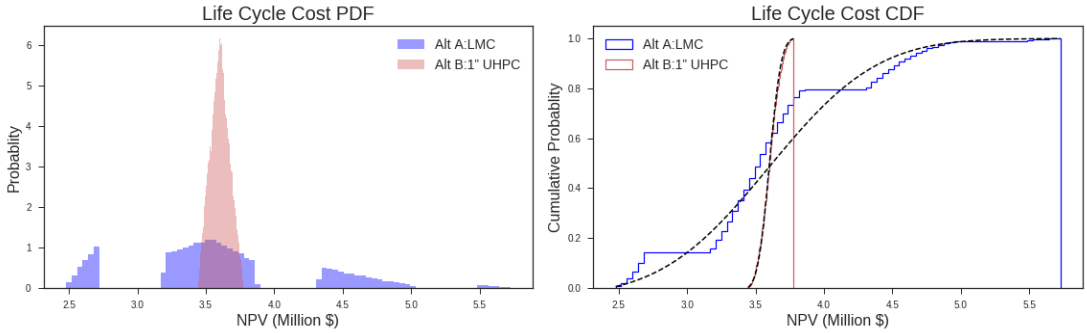

(c) PDFs and CDFs of total life-cycle cost

Figure 7-3 Costs of LMC and 1 in. UHPC overlay with probabilistic service life: (a) agency cost; (b) user costs; (c) total life-cycle cost

7.6.2. Construction unit cost

LMC is assumed to have a triangular distribution in terms of the construction unit cost with a minimum, most likely, and maximum values of 18, 20, and 39, respectively. The 1 in. UHPC is assumed to have a triangular distribution for the construction unit cost with a minimum, most likely, and maximum values of 15, 22.5, and 30, respectively. The lower and upper bound

values are based on the recent UHPC overlay study by FHWA (Harber et al., 2017). All other input parameters are fixed.

Since the agency cost of Alternative B (1 in. UHPC) is 15.8% less than that of Alternative A (LMC) in terms of their mean values, UHPC overlay is preferred if only agency cost is considered, as shown in Figure7-4(a). The life cycle cost results also indicate that the 1 in UHPC is less expensive (3.60 million dollars) compared with the LMC (3.94 million dollars) in terms of their mean life cycle cost (LCC) values, as shown in Figure 7-4(c). However, when the difference of the mean LCC value is less than 10%, these two alternatives should be considered similar or equivalent if both the user and agency costs are considered. The user cost is deterministic under this scenario because probabilistic input parameter "construction unit cost" is not involved in the user cost calculation, as shown in Figure 7-4(b).

7.6.3. Service life and construction unit cost

Figure 7-5 shows the joint probabilistic approach for both service life and construction unit cost. Alternative B (1 in UHPC) is 17%, 5%, and 11% less expensive compared with Alternative A (LMC) in terms of their mean values of the agency, user and life cycle costs, respectively. From the CDF of total life-cycle cost (Figure 7-5(c)), there is 100% chance that Alternative B (1 in UHPC) will have a life cycle cost less than 4.3 million dollars while there is only 68% chance that Alternative A (LMC) will have a life cycle cost less than 4.3 million dollars.

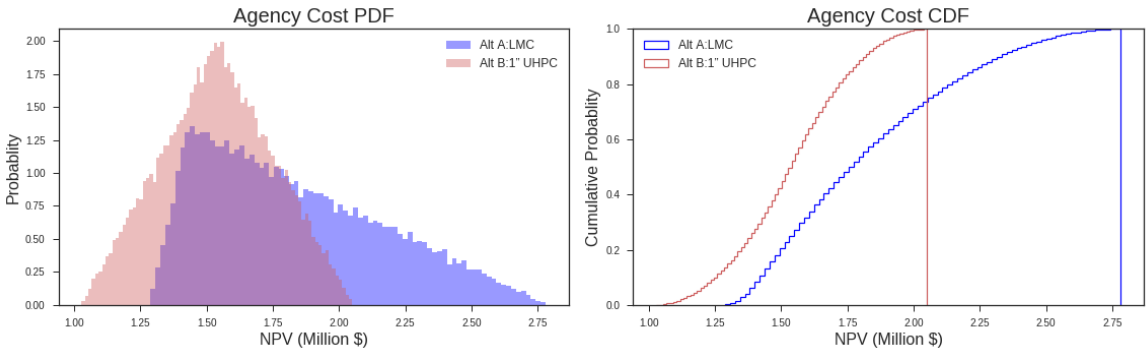

(a) PDFs and CDFs of agency cost

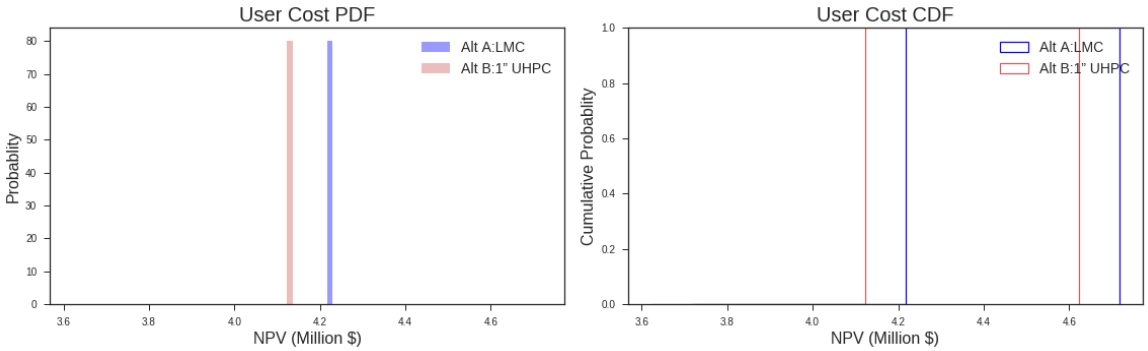

(b) PDFs and CDFs of user costs

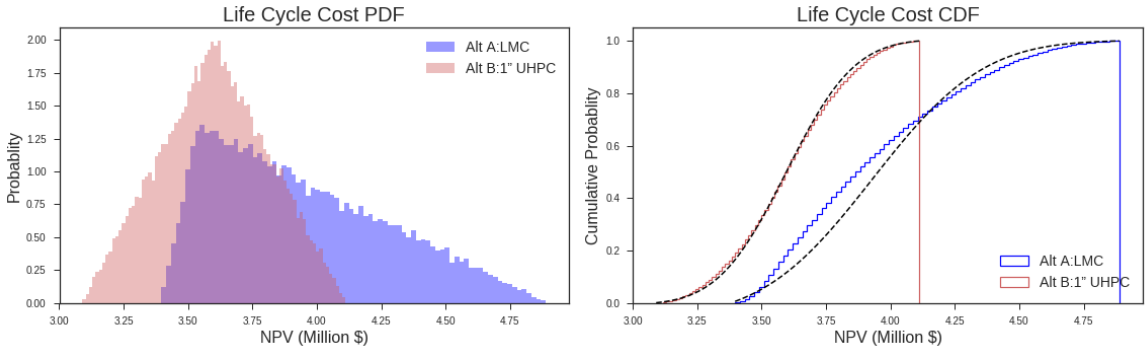

(c) PDFs and CDFs of total life-cycle cost

Figure 7-4 Costs of LMC and 1" UHPC overlay with probabilistic construction unit cost: (a) agency cost; (b) user costs; (c) total life-cycle cost

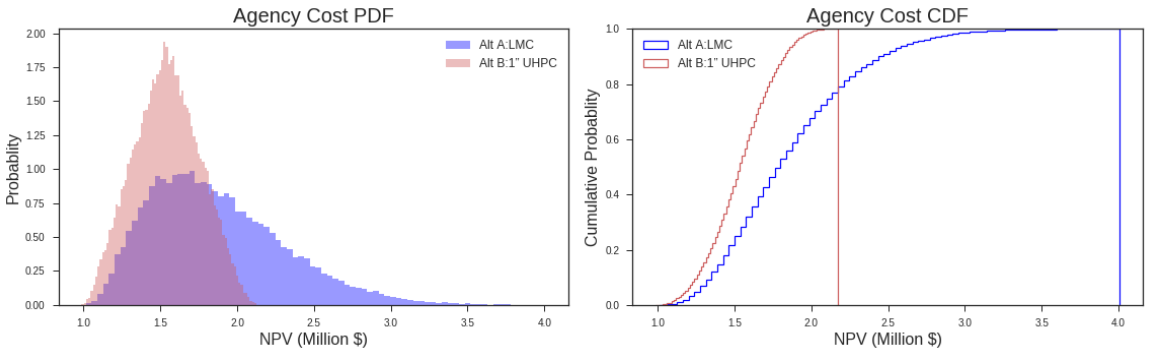

(a) PDFs and CDFs of agency cost

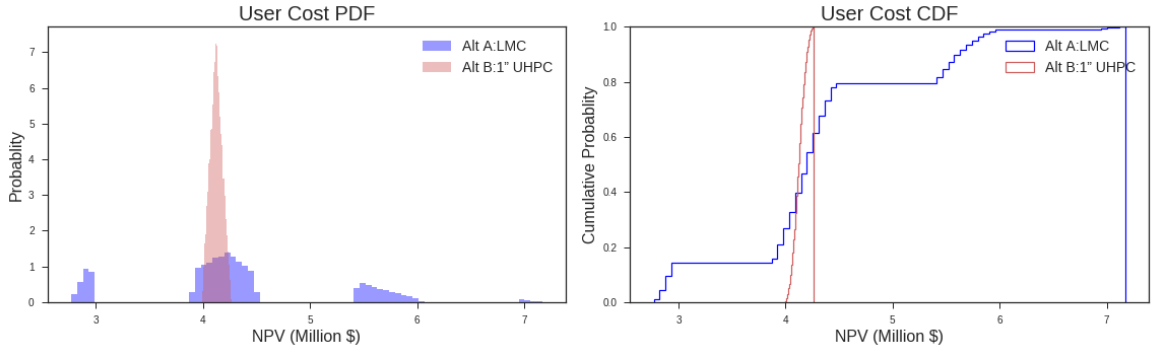

(b) PDFs and CDFs of user costs

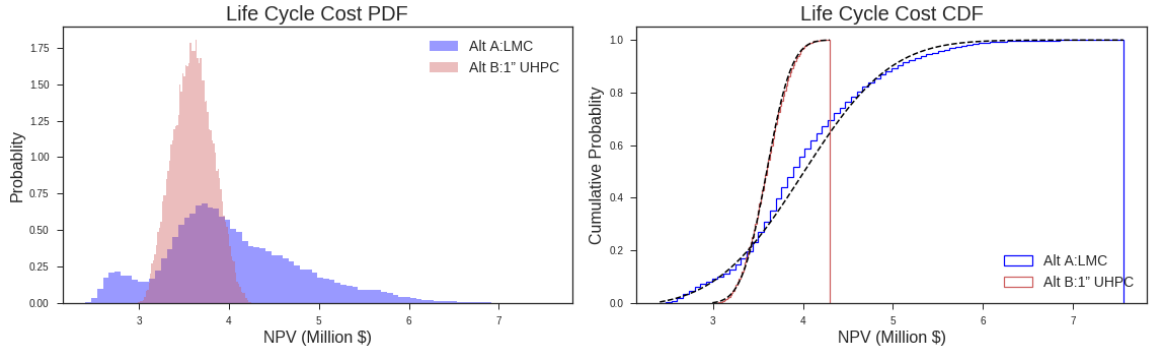

(c) PDFs and CDFs of total life cycle cost

Figure 7-5 Costs of LMC and 1" UHPC overlay with probabilistic construction unit cost: (a) agency cost; (b) user costs; (c) total life cycle cost

7.7. SUMMARY

Life cycle cost analysis was determined for selected concrete mixtures with different mixture compositions and performance characteristics. Based on the results, the following conclusions can be drawn:

(1) UHPC offers various advantages, such as speed of construction and superior durability, which makes it possible to form a thinner overlay. These advantages can be translated into reduced maintenance and a longer lifespan for the treated pavement and bridge deck.

(2) An UHPC overlay is recommended for potential field implementation when compared with a conventional PCC overlay, especially for large-scale construction projects while time-saving is a major consideration for the agency.

(3) Based on both deterministic and probabilistic results, the 1 in. thick UHPC overlay seems to be more cost-effective when compared to LMC overlay applications. However, as the difference between LMC and UHPC overlay becomes relatively small under some scenarios, further evaluation is suggested when more laboratory and field implementation data become available. In addition, some of the UHPC costs, especially material unit cost, may decrease in the future as the technology matures and the market demands mass production.

(4) The final selection of the overlay material should also consider the technical performance of the material, including its resistance to cracking, delamination, bond to substrate, and durability.

8. SUMMARY AND CONCLUSIONS

The research presented in this project was undertaken to develop a cost-effective UHPC material for thin bonded overlays targeted for bridge deck applications. A comprehensive investigation involving laboratory material performance evaluation was conducted to develop the mixture design methodology and validate the material performance. The robustness of UHPC made with silica fume, Class C fly ash, and ground granulated blast-furnace slag placed at different casting and curing temperatures of 10, 23, and 30 °C (50, 73.4, and 86 °F). The effect of LWA, EXC, EXM, and SRA on autogenous and drying shrinkage of thin overlays made with UHPC was thoroughly evaluated. The performance of optimized UHPC mixtures for thin-bonded overlay application was verified by casting thin overlays of various thicknesses on concrete pavement sections used as substrate. Finally, life cycle cost analysis (LCCA) of the selected concrete mixtures with different mixture compositions and performance characteristics was investigated. Based on the test results from this comprehensive research program, the following conclusions can be drawn:

8.1. OPTIMIZATION AND PERFORMANCE OF COST-EFFECTIVE UHPC

A mixture design methodology was presented for producing cost-effective UHPC with high-volume of SCMs and conventional concrete sand. Based on the reported studies, the following conclusions can be made:

(1) The minimum water content (MWC) can first be used as an indicator of the packing density of binders in wet condition to narrow down binder systems and reduce the required number of experiments. The binder composition of UHPC can then be optimized with consideration of the HRWR demand, rheological properties, MWC, relative water demand (RWD), and compressive strength properties. A radar chart approach that takes into consideration several key properties can be employed for the analysis. Based on this approach, the following binder combinations were selected: G50, G50SF5, FAC60, and FAC40SF5.

(2) The second step involves the determination of the preliminary w/cm based on the 28-d compressive strength and HRWR demand value for paste mixtures prepared with the

optimum binder combinations with w/cm of 0.18-0.23. The optimum value for the selected binders was 0.20.

(3) The modified Andreasen and Andersen model can be used to optimize the sand gradation. In this study, 70% river sand and 30% masonry sand were selected to achieve the highest packing density.

(4) The next step involves the determination of the binder-to-sand volume ratio (Vb/Vs). Mortar mixtures made with the selected w/cm and G50SF5 binder were prepared with Vb/Vs values of 0.6, 0.7, 0.8, 0.9, 1.0 and 1.3. Based on flow properties and 28-d compressive strength, the optimum Vb/Vs was determined to be 1.0.

(5) The optimum fiber content for the UHPC is experimentally determined given the flowability and flexural properties of UHPC made with various fiber contents. For the steel fibers considered in this study, 2% fiber volume was selected.

(6) For the UHPC mixtures prepared with the various binder systems and optimized mixture proportioning, the UHPC mixtures were self-consolidating, stable, and had 28 d compressive strengths of 120 - 125 MPa (17.4 - 18.1 ksi) under standard curing condition. The strength can reach up to 178 MPa (25.8 ksi) by applying heat curing at a maximum temperature of 90 °C (194 °F) for one day followed by 7 d moist curing. For the selected UHPC mixtures, the 28 d splitting tensile strength, modulus of elasticity, flexural strength, and toughness (T150) were 11.6-14.3 MPa (1.7-2.1 ksi), 48.8-51.6 MPa (7.1-7.5 ksi), 20.2-21.3 MPa (2.9-3.1 ksi) and 50 ± 1.5 kN mm (439 ± 13.2 lb in.), respectively.

(7) The designed UHPC mixtures exhibited relatively low autogenous shrinkage and drying shrinkage. The G50 mixture had the lowest autogenous and drying shrinkage of 253 με at 28 d and 56 με at 98 d, respectively. All tested UHPC mixtures exhibited a very high electrical resistivity and excellent frost durability.

(8) The unit cost per compressive strength of the UHPC mixtures designed with high volume of SCMs and concrete sand can range between 3.5 and 4.7 $/m3/MPa (455 and 528 $/yd3/psi). The mixture FAC60 was the most cost-effective mixture, which also developed better workability and lower unit cost per compressive strength of 3.7 $/m3/MPa (411 $/yd3/psi) than other.

8.2. ROBUSTNESS OF UHPC AT DIFFERENT CASTING AND CURING TEMPERATURES

The effect of casting and curing temperatures on workability, setting time, mechanical properties as well as autogenous and drying shrinkage of UHPC was investigated. The UHPC was mixed and cured at 10, 23, and 30 ºC (50, 73.4, and 86 ºF). Based on the reported studies, the following conclusions can be drawn:

(1) Regardless of the investigated UHPC mixture, the HRWR demand increased with the increase in temperature. UHPC made with FA required less HRWR content compared to that with GGBS and the reference mixture (25% SF). The FA60 mixture with 0.46% HRWR at 10 °C (50 °F) and G50SF5 mixture with 1.58% HRWR at 30 °C (86 °F) exhibited the lowest and highest HRWR demands, respectively.

(2) Mini V-funnel flow time decreased by up to 45%, with the increase in temperature from 10 to 30 ºC (50 to 86 °F). Increasing the temperature accelerated the initial and final setting times by up to 4.5 and 5 h, respectively. Yield stress increased by up to 55% and plastic viscosity decreased by up to 45% with increasing the temperature from 10 to 30 ºC (50 to 86 °F). UHPC made with GGBS exhibited the highest values of plastic viscosity and the lowest yield stresses compared to the reference mixture and UHPC made with FA.

(3) Temperature variation can significantly affect the development of mechanical properties of UHPC. Results indicated that mechanical properties of different UHPC mixtures improved with the increase in temperature. Increasing temperature from 10 to 30 ºC (50 to 86 °F) improved the 28 d compressive strength of the G50, G50SF5, FA60, and FA40SF5 mixtures by 65%, 70%, 43%, and 42%, respectively. The flexural toughness (T150) was enhanced by up to 65% with the increase in temperature. All mixtures had their minimum and maximum toughness at 10 and 30 ºC (50 to 86 °F), respectively.

(4) Increasing the temperature from 10 to 30 ºC (50 to 86 °F) led to increasing autogenous and drying shrinkage. UHPC made with GGBS or FA exhibited a reduction in autogenous and drying shrinkage by up to 300 and 350 με, respectively, compared to the reference mixture at 56 d. UHPC made with FAC and GGBS were more robust than the

reference mixture made with 25% SF. In general, the FA60 and FA40SF5 mixtures resulted in greater robustness than other UHPC mixtures.

8.3. COUPLED EFFECT OF SATURATED LIGHTWEIGHT SAND AND SHRINKAGE-MITIGATING ADMIXTURES ON PERFORMANCE OF UHPC

The effect of LWS, SRA, EXC, and EXM on compressive strength, autogenous and drying shrinkage of UHPC was investigated. Based on the results, the following conclusions can be drawn:

(1) The incorporation of 25% to 60% pre-saturated LWS resulted in considerable decrease in HRWR demand (1.23% to 1.05%) compared to the EXC7.5 mixture (2.3%) required to secure self-consolidating characteristics. The EXC5LW60 and EXC7.5 mixtures exhibited the lowest and highest values of HRWR demand, respectively. The content of LWS necessary to compensate chemical shrinkage for the investigated UHPC was 35%, by volume of sand.

(2) The combined use of 60% LWS and EXC, EXM, or SRA had a positive effect on reducing mini-slump flow and mini V-funnel losses with time. The fastest and slowest flow times after 70 min were obtained in the EXC7.5LWS60 and EXC7.5 mixtures. The combined use of EXC, EXM, or SRA with LWS significantly shortened the final setting times. The reference G50 mixture had final setting time of 17.5 h and decreased to 6-8 h for the mixtures with LWS and 7.5% EXC.

(3) The coupled effect of incorporating EXC with 60% LWS resulted in a significant effect on controlling autogenous shrinkage of UHPC. The EXC10LWS60 mixture had the highest expansion of 865 με and exhibited expansion value of 580 με at 91 d compared to the reference G50 mixture that had a shrinkage of 530 at 91 d.

(4) The coupled effect of LWS and EXC for different curing conditions indicate that increasing LWS and EXC replacement levels along with extending moist curing significantly improved expansion during moist curing period and reduced total shrinkage thereafter. The EXC10LWS60 mixture had the best performance in terms of total shrinkage (expansion of 110 με at 91 d) following 7 d of moist curing. The use of SRA or EXM in combination with 60% LWS was effective in reducing total shrinkage by up to 30%.

(5) The increase in the period of moist curing from 1 to 3 and 7 d had a significant effect on the 91 d compressive strength of UHPC. Such increase was by up to 35% for UHPC with no LWS and 15% for that with 60% LWS.

(6) The combined use of either EXC, EXM, or SRA with 60% LWS decreased 91 d compressive strength under 7MC ranging from 8 to 20 MPa (1.2 to 2.9 ksi) compared to 60% LWS. Further increase in EXC content from 5% to 10%, EXM from 5% to 7%, and SRA from 1.5% to 3% in mixtures subjected to 7 d of moist curing resulted in 91 d compressive losses of 10, 6, and 5 MPa (1.5, 0.9, and 0.7 ksi), respectively.

8.4. UHPC PERFORMANCE AS BONDED OVERLAY

In this task, 16 slabs made of different mixture proportions were constructed to compare the performance of UHPC overlay materials to those of LMC and conventional portland cement concrete overlays. Based on the results, the following conclusions can be drawn:

(1) The results of shrinkage deformation were shown to be a function of concrete mixture design, location, and UHPC overlay thickness.

(2) The incorporation of EXC at replacement levels of 5% and 10%, combined with 60% LWS resulted in considerable decrease in total shrinkage. The UHPC overlay mixture made with 10% EXC combined with 60% LWS with 25 mm (1 in.) in thickness exhibited the highest expansion of 850 με at 7 d. The same mixture with 38 (1.5 in.) and 50 mm (2 in.) showed 660, and 485 με maximum initial expansions at 7 d, respectively.

(3) Temperature variations showed a high temperature during the first 24 h of casting by up to 40 °C (104 °F) for all of the investigated mixtures. However, after 24 h, the temperature gradually reached close to the ambient temperature varying between 20 to 50 °C (68 to 122 °F). All mixtures exhibited a saturated condition (100% RH) during the wet curing period. The RH gradually dropped right after exposing the slabs to air drying. RH variations reached stabilized range of 65% to 80%, depending on the overlay mixture type and thickness. Visual and microscopic inspections of UHPC overlays at the surface and interface layer showed no signs of cracking and debonding after more than 200 d of casting.

(4) UHPC made with 50% GGBS, 5% to 10% EXC, and 60% LWS reinforced with 2% steel fiber (by volume), was recommended for field implementation. A clean aggregate

exposed surface on the substrate concrete is of critical importance to a long-lasting bond, which can be attained by hydrodemolition method. It is recommended to apply at least 7 d moist curing (wet burlap covered by a plastic sheet) immediately after UHPC casting.

8.5. LIFE CYCLE COST ANALYSIS OF UHPC OVERLAY

Life cycle cost analysis was determined for selected concrete mixtures with different mixture compositions and performance characteristics. Based on the results, the following conclusions can be drawn:

(1) UHPC offers various advantages, such as speed of construction and superior flexural strength, and durability, which make it possible to form a thinner overlay. These advantages can be translated into reduced maintenance and a longer lifespan for the treated structure.

(2) An UHPC overlay is recommended for potential field implementation when compared with conventional portland cement concrete overlay, especially for large-scale construction projects while time-saving is a major consideration for the agency.

(3) Based on both deterministic and probabilistic results, 1 in. UHPC overlay is more cost-effective compared to latex modified concrete (LMC) applications. However, as the difference between LMC and UHPC overlay becomes relatively small under some scenarios, further evaluation is suggested when more laboratory and field implementation data become available. In addition, some of the UHPC costs, especially material unit cost, may decrease in the future as the technology matures and the market demands mass production.

8.6. FUTURE RESEARCH

Based on the findings presented in this research work, the following aspects are recommended for future investigation:

(1) Validate further the performance of the 16 slab specimens by storing them outdoors to evaluate the performance under seasonal environmental variations. Pull-off tests can be conducted on the slabs to assess the bond performance at the interface layer and its variation with time.

(2) Portions of the slabs can be saw-cut to subject and stored in a freeze/thaw chamber to monitor the performance of the various UHPC overlays in terms of debonding, delamination, and crack propagation.

(3) Sections of the cast slab elements can be cut to conduct flexural testing to evaluate the quality of the interface between the subbase concrete and UHPC overlay.

(4) In this study, the performance of the developed UHPC mixtures for bonded bridge deck overlays was evaluated through laboratory-scale investigation and validated on concrete pavement sections. However, for further validation, the performance (i.e., deformation and structural behavior) of such concrete should be verified under actual field conditions. This can involve the casting of overlays with thicknesses of 25, 38, and 50 mm (1, 1.5, and 2 in.) using proven UHPC and comparing their behavior with those of LMC used in actual bridge deck applications.

9. REFERENCE

Ahlborn, T. M., Misson, D. L., Peuse, E. J., & Gilbertson, C. G. (2008). Durability and Strength Characterization of Ultra-High Performance Concrete under Variable Curing Regimes. In Proc. 2nd Int. Symp. on Ultra High Performance Concrete, Fehling, E., Schmidt, M., & Stürwald, S.(Eds.) Kassel, Germany, 197-204.

Ahlborn, T. M., Peuse, E. J., & Misson, D. L. (2008). Ultra-High-Performance-Concrete for Michigan Bridges Material Performance–phase I (No. MDOT RC-1525).

Alhassan, M., & Ashur, S. (2014). Fibrous Latex-Modified Concrete Overlay for Bridge Decks: Installation and Life-Cycle Cost Analysis. Journal of Advanced Science and Engineering Research Vol, 4(2), 74-87.

Aïtcin, P. C. (2011). High Performance Concrete. CRC press.

Aitcin, P. C., Delagrave, Y., & Beck, R. (2000). A 100-M High Prefabricated Concrete Pole: Why Not?. In Transmission and Distribution Construction, Operation and Live-Line Maintenance Proceedings. 2000 IEEE ESMO-2000 IEEE 9th International Conference, 365-374.

Akçaoğlu, T., Tokyay, M., and Çelik, T. (2005). Assessing the ITZ Micro cracking via Scanning Electron Microscope and its Effect on the Failure Behavior of Concrete. Cem. Concr. Res. 35(3), 58-63.

Bao, Y., and Chen, G. (2016). Temperature dependent Strain and Temperature Sensitivities of Fused Silica Single Mode Fiber Sensors with Pulse Pre-Pump Brillouin Optical Time Domain Analysis. Mes. Sci. Technol. 27, 65, 101-111.

Bao, Y., Meng, W., Chen, Y., Chen, G., & Khayat, K. H. (2015). Measuring Mortar Shrinkage and Cracking by Pulse Pre-Pump Brillouin Optical Time Domain Analysis with a Single Optical Fiber. Materials Letters, 145, 344-346.

Bao, Y., Tang, F., Chen, Y., Meng, W., Huang, Y. and Chen, G. (2016). "Concrete Pavement Monitoring with PPP-BOTDA Distributed Strain and Crack Sensors" Smart Struct. Sys. (18) 405-23.

Bentz, D. P. (2000). Fibers, Percolation, and Spalling of High Performance Concrete ACI Mater. J. 97 (35), 1-9.

Beushausen, H., & Alexander, M. G. (2007). Localized Strain and Stress in Bonded Concrete Overlays Subjected to Differential Shrinkage. Materials and Structures, 40(2), 189-199.

Blais, P. Y., & Couture, M. (1999). Precast, Prestressed Pedestrian Bridge: World's First Reactive Powder Concrete Structure. PCI journal, 44(5), 60-71.

Bonen, D., Deshpande, Y., Olek, J., Shen, L., Struble, L., Lange, D., and Khayat, K. (2007). Robustness of Self-Consolidating Concrete, In Proceedings of the Fifth International RILEM Symposium on Self-Compacting Concrete, 33-42.

Bonneau, O., Poulin, C., Dugat, M., & Tcin, P. C. A. (1996). Reactive Powder Concretes: From Theory to Practice. Concrete International, 18(4), 47-49.

Broomfield, J. (2011). Measuring Concrete Resistivity to Assess Corrosion Rates. Concrete Report from the Concrete Society/ Institute of Corrosion Liaison Committee, 37-39.

Bruhwiler, E., Denarié, E. (2013). Rehabilitation of Concrete Structures Using Ultra-High Performance Fibre Reinforced Concrete." In: Proceedings of the second international symposium on ultra high performance concrete, Kassel, 1-8.

Brühwiler, E. (2012). Rehabilitation and Strengthening of Concrete Structures Using Ultra-High Performance Fiber Reinforced Concrete. In Concrete Repair, Rehabilitation and Retrofitting III: 3rd International Conference on Concrete Repair, Rehabilitation and Retrofitting, ICCRRR-3, 3-5 September 2012, Cape Town, South Africa (p. 30). CRC Press.

Castellote, M., Llorente, I., Andrade, C., & Alonso, C. (2003). Accelerated Leaching of Ultra High Performance Concretes by Application of Electrical Fields to Simulate Their Natural Degradation. Materials and Structures, 36(2), 81-90.

Chan, Y. W., and Li, V. C. (1997). Age Effect on the Characteristics of Fiber/Cement Interfacial Properties" J. Mater. Sci. 32. 5287-92.

Chen, G., Zhou, Z., Xiao, H., and Huang, Y. (2012). Pilot Study on Rugged Fiber Optic Brillouin Sensors for Large-strain Measurements to Ensure the Safety of Transportation Structures. Report: MATC-25-1121-0001-114 and MATC- 25-1121-0001-242 Mid-America Transportation Center.

Cusson, D., & Hoogeveen, T. (2007). An Experimental Approach for the Analysis of Early-Age Behaviour of High-Performance Concrete Structures under Restrained Shrinkage. Cement and Concrete Research, 37(2), 200-209.

De Matteis, D., Novain, M., Marchand, P., Fabry, N., Petel, A., Chanut, S. (2008). A Fifth French Bridge Including UHPFRC Components, the Widening of the Pinel Bridge, in Rouen (France). Proceeding of the Second International Symposium on Ultra High Performance Concrete, Kassel, Germany, 795-803.

Denarie, E., Bruhwiler, E., and Znidaric, A. (2005). Full Scale Application of UHPFRC for Rehabilitation of Bridges-From the Lab to the Field, in 5th FWP/ SAMARIS Sustainable and Advanced Material for Road Infrastructures.

Droll, K. (2004). Influence of Additions on Ultra High Performance Concretes–Grain Size Optimisation. In Proceedings of the International Symposium on Ultra-High Performance Concrete, Kassel, Germany, Sept. 13, Vol. 15, 285-301.

Dudziak, L., Mechtcherine, V. (2008). Mitigation of Volume Changes of Ultra-High Performance Concrete (UHPC) by Using Super Absorbent Polymers." In: Proceedings of the second international symposium on ultra high performance concrete, Kassel, 425-432.

Dugat, J., Roux, N., & Bernier, G. (1996). Mechanical Properties of Reactive Powder Concretes. Materials and structures, 29(4), 233-240.

EFNARC. (2002). Specification and Guidelines for Self-Compacting Concrete, English edn. European Federation for Specialist Construction Chemicals and Concrete Systems, Norfolk.

Erdem, T. K., Khayat, K. H., & Yahia, A. (2009). Correlating Rheology of Self-Consolidating Concrete to Corresponding Concrete-Equivalent Mortar. ACI Materials Journal, 106(2), 154.

Feng, X., Zhou, J., Sun, C., Zhang, X., and Ansari, F. (2013). Theoretical and Experimental Investigations into Crack Detection with BOTDR distributed Fiber Optic Sensors. J. Eng. Mech. 139(1), 797-807.

Ferraris, C. F., Obla, K. H., & Hill, R. (2001). The Influence of Mineral Admixtures on the Rheology of Cement Paste and Concrete. Cement and concrete research, 31(2), 245-255.

Gao, R., Liu, Z. M., Zhang, L. Q., & Stroeven, P. (2006). Static Properties of Plain Reactive Powder Concrete Beams. In Key Engineering Materials, Vol. 302, 521-527.

Gettu, R., Nawaz Shareef, S., and Ernest, K. (2009). Evaluation of The Robustness of SCC, Indian Concrete Journal, 83 (6) 13-19.

Graybeal, B. A. (2006). Material Property Characterization of Ultra-High Performance Concrete (No. FHWA-HRT-06-103).

Griffin, J. J., Harik, I. E., & Choo, C. C. (2006). Performance Evaluation of Bridges with Structural Bridge Deck Overlays (SBDO).

Habel, K., Charron, J. P., Denarié, E., & Brühwiler, E. (2006). Autogenous Deformations and Viscoelasticity of UHPFRC in Structures. Part I: Experimental Results. Magazine of Concrete Research, 58(3), 135-145.

Haber, Z. B., Munoz, J. F., & Graybeal, B. A. (2017). Field Testing of an Ultra-High Performance Concrete Overlay (No. FHWA-HRT-17-096).

Houst, Y. F., Flatt, R. J., Bowen, P., Hofmann, H., Mäder, U., Widmer, J., ... & Sika, A. G. (1999, March). Influence of Superplasticizer Adsorption on the Rheology of Cement Paste. In International symposium on: the role of admixtures in high performance concrete, Monterrey, Mexico, 387-402.

Hwang, S., & Khayat, K. H. (2005). Effect of Various Admixture-Binder Combinations on Workability of Ready-Mix Self-Consolidating Concrete. ACI Special Publications, 233, 25-44.

Joe, C. D., & Moustafa, M. A. (2016). Cost and Ecological Feasibility of Using UHPC in Bridge Piers. In First International Interactive Symposium on UHPC, 18-20.

Jolicoeur, C., Sharman, J., Otis, N., Lebel, A., Simard, M. A., & Page, M. (1997). The Influence of Temperature on the Rheological Properties of Superplasticized Cement Pastes. Special Publication, 173, 379-406.

Kaan Ozbay, J.G. (2016). Draft Report on Life Cycle Cost Analysis for Research on Concrete Applications for Sustainable Transportation (RE-CAST).

Khayat, K. H., Kassimi, F., & Ghoddousi, P. (2014). Mixture Design and Testing of Fiber-Reinforced Self-Consolidating Concrete. ACI Materials Journal, 111(2), 143-152.

Khayat, K. H., Mitchell, D., Long, W. J., Lemieus, G., Hwang, S. D., Yahia, A., Cook, W. D., Baali, L. (2007). Self-Consolidating Concrete for Precast, Prestressed Concrete Bridge Elements. NCHRP Project 18-12. University of Sherbrooke, Quebec.

Kim, D. H., Fowler, D. W., Ferron, R. P., Trevino, M. M., & Whitney, D. P. (2012). Materials Selection for Concrete Overlays. (No. FHWA/TX-11/0-6590-2).

Kishida, K., and Li, C. H. (2006). Pulse Pre-Pump-BOTDA Technology for New Generation of Distributed Strain Measuring System. Proc. Structural Health Monitoring and Intelligent Infrastructure (London, UK, 2006), 471-477.

Knight, M., Wilson, G., Seger, W., & Mahadevan, S. (2004). Overlay Types Used as Preventive Maintenance on Tennessee Bridge Decks. Transportation Research Record: Journal of the Transportation Research Board, (1866), 79-84.

Koehler, E., Fowler, D. (2007). Aggregate in Self-Consolidating Concrete. In: ICAR project 108. The University of Texas at Austin: International Center for Aggregates Research.

Krauss, P. D., Lawler, J. S., & Steiner, K. A. (2009). Guidelines for Selection of Bridge Deck Overlays, Sealers and Treatments. NCHRP Project, 20-07.

Krstulovic-Opara, N., Haghayeghi, A. R., Haidar, M., & Krauss, P. D. (1995). Use of Conventional and High-Performance Steel-Fiber Reinforced Concrete for Bridge Deck Overlays. ACI materials journal, 92(6), 669-677.

Lange, D., & Shin, H. C. (2001). Early Age Stresses and Debonding in Bonded Concrete Overlays. Transportation Research Record: Journal of the Transportation Research Board, (1778), 174-181.

Li, L. G., & Kwan, A. K. (2011). Mortar Design Based on Water Film Thickness. Construction and Building Materials, 25(5), 2381-2390.

Li, V. C., Lim, Y. M., and Foremsky, D. J. (1995). Interfacial fracture toughness of concrete repair materials Fracture Mechanics of Concrete Structures, Proc. FRAMCOS-2 ed F H Wittmann, 1329-44.

Lou, P., Nassif, H., Su, D., & Truban, P. (2016). Effect of Overweight Trucks on Bridge Deck Deterioration Based on Weigh-in-Motion Data. Transportation Research Record: Journal of the Transportation Research Board, (2592), 86-97.

Mechtcherine, V., Secrieru, E., & Schröfl, C. (2015). Effect of Superabsorbent Polymers (Saps) on Rheological Properties of Fresh Cement-Based Mortars development of Yield Stress and Plastic Viscosity over Time. Cement and Concrete Research, 67, 52-65.

Meng, W., Khayat, K. H. (2017). Effects of Saturated Lightweight Sand Content on Key Characteristics of Ultra-High-Performance Concrete. Cement and Concrete Research, 46-54.

Meng, W., Valipour, M., & Khayat, K. H. (2017). Optimization and Performance of Cost-Effective Ultra-High Performance Concrete. Materials and Structures, 50(1), 29.

McDonagh, M.D., and Foden, A.J. (2016). Benefit of Ultra-High Performance Concrete for the Rehabilitation of the Pulaski Skyway'. Proc. First International Interactive Symposium on UHPC, Des Moines, Iowa, USA.

Misson D. L. (2008). Influence of Curing Regime on the Durability of an Ultra-High Performance Concrete Material, Thesis. Houghton, MI: Michigan Technological University.

Mo, L., Deng, M., & Tang, M. (2010). Effects of Calcination Condition on Expansion Property of Mgo-Type Expansive Agent Used in Cement-Based Materials. Cement and Concrete Research, 40(3), 437-446.

Naaman, A. E., & Wille, K. (2012). The Path to Ultra-High Performance Fiber Reinforced Concrete (UHP-FRC): Five Decades of Progress. In Proceeding of 3rd International Symposium on UHPC and Nanotechnology for High Performance Construction Materials. Kassel: Kassel University Press, 3-13.

Nassif, A. Y., & Petrou, M. F. (2013). Influence of Cold Weather during Casting and Curing on the Stiffness and Strength of Concrete. Construction and Building Materials, 44, 161-167.

Nunes, S., Figueiras, H., Oliveira, P. M., Coutinho, J. S., & Figueiras, J. (2006). A Methodology to Assess Robustness of SCC Mixtures. Cement and Concrete Research, 36(12), 2115-2122.

Otsubo, Y., Miyai, S., & Umeya, K. (1980). Time dependent Flow of Cement Pastes. Cement and Concrete Research, 10(5), 631-638.

Park, C. K., Noh, M. H., & Park, T. H. (2005). Rheological Properties of Cementitious Materials Containing Mineral Admixtures. Cement and concrete research, 35(5), 842-849.

Park, S. H., Kim, D. J., Ryu, G. S., & Koh, K. T. (2012). Tensile Behavior of Ultra High Performance Hybrid Fiber Reinforced Concrete. Cement and Concrete Composites, 34(2), 172-184.

Plank, J., & Hirsch, C. (2007). Impact of Zeta Potential of Early Cement Hydration Phases on Superplasticizer Adsorption. Cement and Concrete Research, 37(4), 537-542.

Rahman, M. K., Baluch, M. H., & Al-Gadhib, A. H. (2000). Simulation of Shrinkage Distress and Creep Relief in Concrete Repair. Composites Part B: Engineering, 31(6), 541-553.

Rallabhandhi, S. (2016). Evaluation of Ultra High Performance Concrete in Joints of Bridge Girders. Missouri University of Science and Technology.

Resplendino, J. (2012). State of the Art of Design and Construction of UHPFRC Structures in France. Proceedings of Hipermat, 27-41.

Richard, P., & Cheyrezy, M. H. (1994). Reactive Powder Concretes with High Ductility and 200-800 MPa Compressive Strength. Special Publication, 144, 507-518.

RS Means Company. (2013). RSMeans Heavy Construction Cost Data. p. 49.

Russell, H.G., and Graybeal, B.A. (2013). Ultra-High Performance Concrete: A State-Of-The-Art Report for the Bridge Community, No. FHWA-HRT-13-060.

Schmidt, W., Brouwers, H. J. H., Kühne, H. C., & Meng, B. (2014). Influences of Superplasticizer Modification and Mixture Composition on the Performance of Self-Compacting Concrete at Varied Ambient Temperatures. Cement and Concrete Composites, 49, 111-126.

Schober, I., & Flatt, R. J. (2006). Optimizing Polycaboxylate Polymers. Special Publication, 239, 169-184.

Shann, S. V. (2012). Application of Ultra High Performance Concrete (UHPC) as a Thin-Bonded Overlay for Concrete Bridge Decks. Michigan Technological University.

Sprinkel, M.M. (2011). LMC Overlays for Bridge Deck Preservation. Virginia Center for Transportation Innovation & Research, Southeast Bridge Preservation Partnership Meeting, Raleigh NC.

Stovall, T., De Larrard, F., & Buil, M. (1986). Linear Packing Density Model of Grain Mixtures. Powder Technology, 48(1), 1-12.

Tattersall, G.H., Banfill G. (1983). Rheology of Fresh Concrete. Pitman, London.

Tazawa, E. I. (Ed.). (1999). Autogenous Shrinkage of Concrete. CRC Press.

Termkhajornkit, P., Nawa, T., Ohnuma, H. (2001). Effects of Properties of Fly Ash on Fluidity of Paste. Cem Sci Concr Technol 55:163-169.

Toutlemonde, F., Renaud, J. C., Lauvin, L., Brisard, S., & Resplendino, J. (2007). Local Bending Tests and Punching Failure of a Ribbed UHPFRC Bridge Deck. In 6th International Conference on Fracture Mechanics of Concrete and Concrete Structures (Vol. 3, pp. 1481-1489).

Vande Voort, T. L., Suleiman, M. T., & Sritharan, S. (2008). Design and Performance Verification of Ultra-High Performance Concrete Piles for Deep Foundations (No. IHRB Project TR-558).

Walraven, J. C. (2002). From Design of Structures to Design of Materials. In Innovations and Developments in Concrete Materials and Construction: Proceedings of the International Conference held at the University of Dundee, Scotland, UK, 281-293.

Wang, X. H., Jacobsen, S., He, J. Y., Zhang, Z. L., Lee, S. F. and Lein, H. L. (2009). Application of Nano Indentation Testing to Study of the Interfacial Transition Zone in Steel Fiber Reinforced Mortar. Cem. Concr. Res. 39 (70), 1-15.

Wille, K., Graybeal, B. A. (2013). Development of Non-Proprietary Ultra-High Performance Concrete for Use in the Highway Bridge Sector, No.: FHWA-HRT-13-100.

Wong, H. H. C., & Kwan, A. K. H. (2008). Rheology of Cement Paste: Role of Excess Water to Solid Surface Area Ratio. Journal of materials in civil engineering, 20(2), 189-197.

Wu, Q., & An, X. (2014). Development of a Mix Design Method for SCC Based on the Rheological Characteristics of Paste. Construction and Building Materials, 53, 642-651.

Yuguang, Y., Uijl, J. D., and Walraven, J. (2008). Study on Bending Behavior of an UHPC Overlay on a Steel Orthotropic Deck. In Second International Symposium on Ultra High performance Concrete. Kassel, Germany, 639-646.